$44.60

Public-data File 85-53

THE GILMORE DOME TUNGSTEN MINERALIZATION

FAIRBANKS MINING DISTRICT, ALASKA

A

THESIS

By

G.L.Allegro

794 University Avenue, Basement
Fairbanks, Alaska 99709

THE GILMORE DOME TUNGSTEN MINERALIZATION FAIRBANKS MINING DISTRICT, ALASKA

A

THESIS

Presented to the Faculty of the University of Alaska

in Partial Fulfillment of the Requirements

for the Degree of

MASTER OF SCIENCE

By

Gayle L. Allegro B.S.

Fairbanks, Alaska

May 1987

THE GILMORE DOME TUNGSTEN MINERALIZATION

FAIRBANKS MINING DISTRICT, ALASKA

RECOMMENDED:

Chairman, Advisory Committee

Department Head

APPROVED:

Dean, College of Natural Sciences

Director of Graduate Programs

Date

ABSTRACT

Scheelite in the Fairbanks mining district, Alaska occurs in small, discontinuous, stratabound bodies along the northern flank of the Gilmore Dome intrusive up to 3 km away from intrusive contacts within late Precambrian greenschist facies marble, calc-silicate marble, and calcareous quartzite. Detailed studies of these prospects have led to the conclusion, based on gangue mineralogy, structural control, cross-cutting features, and age of mineralization, that the scheelite is of metasomatic origin.

Scheelite occurs in pyroxene (Hd_{90-40}) - garnet (Gr_{82-70}) skarn, ferro-actinolitic hornblende + quartz + calcite retrograde skarn, and muscovite + biotite + chlorite altered zones. Skarns are localized in calcareous horizons cut by veins, felsic dikes and faults. Marble hosted skarns have higher tungsten $\pm$ gold grades and show spatial zoning from proximal garnet to distal pyroxene. Amphibole and white mica from skarns have ages consistant with the cooling age of Gilmore Dome pluton (85 - 91 Ma). These skarns are similar to other tungsten skarns worldwide.

CONTENTS

FIGURES

Figures

PLATES

ACKNOWLEDGEMENTS

Many people have helped make this thesis possible. Funding and assistance was provided by the Alaska Division of Geological and Geophysical Survey, the School of Mineral Industry and Department of Geology and Geophysics at U. of A., Resource Associates of Alaska, Clynt Nauman, and Vince and Linda Monzulla. I wish to express my sincere thanks to my committee members - R.J. Newberry, T.E. Smith, and S.E. Swanson - for their guidance and patience. I would especially like to thank Rainer Newberry for sharing his world of skarns and Tom Smith for his advice, support, and encouragement over many years. Janice Leveille provided statistical and computer assistance, and field and drafting assistance was given by Mary Albanese, Jeff Lindhorst, Mo Aumiller, and Jeff Filut.

I would also like to thank my fellow students and collegues who made working on this project easier and even fun - sometimes. Dave Szumigala was the best office and skarn buddy around while Janice Leveille, Kate Bull, and Nancy Hanneman offered emotional support and comic relief. Finally, through constant support and encouragement, Crandon Randell made finishing this project relatively enjoyable.

INTRODUCTION

The Fairbanks mining district in central Alaska, known primarily for its placer and lode gold production, also has many small lode tungsten occurrences. Gold and tungsten mineralization is concentrated north of Fairbanks along a northeast-southwest trending belt that extends from Ester Dome to the northeast beyond Cleary Summit (fig. 1) (Mertie,1918; Hill, 1931; Byers, 1957; Robinson and others, 1982).

The main tungsten occurrences in the district are found in the Gilmore and Pedro Dome areas (Byers, 1957), with the majority of tungsten mineralization occurring in metasediments along the northern flank of the Gilmore Dome pluton. Numerous prospect pits in the area have shown the mineralization to be widespread but sporadic and of variable grade. In the Pedro Dome area the mineralization is not as pronounced and appears to be much less extensive (Byers, 1957).

Compared with the gold production from the district (approximately 7.5 million troy ounces), tungsten mining has not been important. However, the origin of the tungsten deposits, whether (1) contact metasomatic skarns or (2) syngenetic strata-bound concentrations, recently has been a matter of ongoing debate (Metz and Robinson, 1980).

Early workers in the area described these occurrences as being the result of contact metamorphic processes (Mertie and Overstreet, 1942; Joesting, 1942; Thorne and others, 1948; Byers, 1957). Tungsten mineralization is associated with pegmatitic dikes, along intrusive contacts in calcareous rocks and schists, in quartz veins, and within rocks containing garnet and pyroxene. The occurrences, like many other tungsten deposits worldwide have been reevaluated (Metz, 1977; Metz and Robinson, 1980) in light of the tungsten-mercury-antimony syngenetic strata-bound model proposed by Maucher (1976). Characteristics of the occurrences considered similar to the strata-

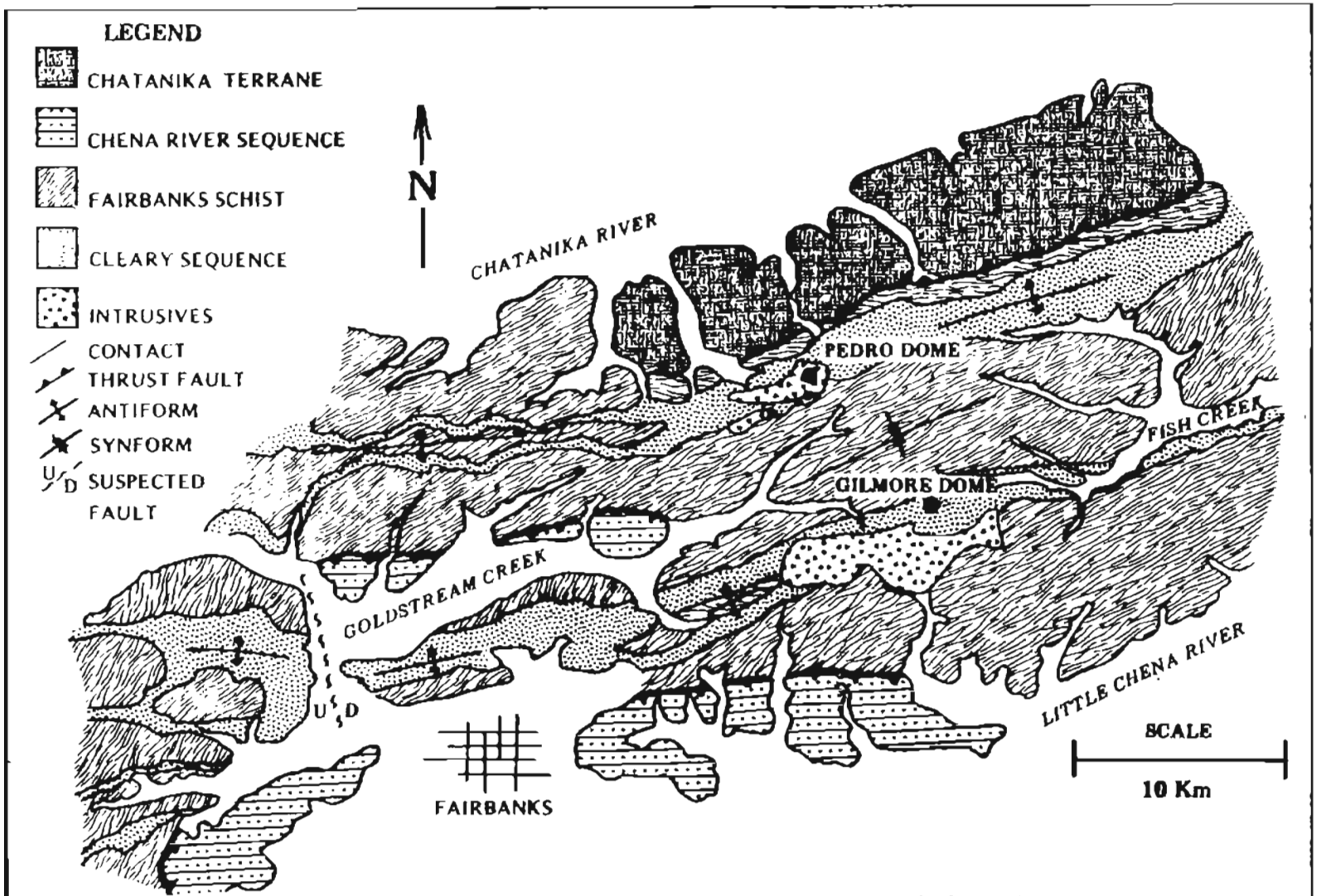

Figure 1. General geology of the Fairbanks mining district, Alaska (modified from Smith and others, 1981 and Robinson and others, 1982).

bound model are the stratiform nature of some of the tungsten mineralization, tungsten occurrences mostly concentrated at considerable distance (up to several kilometers) and extending for great distances along strike of certain lithologic units from intrusive contacts, scheelite associated with amphibole-rich rocks, the presence of mafic volcanic units, and the likely Precambrian to Early Paleozoic age of the host sediments. Unfortunately, criteria for recognition of strata-bound tungsten deposits are not as well established as those for metasomatic skarns, and thus confusion between layer-like metasomatic and syngenetic strata-bound deposits is common. Well established characteristics for tungsten skarns are described by Newberry (1980); Einaudi and others (1981); and Dick and Hodgson (1982). Tungsten deposits interpreted as being strata-bound are Felbertal in Austria (Holl and others, 1972; Maucher, 1976; and Holl, 1977) and the Piriwiri and Bulawayan systems in Rhodesia (Cunningham, 1973).

This study was undertaken to understand the Gilmore Dome mineralization and its possible origins as either a syngenetic strata-bound or metasomatic deposit. Resolution of this question has considerable significance for the tungsten resource potential of the district. If the tungsten is an original constituent of discrete stratigraphic units, then the mineralized beds could be quite extensive, and exploration would consist of following the ore-bearing units. However, if the mineralization is a result of metasomatic processes associated with the intrusion of the Gilmore Dome pluton, exploration would be confined to favprable sites in a limited area surrounding the pluton and would emphasize variations in the igneous rocks.

To resolve the question of origin, detailed mapping and sampling at a scale of 1:120 (2.5 cm to 3 m) and 1:240 (2.5 cm to 6 m) was completed on three prospects in the Gilmore Dome area during the summer of 1982 (pls. 1-7). These prospects are the Spruce Hen, Yellow Pup, and Gil (fig. 2). A total of 212 - 7 kg rock samples were collected and analyzed for tungsten, gold, silver, mercury, antimony, copper, lead, zinc,

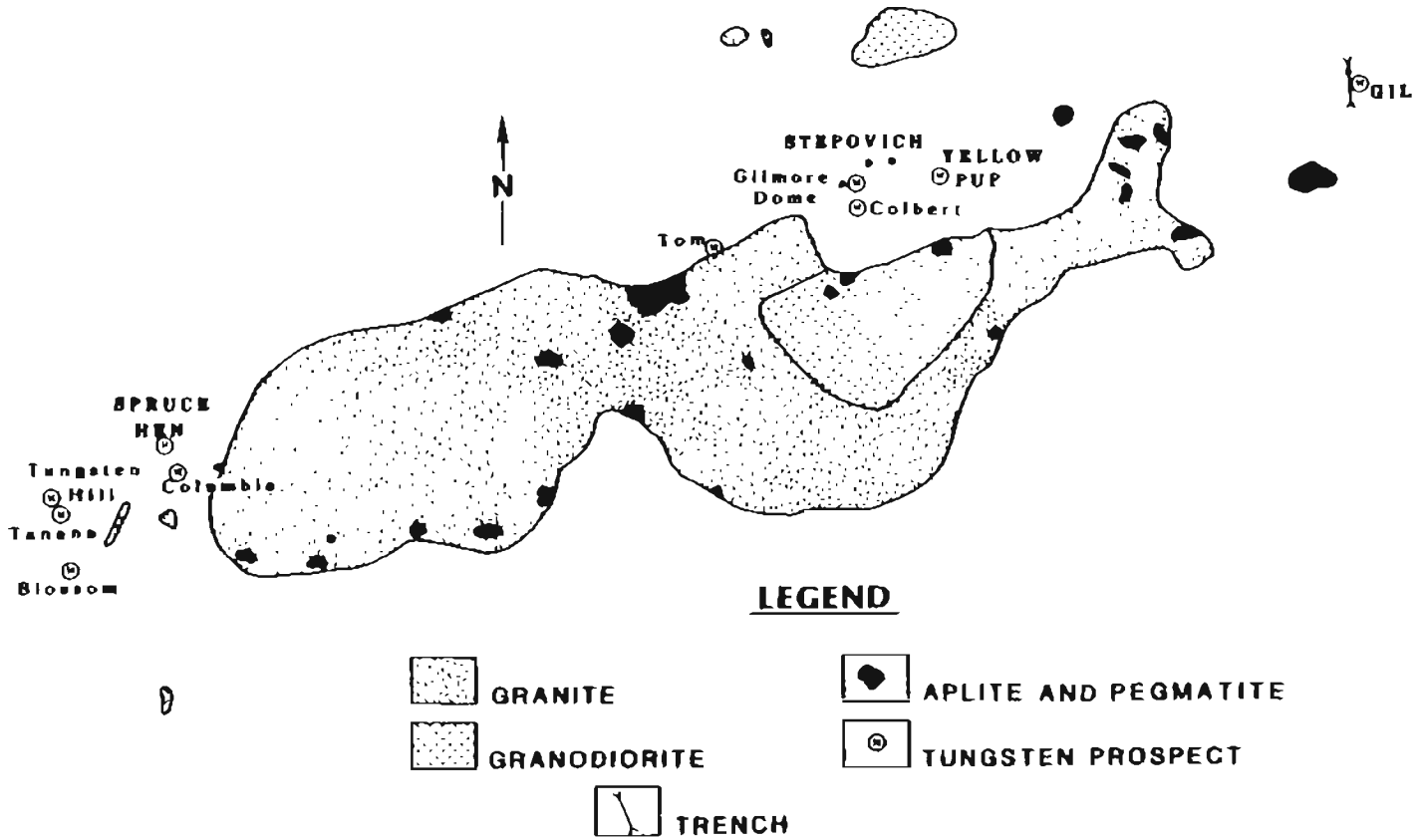

Figure 2. Distribution of tungsten occurrences along the Gilmore Dome pluton, Fairbanks mining district, Alaska (modified from Byers, 1957 and Blum, 1983). Major occurrences are capitalized in figure.

molybdenum, tin, arsenic, and fluorine. Major oxide compositions were obtained on 38 rock samples representing the various types of metasedimentary units in the area. The field work and geochemistry was augmented with petrographic examination of 200 thin sections and microprobe analysis of characteristic minerals.

The study was supported by the Alaska Division of Geological and Geophysical Surveys (DGGS) as one component of a mineral evaluation program of the Fairbanks mining district. The program was undertaken at the request of the Fairbanks North Star Borough and was a joint effort between DGGS and the Mineral Industry Research Laboratory, University of Alaska.

PREVIOUS WORK

Scheelite has been found in many placer deposits in the Fairbanks district, and was first discovered in bedrock in 1915 at the summit of Gilmore Dome (fig. 2) on the property now known as the Stepovich mine (Brooks and others, 1916). Other occurrences were found in the area of First Chance, Steele, and Engineer Creeks approximately 7 km southwest of the summit of Gilmore Dome and include the Spruce Hen, Tanana, Columbia, Tungsten Hill, Anderson, and Blossom claim blocks described by Brooks and others (1916); Mertie (1918); and Chapin and Harrington (1919). Prospecting in the district continued for two or three years until the decline in the market value of tungsten at the end of World War I. Except for the Stepovich mine, little work has been done on most of these properties until recently (Thorne and others, 1948). The Stepovich mine produced approximately 60 tons of concentrate containing 65 to 70 percent WO_3 (tungsten trioxide) during the years 1942 to 1944 (Byers, 1957).

During World War II, the area was reevaluated by the U.S. Geological Survey, Territorial Department of Mines, and U.S. Bureau of Mines for its tungsten potential and possible reserves (Mertie and Overstreet, unpubl. war report, 1942; Joesting, 1942; Thorne and others, 1948). Mertie and Overstreet (published as part of Byers, 1957) described the occurrences along Gilmore Dome as the result of contact metamorphism. At the Stepovich mine, the tungsten ore was found in calcareous zones and occasionally in quartz veins. Below the calcareous horizons, an amphibolite unit was noted. The silicate mineralogy associated with the scheelite within discontinuous limestone lenses included quartz, diopside, and hornblende, with minor garnet, idocrase, apatite, sphene, and clinozoisite.

Joesting (1942) attributed the scheelite in altered limestone or calc-schist as a product of deposition from tungsten-bearing fluids emanating from the underlying

Gilmore Dome pluton, even though most of the deposits were several thousand feet from known intrusive contacts. He also noted that a zone of dark green hornblende frequently accompanied the ore zone and suggested it was formed by replacement directly related to the scheelite deposition. His report notes that the scheelite occurs in two forms: 1) as finely disseminated grains associated with calc-silicate replacement of calcareous horizons, and 2) within and adjacent to rich ore shoots where vertical quartz stringers intersected mineralized calcareous horizons.

More recently Metz (1977) speculated that some of the mineralized rocks in the Fairbanks district are similar to the strata-bound tungsten-antimony-mercury model described by Maucher (1976). By this model, early Paleozoic sediments and volcanic rocks forming near major tectonic lineaments are enriched in tungsten-antimony-mercury from submarine volcanic hydrothermal exhalations. The strata-bound ore can be found in quartzite, graphitic schist, marble, metatuff, amphibolite and other metavolcanoclastic rocks, with the synsedimentary character of the ore said to be preserved (Holl and Maucher, 1972). Maucher stresses that this type of deposit shows an intimate temporal, spatial, and genetic relationship to widespread mafic volcanic activity of the early Paleozoic. Further developing this model, Plimer (1980) has postulated that strata-bound tungsten in early Paleozoic sequences of thick pelitic metasediments containing mafic volcanic rocks and chemically precipitated quartzite and carbonate are the precursors to tungsten deposits associated with anatectic granites. Extending Plimer's hypothesis, Maiden (1981) suggested that metamorphic remobilization of tungsten without the influence of a magmatic event is also potentially a major ore generating process from subeconomic strata-bound deposits.

Metz and Robinson (1980) have proposed that the amphibolites, which represent metamorphosed mafic volcanic rocks in the Fairbanks district, may be the source of the

tungsten and that the tungsten present in calcareous rocks may be the result of remobilization during metamorphism. Initial geological studies at the Yellow Pup mine suggested that tungsten was concentrated in calc-amphibolite layers within the metamorphic sequence (Robinson, 1981).

GEOLOGIC SETTING

The Fairbanks mining district is part of the Yukon-Tanana Upland also called the Yukon Crystalline Terrane (Tempelman-Kluit, 1976) (fig. 3) and is underlain by crystalline rocks of the Yukon-Tanana metamorphic complex (Foster and others, 1973). Parental rocks of the Yukon-Tanana metamorphic complex are believed to be of Precambrian to Late Paleozoic in age (Forbes, 1982) and have experienced at least two periods of metamorphism. The metamorphic grade of the rocks ranges from greenschist to garnet-amphibolite (Forbes, 1982). Within the complex, the dominant rock types are micaceous quartzite, quartz-mica schist, and pelitic schist with subordinate amounts of gneiss, amphibolite, marble, greenschist, calc-magnesium schist, and phyllite (Forbes and Weber, 1982). Igneous rocks ranging in composition from ultramafic to granitic have intruded the complex at various time intervals (Forbes, 1982).

The Yukon-Tanana complex within the Fairbanks mining district has been subdivided into three metamorphosed stratigraphic packages (fig. 1) based on rock type and metamorphic grade (Smith and others, 1981). These packages appear to be in thrust contact. The lowermost package, the Fairbanks schist, consists dominantly of greenschist facies rocks, including brown to gray quartzite, micaceous quartzite, white mica quartz schist, and minor graphitic schist with local variants containing biotite, feldspar, garnet, and chlorite.

Interstratified within the Fairbanks schist is an interval, informally known as the Cleary sequence, which is interpreted as being partially of distal volcanogenic origin (Smith and others, 1981). Along with the dominant micaceous quartzite and quartz mica schist that are indistinguishable from similar rock units in the Fairbanks schist, there are units of marble, calc-silicate marble, metabasite and metarhyolite, chloritic or actinolitic greenschist, finely laminated white micaceous quartzite, felsic schist, and

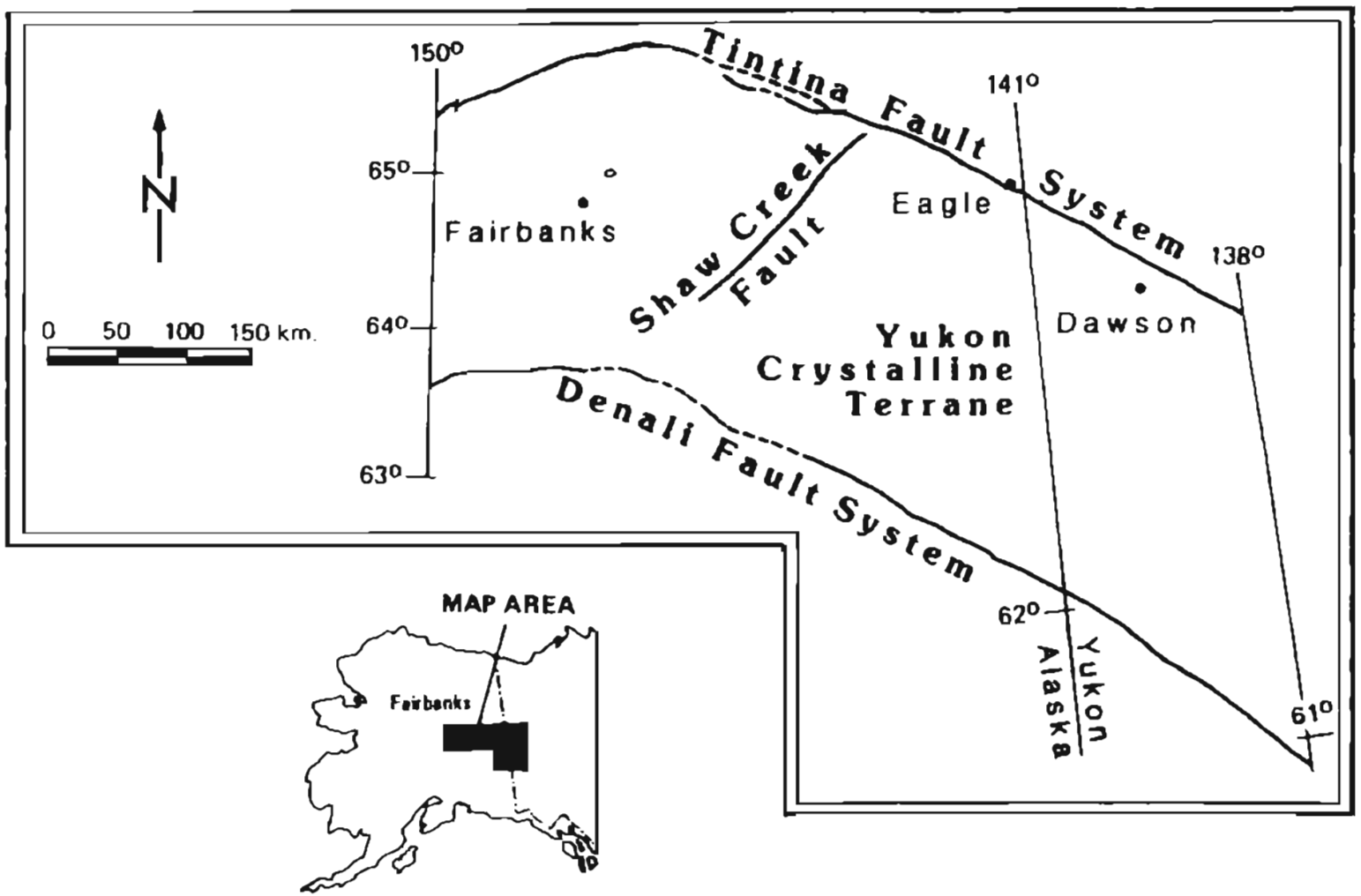

Figure 3. Map of the Yukon Crystalline Terrane showing location of Fairbanks.

minor graphitic schist (Smith and others, 1981). The Cleary sequence appears to host most of the lode mineral occurrences and is found upstream from most of the significant placer deposits. Tungsten occurrences along Gilmore Dome are located within this stratigraphic sequence (fig. 2).

The trench at Gil (pl. 7, fig. 4) exposes both the Cleary sequence and the Fairbanks schist. The distinction between the Fairbanks schist and the Cleary sequence noted at Gil is based primarily upon lithological differences. The Fairbanks schist is comprised of quartzite, quartz-mica and mica-quartz schist, and graphitic schist (pl. 7). Quartzite, the dominant lithology, is usually slightly micaceous with variable amounts of feldspar (0-10 percent) that occur as layers or porphyroblasts along with biotite and white mica. Thick, monotonous quartzite units are separated by thin graphitic layers or grade into schist. The schists are, in general, gray to tan, white mica-rich with subordinate biotite, feldspar, graphite, and rare garnet.

Cleary sequence rocks are dominated by quartzite and schist similar to that found in the surrounding Fairbanks schist, however, the ratio of quartzite to schist is much lower in the Cleary sequence. There is also greater variability in the composition of the quartzite and schist within the Cleary sequence. Most of the quartzite is micaceous and contains feldspar, biotite, white mica, and calcite. Some quartzite units are thin, white, feldspathic and finely laminated; they are locally stained by iron and/or manganese along fractures and foliation. Calcareous quartzite is thinly interlayered with quartz-bearing marble and schist throughout the northern section of the trenches. The schists have a wide range of compositions from pelitic to quartzose, iron-rich to calcareous. They include graphitic schist, biotite-white mica schist, quartz mica schist and mica quartz schist with significant amounts of white mica, biotite, feldspar, garnet, chlorite and locally magnetite. Quartzite and schist units of the Cleary sequence are

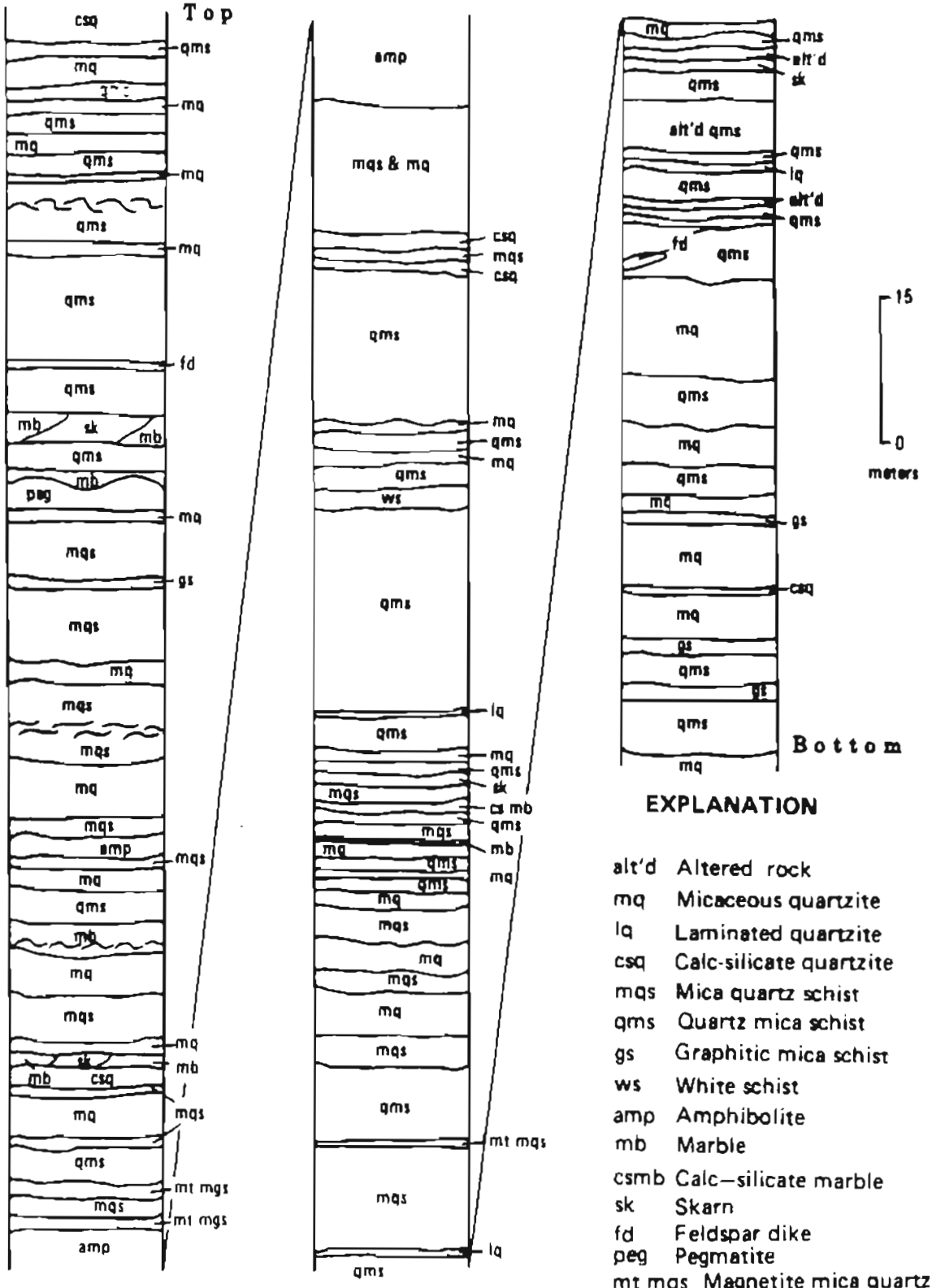

Figure 4. Stratigraphic column of the Gil trenches, Fairbanks mining district.

generally thinner and alternate more frequently than the units within the Fairbanks schist sequence.

The Cleary sequence also contains marble and amphibolite. At Gil there are six thick marble horizons (0.3 to 2.0 meters thick) and a number of thin units (1.0 cm to 0.3 m thick) interlayered with quartzite and schist. Some of the marble units contain up to 10 percent metamorphic pyroxene, quartz, tremolite, iron oxides, and feldspar as small interstitial anhedral grains in a medium-grained (0.3 - 0.9 mm) calcite mosaic. Other marble units contain wispy feldspar layers comprising less than 5 percent of the rock. Protoliths of these metamorphic rocks were siliceous dolomitic limestone and argillaceous limestone. The metamorphic calc-silicate phases define a crude layering that is often only perceptible in thin section. Weathering of the marble results in a brown granular material; in many places, the presence of this weathered material is the only means of recognizing the very thin marble units interlayered with quartzite and schist.

Five distinct units of amphibolite (1 m to 17 m thick) are interlayered within the section at the Gil property. Major oxide analysis of the units suggests the protoliths were tholeiitic basalts of probable non-MORB (Gill, 1981) and non-island arc (Perfit and others, 1980) affinities (fig. 5, appendix IV, table 5). It is not clear from field evidence whether these units represent sills, flows, or tuffs. They are composed of 80 to 90 percent amphibole with lesser amounts of epidote, biotite, plagioclase, sphene, ilmenite, chlorite, quartz, calcite, and garnet. Units show heterogeneous textures that range from fine-grained and well foliated to coarse-grained and massive.

A small body of pegmatite is present in the northern section of the trenches near a marble and skarn unit. Other thin quartz and feldspar veins are present throughout the trench area.

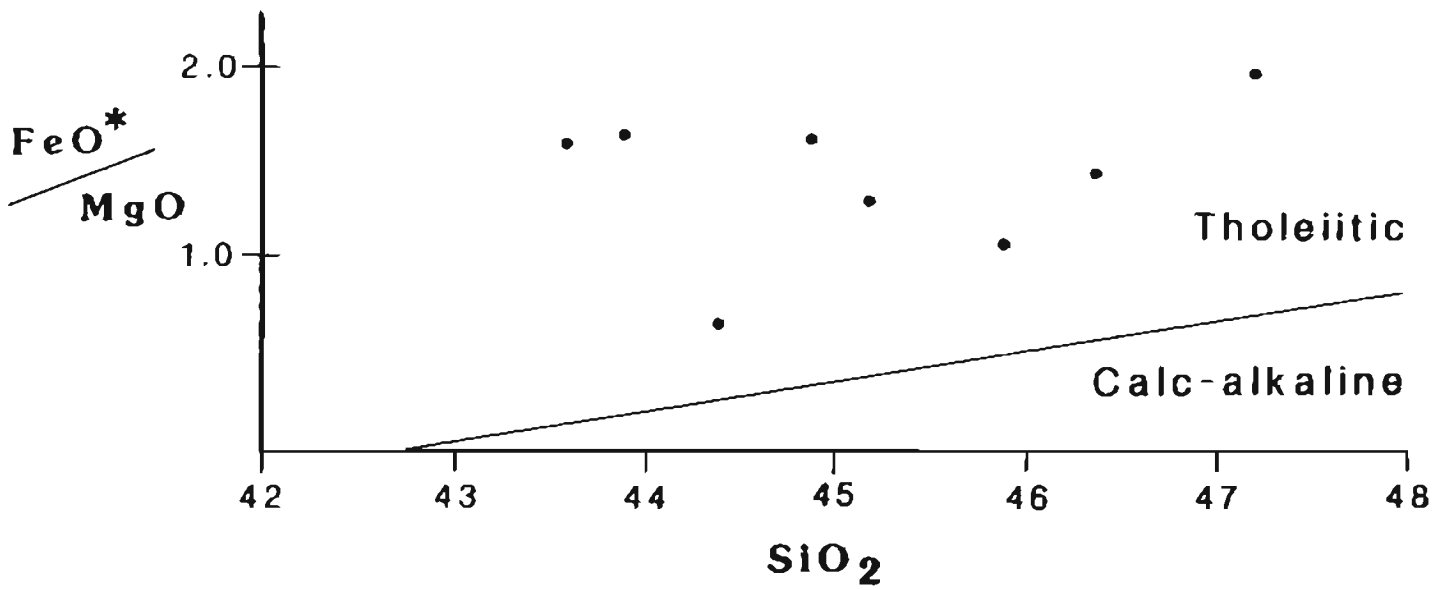

Figure 5. Major oxide data from Gilmore Dome amphibolites (discriminant plot from after Miyashiro, 1974).

Representative samples of schists and amphibolites analysed for major oxides from the Gil trenches (appendix IV) are plotted on an ACF diagram (fig. 6) with fields for sedimentary and igneous protoliths. Quartzites were not included in the figure due to the distorted placement resulting from a minor amount of components in a dominantly quartzose rock. Many of the schists plot in the Al-rich clay and shale field. The rest are transitional between Al-clays and greywackes. A slight trend in schist towards the amphibolites may represent mixing of volcanic and sedimentary material.

A ground magnetic survey by Resource Associates of Alaska (RAA) revealed that the Cleary sequence rocks overall have a higher magnetic signature than those of the enclosing Fairbanks schist. This is a reflection of the magnetite-bearing schists and amphibolite units present in the Cleary sequence.

Structurally above the Fairbanks schist is the Chena River sequence, amphibolite facies rocks that include coarse-grained garnet-mica schist, quartzite, black argillite, marble, amphibolite, and calc-silicate units. Along the northern part of the district, rocks of the Chatanika terrane consist of garnet-clinopyroxene rock, garnet amphibolite, black quartzite, and pelitic schist of amphibolite facies metamorphic grade (Smith and others, 1981; Robinson and others, 1982).

Bedrock units within the Fairbanks district exhibit evidence of two periods of deformation. An early event is defined by northwest-trending isoclinal-recumbent folds and mineral lineations. Superimposed on these structures, recording the most recent structural event (90 to 120 m.y.), are large open and upright sinuous anticlines and synclines that trend northeast (Forbes, 1982; Hall, 1985).

In a structural analysis of the district, Hall (1985) defined four phases of folds and suggested the folding was derived from nappe and tectonic slide development. He proposed the dislocation structures which host the Cleary belt mineralization, were

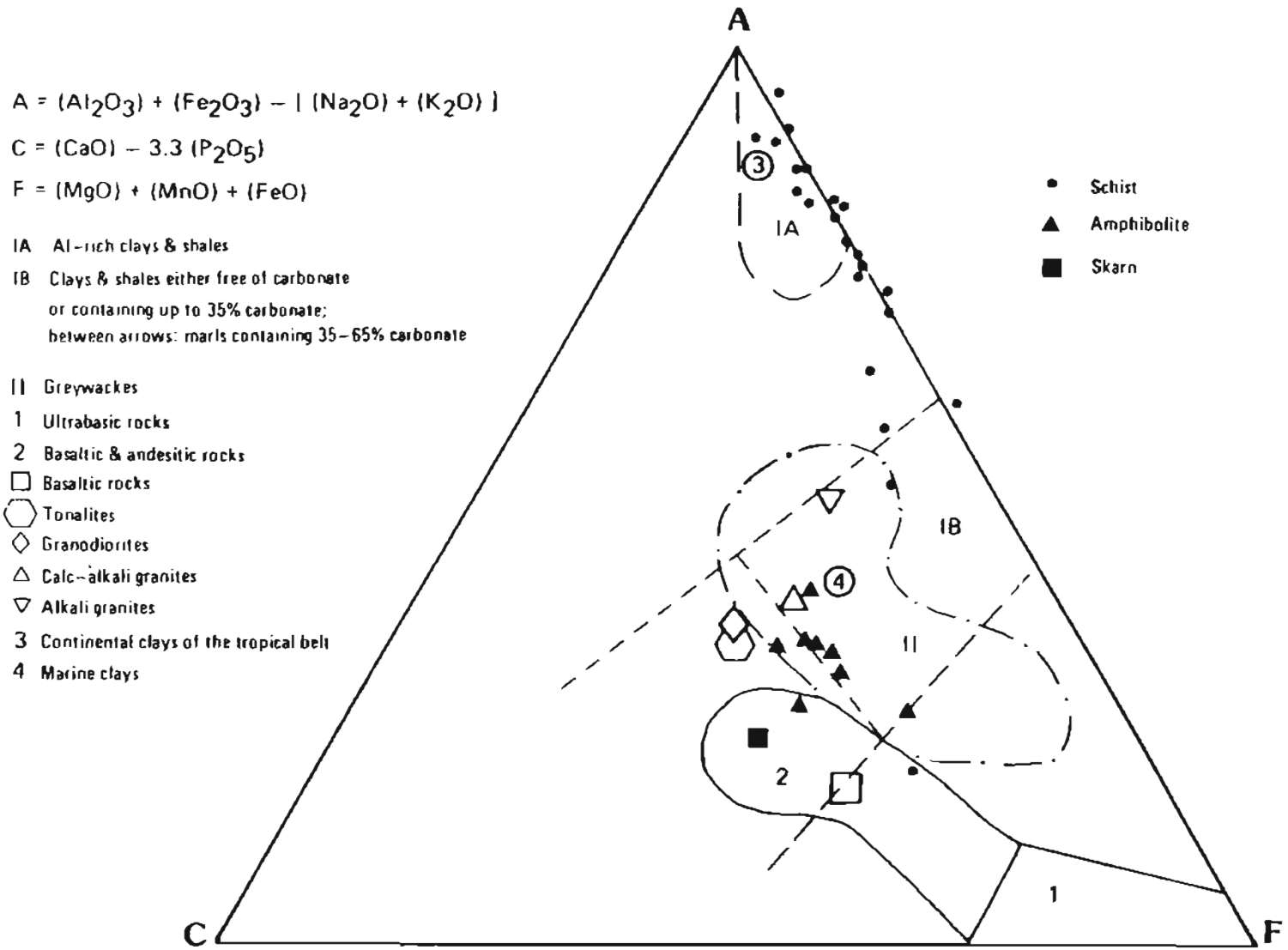

Figure 6. Major oxide data of schists and amphibolites from the Gilmore Dome area (after Winkler, 1979).

related to the plutonic event and changed during fluid introduction from dominantly ductile to brittle deformation.

During the waning stages of the last deformational event, granodiorite and granite stocks (classification of Streikeisen, 1976) intruded the metamorphic country rock along the axis of the two dominant antiforms (Blum, 1983). Blum reported radiometric dates of 91 m.y. for the plutons and estimated a depth of emplacement of 3 to 5 km. Initial $^{87}Sr/^{86}Sr$ ratios of 0.712 suggests some crustal source component to the magma.

The Gilmore Dome pluton is composed primarily of porphyritic coarse-grained granite with several small areas of porphyritic fine- to medium-grained granodiorite. Biotite is the dominant mafic phase, with local hornblende. Aplite-pegmatite dikes, 2 to 20 cm wide, are common along the edges of the pluton (Blum, 1983) (fig. 2). Due to the extreme lack of outcrop, contacts between the intrusion and country rock are approximate and the extent of thermal metamorphic effects is poorly defined.

GENERAL FEATURES OF THE TUNGSTEN OCCURRENCES

During field evaluation of the various tungsten properties, it became clear that the character of the mineralized zones varied from prospect to prospect and that the rocks within and many of those near the mineralized horizons had experienced some degree of alteration. Ore horizons were sporadic and discontinuous along strike, often localized along structural surfaces and cross-cut stratigraphy, and were commonly associated with abundant quartz veining, surrounded by rocks that were bleached or "silicified", and had variable gangue mineralogy. Subsequent petrographic examination of the many rock types confirmed initial impressions and defined alteration types. This data led to the conclusion that the mineralization is largely present as tungsten skarns. Following the nomenclature of Einaudi and Burt (1982), the term skarn used in this study refers to the result of infiltration and diffusion of metasomatic fluids carrying exotic components into predominantly carbonate rocks. Exoskarns are formed when the host rocks are carbonates whereas endoskarns are formed from rocks of igneous, volcanic, or shaley sedimentary origin. Commonly in skarns the most notable mineralization is localized within the exoskarns (Einaudi, and others, 1981).

Traditionally the term endoskarn has referred to skarn formation in igneous rocks adjacent to marble skarn that, through appearance and mineral phases, resembles marble skarn. Skarn development is not limited to marble or adjacent igneous rocks but can be found in volcanic and sedimentary rocks (Einaudi and others, 1981; Shimazaki, 1982). Wallrock alteration in adjacent units is also common in some skarn deposits (eg., MacTung; Hodgson and Dick, 1982).

Along Gilmore Dome the character of the tungsten skarns reflects the type of the host rock the skarn formed in. The skarns are limited to the Cleary sequence belt due to the calcareous nature of some of these rocks. Skarns formed near the intrusive

in relatively thick marble such as at Spruce Hen are distinctive in their traditional exoskarn characteristics, whereas skarns formed further from the intrusive and in rocks dominated by very thin, sparsely spaced marble and calc-silicate marble layers such as at Yellow Pup show a wider diversity in skarn characteristics. In these areas, endoskarn becomes more important as the host for mineralization.

Complexity of the skarns is also caused by the presence of calc-silicate minerals formed during both the regional metamorphic and thermal contact events. Fine-grained recrystallized hornfels is not found at these prospects, but a certain degree of contact metamorphic recrystallization is present in the rocks, especially in the impure marbles. Bimetasomatic or reaction skarns (Einaudi and Burt,1982) have also formed along contacts of marble and schist due to isochemical diffusion. Commonly these metamorphic calc-silicate minerals are overprinted by skarn mineral assemblages.

Finally, the skarn event occurred over a range of temperatures expressed by changing mineral assemblages. Mineral stability relationships used for this study are from Burt (1972), Einaudi (1981), and Einaudi and others (1981). For this study the exoskarn event has been divided into an early (prograde) event characterized by anhydrous calc-silicate formation and a later (retrograde) event of anhydrous calc-silicate destruction and hydrous mineral formation with accompanying quartz and calcite.

Mineralized skarn along Gilmore Dome formed in a variety of host lithologies. Minerals formed during skarn processes reflect the host lithology as well as the composition and temperature of the fluids. The resultant skarn mineral assemblages do not always fit within the traditional use of the present skarn terminology. Transitional contacts between metasomatically altered units also complicate descriptions. The term endoskarn as used in this study does not necessarily imply the presence of calc-silicate minerals but includes rocks dominated by white mica and chlorite. This later alteration

is considered genetically related to and contemporaneous with to slightly later than pyroxene-garnet skarn formation. Terms such as greisen and propylitic do not seem appropriate for these rocks, as they are traditionally associated with Sn and Cu deposits (respectively). Therefore, in this study the term endoskarn is used to denote rocks other than marbles that have experienced substantial fluid interaction along with the introduction of exotic components resulting in the formation of calc-silicate and/or phyllosilicate mineral phases and ore minerals. Wallrock alteration is used to denote areas surrounding ore zones that show signs of recrystallization and minor addition or subtraction of components, but where the overall bulk composition of the rocks has not been significantly changed. Where endoskarn development ceases and wallrock alteration begins is highly variable and often only perceptible on the thin section scale.

Distinguishing between metamorphic and metasomatic calc-silicate minerals can be difficult, especially where metamorphic calc-silicate minerals have been overprinted by the skarn-forming event. Criteria described by Newberry (1980) were used to distinguish the types of calc-silicate minerals. Microprobe analysis augmented the petrographic data. For this study, the criteria used to distinguish metamorphic calc-silicate minerals are: fine-grain sizes, irregularly shapes, inclusion-rich, iron and manganese poor, pale color, preservation of sedimentary layering, and absence of veining. Metasomatic calc-silicate phases are: medium- to course-grained, subhedral to euhedral, nonpoikiolitic, iron and manganese enriched, dark in color, occur in irregular pods and lenses, and are associated with abundant veining and other evidence of fluid flow. These characteristics will be described in more detail in the following sections.

TUNGSTEN OCCURRENCES

Three tungsten occurrences along the northern flank of the Gilmore Dome pluton were studied in detail. These are the Spruce Hen, Yellow Pup, and Gil properties (fig. 2, pls. 1-7). All the tungsten occurrences are believed to be within the Cleary sequence which roughly parallels the northeasterly trending pluton. None of the known mineralized areas are along the plutonic contact. Based on current knowledge of the contact, the Spruce Hen is nearest the pluton, the Yellow Pup is farther away, followed by the Gil, which is approximately 3 km from the pluton. These properties were chosen for study because of their accessibility and higher degree of exposure through trenching and underground workings. Other tungsten occurrences along this belt were examined briefly and were found to have similar characteristics to those studied in detail. At the time field work was being completed access to the Stepovich property only consisted of material on the old dumps. Since that time new trenching and drilling has been done by Resources Associates of Alaska. Much of this data has been examined, but is considered confidential and is not formally included here.

Spruce Hen Property

Introduction

The Spruce Hen property, also known as Tungsten Hill, is located on the northwest end of the Gilmore Dome pluton on the divide between the headwaters of Steele Creek and First Chance Creek (fig. 2). Prospecting in the area in 1916 resulted in the location of five prospects: the Spruce Hen, Columbia, Blossom, Tanana, and Tungsten Hill (Mertie, 1918). Numerous trenches and several adits were put in the area

prior to 1918, when all work ceased. On the southwest end of the Spruce Hen property an inclined shaft was reportedly sunk 20 meters, following an orebody approximately one meter wide (Byers, 1957). Another shaft was sunk on the northeast end of the property in search of gold (Byers, 1957). Resource Associates of Alaska began work on the property in 1982 reopening a small pit for evaluation purposes. Three diamond drill holes totaling 95 meters were drilled in the summer of 1983.

General Geology

The Spruce Hen property is approximately 600 meters northeast of intrusive outcrop. The open pit at the property exposes a sequence of interlayered schist, quartzite, and marble (pl. 1 and 2). Units, striking N. 40-50^{0} E. with an average northwesterly dip of 40 degrees, have a foliation that is roughly parallel to compositional layering. The most abundant schists are fine- to medium-grained mica (biotite + white mica) quartz schist, quartz mica (biotite and/or white mica) schist, mica (biotite + white mica) schist, and minor graphite schist. Chlorite, albite, garnet, and feldspar in minor amounts are present in some of the rocks. Accessory minerals include tourmaline, apatite, and opaque phases. In thin section, the micaceous layers show signs of contact metamorphism with secondary biotite and white mica rosettes and tourmaline crystals cross-cutting the foliation. Quartzite is, for the most part, micaceous with accessory white mica, biotite, chlorite, and feldspar. Both schist and quartzite contain variable amounts of opaque phases, with some rocks containing up to 5 percent.

Two marble horizons, each approximately 1 to 2 meters wide, have an exposed strike length of at least 90 meters and appear to represent limbs of a fold (pl. 1). Unaltered marble is composed of 80 to 90 percent calcite with variable amounts of metamorphic idocrase, diopside, garnet, wollastonite. Within the marble, layers of

poikilitic, subhedral brown idocrase crystals up to 1.5 cm and small amounts of anhedral garnet, representing original argillaceous layers, parallel the foliation of the surrounding schist. The abundance of metamorphic idocrase over pyroxene within these layers implies the pelitic protolith was aluminous. On weathered surfaces, the metamorphic calc-silicate layers stand out as resistant bands above the more easily weathered marble (fig. 7). Minor diopside (2 to 4 percent) is disseminated throughout the marble as small (0.2 mm) anhedral grains and aggregates interstitial to calcite. The presence of interstitial diopside implies the limestone protolith was also slightly dolomitic.

The large size of the idocrase crystals is presumably a result of the relatively high contact metamorphic temperatures experienced at the Spruce Hen property due to the close proximity of the Gilmore Dome stock. Distinct large idocrase in marble layers were seen in only one other locality in the district where marble is in direct contact with the intrusive (Tom property, fig. 2).

Also exposed in the Spruce Hen pit are several felsic dikes 3 to 8 cm wide that cut across the pit, subparallel to the dominant foliation. Dikes are composed of potassium feldspar, plagioclase (An_{30-54}), and quartz with an average grain size of 0.5 to 1.0 mm. Blum (1983) noted the abundance of dikes on the northwestern end of the Gilmore Dome stock. In some places, felsic dikes contain significant concentrations of tungsten, silver, arsenic, lead, zinc, antimony, and gold. South of the Spruce Hen pit, a thick unit of amphibolite is exposed in old trenches. The rock is composed of hornblende and plagioclase with minor quartz and calcite.

Alteration and Mineralization

Scheelite mineralization at the Spruce Hen property is localized within a dense, nonfoliated, calc-silicate skarn (exoskarn) that contains irregular pods of barren marble.

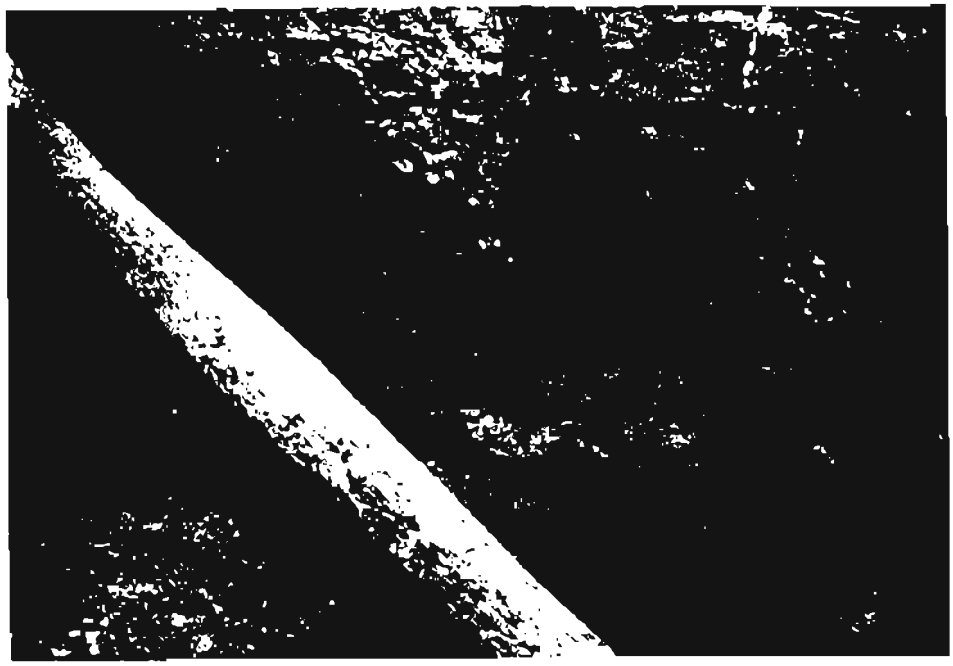

Figure 7. Outcrop of zoned garnet-pyroxene vein cutting across skarn and marble units at Spruce Hen. Resistant idocrase and garnet layers mimic sedimentary layering in marble. Hammer handle approximately 30 cm in length.

Figure 8. Outcrop of remnant marble surrounded by pyroxene-garnet skarn and pyroxene-plagioclase endoskarn along hanging wall contact at Spruce Hen. Note garnet veins parallel to and cutting across general foliation. Detailed alteration shown in fig. 9. Quarter for scale.

Along strike, the skarn abruptly changes into marble (pl. 1). Within the pit exposure, approximately 80 percent of the marble has been replaced by calc-silicate minerals. It is unlikely that the original components available within the slightly impure marble during isochemical metamorphism could account for the bulk of the calc-silicate mineralogy present. Mineralogic evidence suggests that the primary components added to the host rocks by the hydrothermal fluids were silicon, iron, aluminum, magnesium, manganese, fluorine, and tungsten. Other evidence pointing to the secondary nature of the calc-silicate rock are (1) zoned calc-silicate veins cutting through marble as well as through massive calc-silicate rock (fig. 7) and (2) a crudely developed zoning within the calc-silicate rock. In the replacement zone both anhydrous and hydrous calc-silicate minerals are present.

Petrographic evaluation of textures has shown the anhydrous phases to be an early event followed by retrogressive replacement by hydrous phase assemblages. Alteration is not limited to the marble units but is also found to a lesser degree in the hanging and footwall schist and quartzite. Alteration is present especially along the country rock-marble contact (figs. 8 + 9). Each type of alteration noted at the Spruce Hen is discussed below.

Exoskarn

Early skarn Pyroxene and garnet are the characteristic minerals associated with the early stage of skarn formation. They form as massive replacement of marble and as veins within the marble (figs. 7 + 8). Where replacement of the marble is complete, the skarn is a very dense, mottled, green and reddish brown nonfoliated rock. Metamorphic idocrase layers, where not totally replaced by garnet or pyroxene, give a slightly layered appearance to the skarn. Other minerals present in the early skarn are idocrase, wollastonite. quartz, and scheelite.

Zoning within the calc-silicate skarn is developed on the macroscopic scale along marble-schist contacts and calc-silicate veins as well as on the microscopic scale along metamorphic idocrase layers. A zoning pattern often observed away from the marble-schist contact or the idocrase layers is:

schist or idocrase layer	----> garnet + pyroxene ± quartz	----> pyroxene + garnet + scheelite	----> idocrase ± wollastonite ± pyroxene ± scheelite ± quartz	----> marble

Zoning is not always well defined nor are all zones always present. The idocrase-wollastonite zone is often missing. The pyroxene zone locally may contain abundant quartz. In most cases, the marble-schist contact is altered, however, irregular pods of remnant marble remain in the central area of the original limestone unit (fig. 8). The zoning pattern developed in the skarn suggests that metasomatic fluids migrated along lithologic contacts and along the metamorphic idocrase-garnet layers within the marble. This pattern, with garnet furthest from marble, is not expected for bimetasomatic skarn growth (Kerrick, 1977).

Pyroxene-garnet veins in unaltered marble show the same zoning sequence as seen along the contact zone (fig. 7). In the veins, garnet cores are surrounded by pyroxene selvages and locally idocrase and wollastonite. These veins cut across foliation and branch out along idocrase layers. Garnet and garnet-quartz veins (1 cm to 30 cm thick) commonly cut skarn and unaltered marble (figs. 8 + 9). Garnet veins can be traced from the dominantly garnet zone through the pyroxene zone to the marble where the veins open out to form another massive garnet zone.

Pyroxene grains in the skarn are pale to medium green, coarse-grained (0.1 to 1.5 cm), subhedral to euhedral, and form up to 70 percent of the skarn (fig. 10).

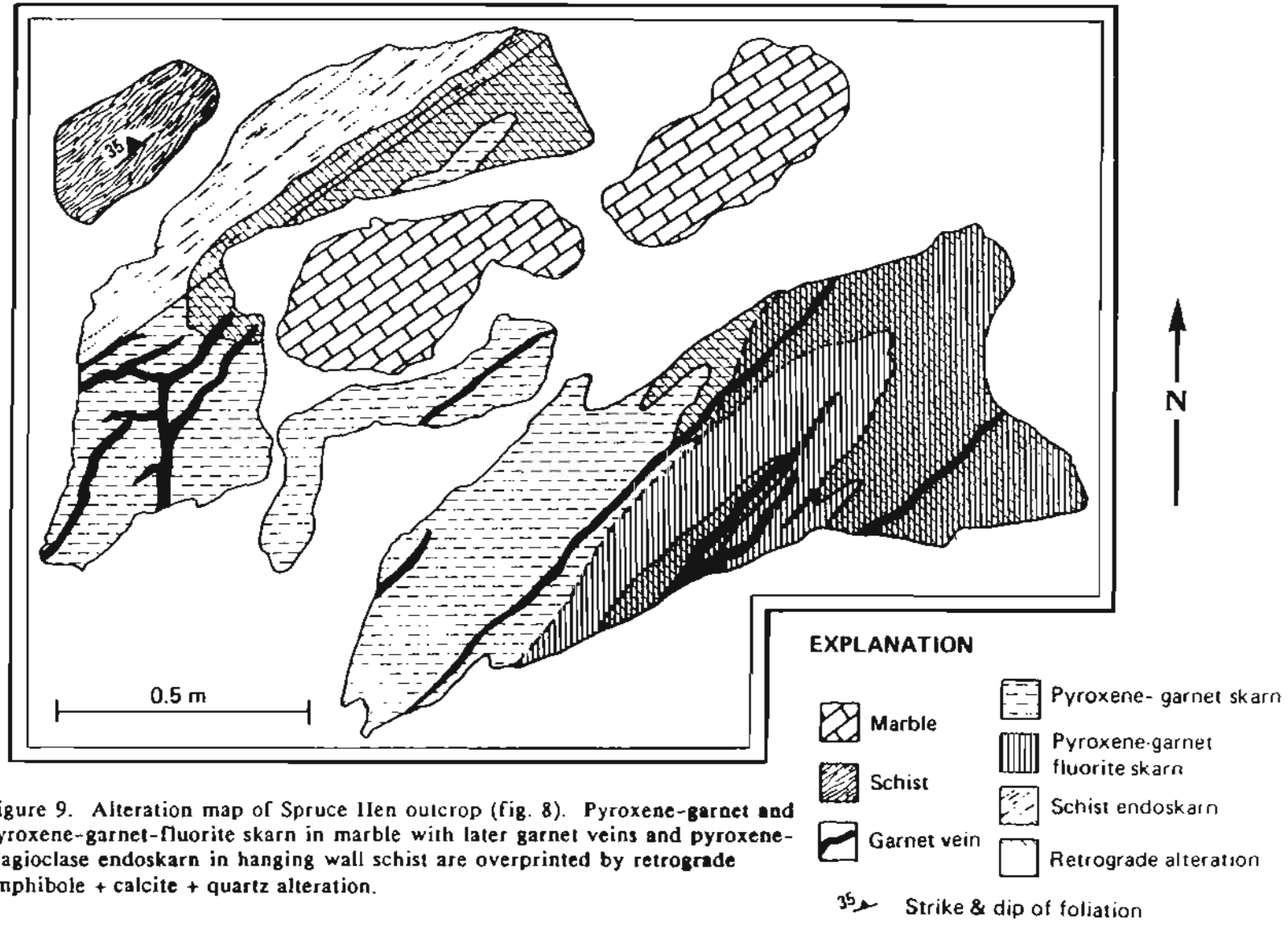

Figure 9. Alteration map of Spruce Hen outcrop (fig. 8). Pyroxene-garnet and pyroxene-garnet-fluorite skarn in marble with later garnet veins and pyroxene-plagioclase endoskarn in hanging wall schist are overprinted by retrograde amphibole + calcite + quartz alteration.

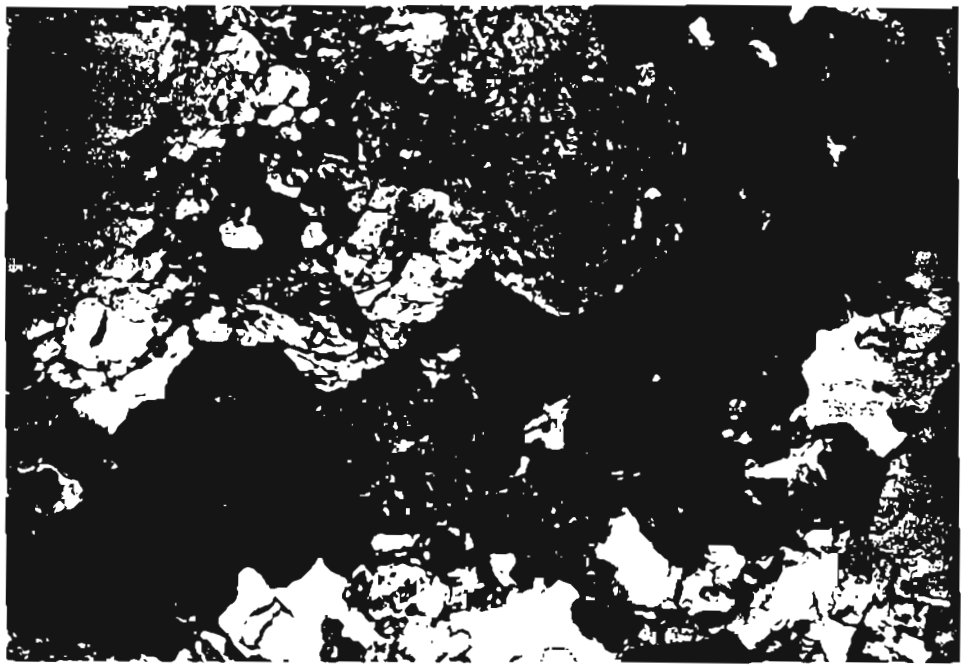

Figure 10. Photomicrograph of pyroxene (pink, yellow, blue) garnet (isotropic) skarn with scheelite (high relief, yellow and grey) at Spruce Hen. Garnet fills vugs and replaces pyroxene. Cross polars, field of view 2.35 mm.

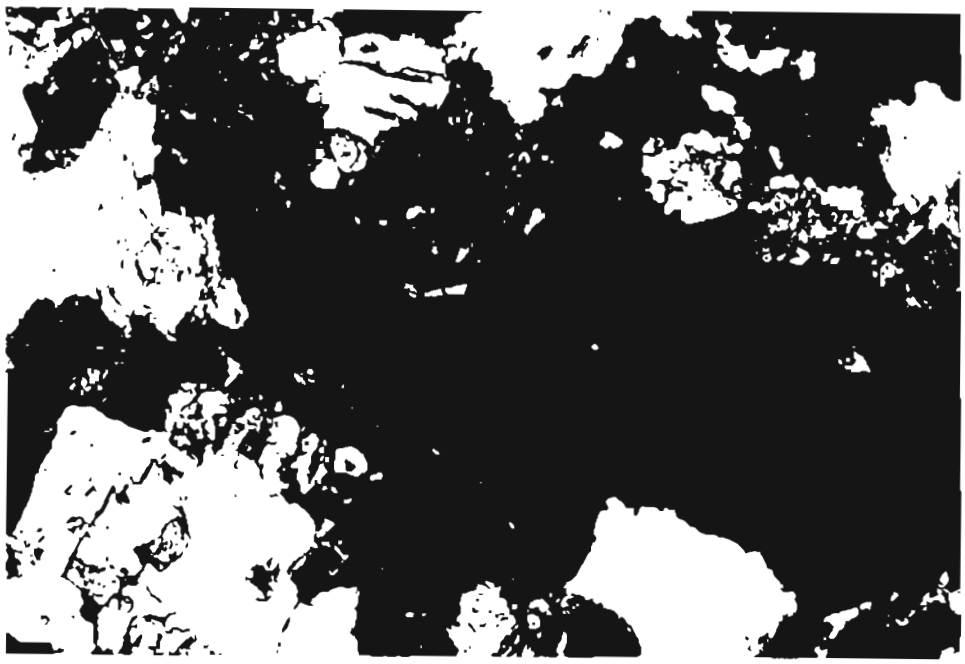

Figure 11. Photomicrograph of zoned garnet at Spruce Hen. Euhedral garnet (black) with anisotropic bands and quartz (grey + white) fill vug in pyroxene skarn. Cross polars, field of view 2.35 mm.

The pyroxene to garnet ratio is about 3:5. Metamorphic idocrase is in some places partially replaced by pyroxene. With increasing distance from idocrase layers, the pyroxene grain size, euhedral shape, and concentration usually increases as the amount of garnet decreases.

Early skarn garnet usually rims and replaces pyroxene and idocrase. Based on variations of color and birefringence, the composition of garnet appears to have changed with time. Light pink, isotropic to slightly birefringent garnets are disseminated throughout the pyroxene skarn and form the cores of darker orange, birefringent, zoned garnets. Orange garnets are found as veins in pyroxene skarn and in zones along contacts with idocrase layers or schist units. The size and shape of the garnets appears to be a function of the mineral phase being replaced. Garnets replacing other calc-silicate minerals form fine- to medium-grained anhedral aggregates whereas garnets replacing calcite are medium- to coarse-grained euhedral crystals (fig. 11). Quartz is commonly associated with the darker birefringent garnets. Dark orange garnet also forms selvages on large, massive, barren quartz veins that cut both marble and skarn.

Idocrase appears to have formed during regional or contact metamorphism and during the metasomatic stage. A metasomatic origin for idocrase crystals is suggested by their large euhedral shape, lack of inclusions, lack of any alteration, and appearance with wollastonite in zoned skarns. Where calc-silicate zoning is present, idocrase forms near the marble front.

Minor wollastonite is found in the calc-silicate skarn, occurring as bladed masses between the pyroxene zones and unaltered marble. Several small areas along the strike length of the marble unit are composed primarily of highly weathered wollastonite, idocrase, and marble.

Scheelite is not present in unaltered marble but is finely disseminated throughout the pyroxene-garnet skarn. Texturally it appears to have formed contemporaneously with these minerals (fig. 12). Scheelite is most abundant in pyroxene rich zones and, where present, in the idocrase-wollastonite zone, but much less so in garnet dominant zones. Scheelite usually occurs as 0.2 to 0.4 mm, subhedral to anhedral grains, both as isolated crystals and as aggregates. Euhedral crystals are relatively rare at Spruce Hen. Both blue fluorescing, relatively pure scheelite and cream fluorescing scheelite with a significant powellite component ($CaMoO_3$) are present at the Spruce Hen. Mo-rich scheelite is often surrounded by Mo-poor scheelite.

Fluorite is very abundant at the Spruce Hen (up to 20 to 30 percent locally). The formation of fluorite appears to have been transitional between early and late skarn. Fluorite grains, mostly colorless in hand specimen, are subhedral, 0.2 to 1.4 mm in size, and occur in aggregates of calcite and quartz that surround or fill vugs in earlier calc-silicate minerals. The assemblage pyroxene -garnet - idocrase - quartz - fluorite $\pm$ calcite is present in both massive skarn and in veins cutting marble. Where zoning is present, fluorite is predominantly found with pyroxene near the marble front. Fluorite is replaced by amphibole and iron oxides and rimmed by opaque phases. Thus it appears to be earlier than the main hydrous event.

Late skarn Late hydrous retrograde alteration of the earlier formed pyroxene-garnet skarn occurs sporadically throughout the Spruce Hen skarn. Retrograde fluids followed, in most cases, many of the same pathways used by the earlier fluids resulting in higher concentrations of retrograde minerals along lithologic contacts, metamorphic idocrase layers, and along the edges of cross-cutting garnet and quartz-garnet veins (fig. 9). The retrograde event was responsible for the formation of amphibole $\pm$ calcite + quartz (after pyroxene), clinozoisite $\pm$ quartz - calcite (after garnet and idocrase),

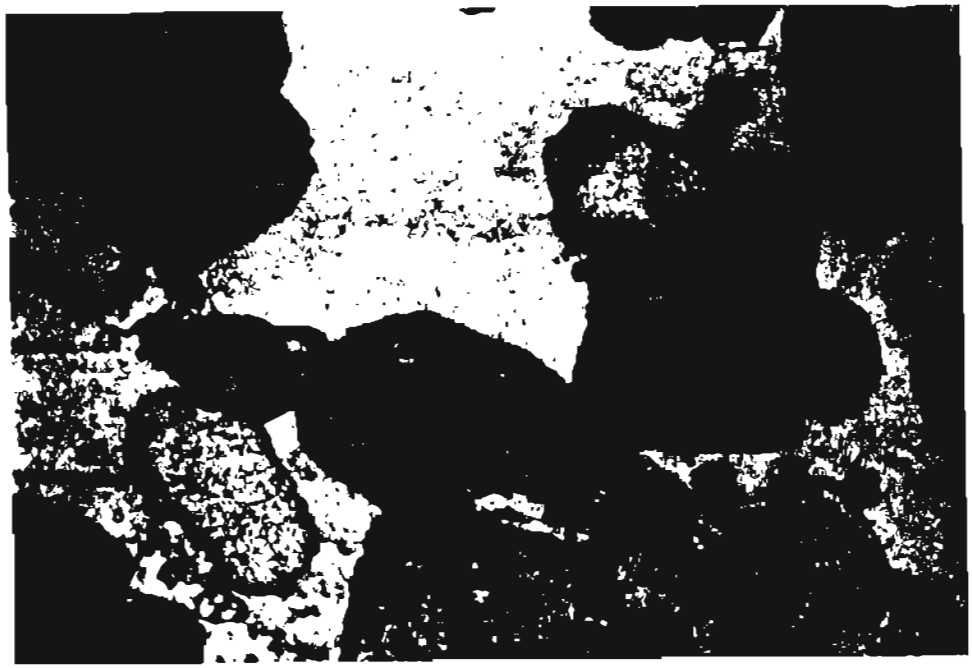

Figure 12. Photomicrograph of pyroxene (blue) skarn with scheelite at Spruce Hen. Scheelite (subhedral, purple) has pyroxene inclusions and intergrowths along the edge. Cross polars, field of view 1.25 mm.

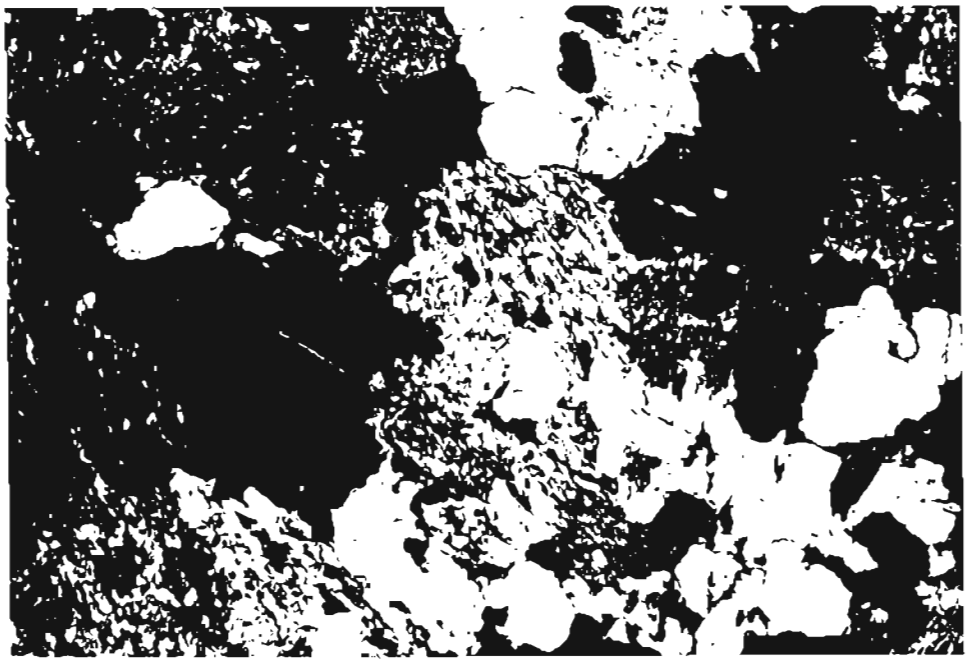

Figure 13. Photomicrograph of ragged amphibole + quartz replacing pyroxene (high birefringence) in skarn. Note scheelite (light to dark grey, high relief) and fluorite (isotropic). Crossed polars, field of view 2.35 mm.

higher grade scheelite, and minor chlorite, biotite, iron oxides, and sulfides. Even though the retrograde event has in places totally replaced the earlier formed minerals, in general this type of alteration is not dominant at Spruce Hen.

Amphibole is the main retrograde mineral, replacing pyroxene and calcite. The degree of pyroxene skarn destruction in the hydrous phase is variable. Complete replacement by amphibole occurs in places, especially along the contacts between skarn and schist. Quartz and calcite are almost always present with amphibole in retrograde zones. Darker green amphibole forms ragged pseudomorphs after pyroxene and lighter green amphibole forms tiny randomly oriented needles in quartz, calcite, and fluorite (fig. 13). Garnet is also locally replaced by amphibole. In some skarn, the concentration of secondary amphibole after pyroxene decreases away from metamorphic idocrase layers. This suggests retrograde fluids used the same pathways as the earlier pyroxene forming fluids.

Other retrograde replacements include clinozoisite + calcite + quartz replacing garnet and idocrase, biotite + calcite replacing garnet, biotite + chlorite replacing pyroxene, and quartz and calcite replacing everything.

Scheelite is not always present in the retrograde zones but where present, significantly higher tungsten grades (up to 8 percent over small areas) are common. Scheelite is often in crystal aggregates up to 1.5 mm in diameter but smaller more euhedral crystals of scheelite within calcite are also common. In retrograded skarn scheelite is nearly always surrounded by amphibole $\pm$ calcite + quartz (fig. 13). Inclusions of calcite, pyroxene, clinozoisite, and fluorite are found in scheelite.
The last event to affect the skarn at Spruce Hen was the introduction of iron as sulfide and oxide. Minor amounts of pyrite, pyrrhotite, chalcopyrite, and arsenopyrite are present along the strongly retrograded contacts between marble and country rock. Iron oxide is found along grain boundaries and cleavage and fracture planes in preexisting

minerals. This stage of fluid introduction was intense enough to significantly alter several areas of skarn. With subsequent weathering, these areas now show near total destruction of rock fabric or have a saprolitic-like texture. Scheelite is often present in these zones along with remnant idocrase, garnet, pyroxene, and concretionary iron oxides.

Endoskarn and wallrock alteration

At the Spruce Hen, all the contacts between the marble units and the hanging and footwall schist and micaceous quartzite have been obscured by alteration. Marble skarn and quartzite or schist endoskarn overlap and blend to form a dense, nearly uniform skarn zone (figs. 8 + 9). With careful inspection, however, endoskarn shows a fine layering parallel to foliation and remnant lenses of unaltered schist, which are not present in the marble skarn. Under ultraviolet light, the contact between marble and country rock is quite evident as scheelite is almost exclusively localized within the marble skarn. Thickness of the endoskarn varies from 15 cm to over one meter.

Mineralogical and textural variations in endoskarn are more complex and variable than in marble skarn due to the variety of original compositions in schist and micaceous quartzite. In general, an alteration zoning sequence from marble to schist of:

mb	--->	pyx	--->	pyx	--->	pyx	--->	amph	--->	bio	--->	ct rk
skn		±		+		+		+		+		schist
		garn		pl		pl		pl		chl		
						+		+		±		
						sph		sph		pl		

is present (see appendix I for abbreviations). However, not all zones occur in one sample and repetition of zones is common. In most cases alteration minerals lie in the plane of preexisting foliation (fig. 14). Within schist and quartzite, pyroxene, amphibole, biotite, chlorite, sphene, and minor sulfides are concentrated in biotite-rich layers, whereas plagioclase favors white mica layers. Metamorphic quartz layers are

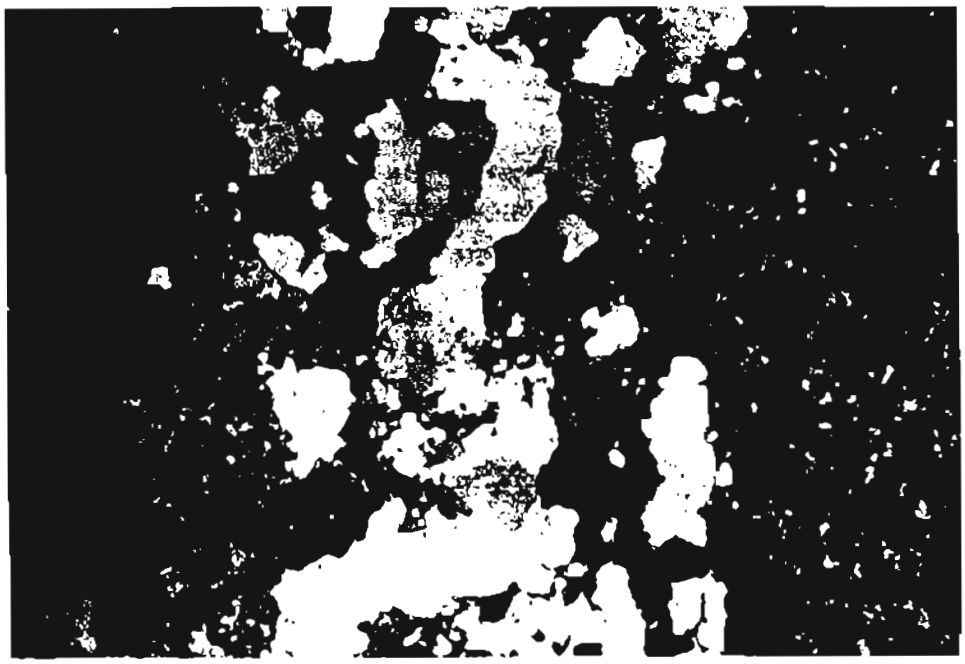

Figure 14. Photomicrograph of endoskarn in schist. Pyroxene (purple + yellow, left side) + clinozoisite (grey to blue, right side) form in feldspar + mica schist along the edge of a thin quartzite band (light grey, center). Cross polars, field of view 3.3 mm.

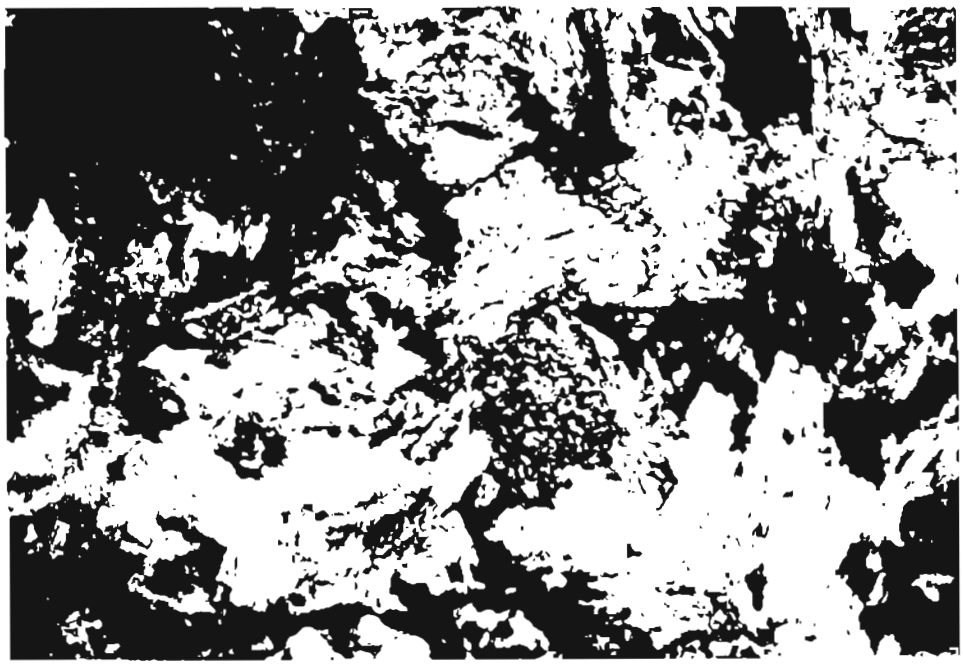

Figure 15. Photomicrograph of altered felsic dike at Spruce Hen. Scheelite (upper left, yellow to dark grey) and white mica (bluish blades) are replacing feldspar (light grey). Cross polars, field of view 1.25 mm.

relatively unchanged. Pyroxene, amphibole, and plagioclase also form selvages along quartz veins that cut endoskarn. Metasomatic garnet is rarely present in endoskarn. When present, it occurs along the schist-marble contact. Scheelite was observed in only one sample and was in contact with pyroxene.

It is difficult to distinguish early and late alteration events since the endoskarn lacks distinctive, contrasting mineralogy. Pyroxene, plagioclase, and garnet appear to be early. Some textures such as cross-cutting features clearly indicate a late formation for some minerals. Fluorite, an occasional constituent within endoskarn, is predominantly localized near the marble contact in the pyroxene-plagioclase zone. Clinozoisite is present as an alteration of plagioclase and is generally found in the pyroxene-plagioclase zone. Iron oxides and sulfides rim and cross-cut fluorite as well as all the other phases.

Alteration and mineralization of felsic dikes, is present adjacent to pyroxene-garnet skarn. A thin dike (<20 cm) composed of quartz and plagioclase (An_{30-40}) is altered to fans and spherical aggregates of white mica and chlorite. Scheelite aggregates and large euhedral crystals form up to 5 percent of the rock (fig. 15). Another felsic dike is less altered but shows zoning from the contact with schist of plagioclase altering to chlorite + white mica + calcite + clinozoisite + sphene + scheelite along the contact to white mica + calcite ± chlorite. The schist is also altered to amphibole + clinozoisite + chlorite + calcite + sphene.

Ore Zone

Scheelite mineralization is localized within the altered marble unit and is relatively continuous for at least 50 meters along strike of the marble beds (pl. 3). Scheelite-bearing skarn is also present in trenches along the strike of the marble unit to the east of the main pit and in skarn in the South pit. The possibility for more

tungsten-bearing skarn along strike and down dip in the subsurface appears high, but the lenticular nature of the marble units may be a limiting factor in the extent of skarn formation.

Geochemical analyses of rocks collected at the Spruce Hen property are listed in appendix IV, table 1. The highest tungsten values are found in skarns developed in marble, but minor tungsten is also present in the hanging and footwall endoskarns, altered felsic dikes, and quartz veins. These data agree with visual estimates of scheelite concentration made using a black light. Contacts between altered marble and schist or quartzite are well defined by the general absence of scheelite outside the altered marble unit. Most of the scheelite is evenly disseminated throughout the marble skarn with some retrograded zones containing larger scheelite grains and higher tungsten grades. Saprolitic-like zones along the strike of the marble units locally contain significant amounts of scheelite and gold (appendix IV, table 1).

Yellow Pup Property

Introduction

The Yellow Pup mine is located at the head of Yellow Pup Creek, about 0.8 km east of Gilmore Dome (fig. 2). The mine area is 0.8 km north of the granodiorite phase of the Gilmore Dome stock and 1.2 km south of another satellitic granodiorite stock on Monte Cristo and Melba Creeks. Tungsten was discovered in the Yellow Pup Creek valley in 1943 (Byers, 1957). In an attempt to prove continuity between the Yellow Pup and the Colbert property to the southeast, a number of trenches were put in between the two properties by the Bureau of Mines in 1944 (Thorne and others, 1948). They found the irregular scheelite ore zones to be erratically distributed (both horizontally

and vertically), with evidence of fault displacement in several places. The Colbert property is along strike with the same units seen in the main trench at Yellow Pup. The type of mineralization is very similar to Yellow Pup but of lesser extent. In 1957, Alaska Metals Mining Co. put in an adit to intersect at depth the extension of the Colbert ore zone. The exploratory adit runs roughly perpendicular to compositional layering and has two drifts along the strike of scheelite-bearing horizons (pl. 5). The current owner, Vince Monzulla, has taken ore out of the main trench (pl. 4), concentrated some of it in his mill and stockpiled the rest. At present, the lode mine is not in operation but instead he has a placer operation in upper Yellow Pup Creek which produces placer gold along with scheelite.

General Geology

The Yellow Pup mine area lies within the Cleary sequence (Smith and others, 1981; Robinson and others, 1982; fig. 1). The dominant lithologies, quartz mica schist and micaceous quartzite, are interlayered with a variety of felsic schists, white laminated quartzites, calcareous quartzite, marble, and minor amphibolite. In general, the units trend N 70^{O}E and dip 40^{O} N. Foliation changes within the main trench define a small antiformal structure trending approximately N 65^{O} E and flattening out to the south and with depth (pl. 4). Marble and calc-silicate marble horizons concentrated along the axis of the fold are interlayered with and flanked by feldspathic and quartz mica schist and quartzite. Schist and quartzite vary from a few centimeters to a meter in thickness, whereas the main carbonate horizon, also exposed in the underground workings beneath, is approximately 2 meters thick and contains numerous thin schist and quartzite layers. Another carbonate horizon containing interlayered marble, calc-silicate marble, calc schist, calcareous quartzite, and schist is exposed at the south end

of the adit and along the second drift (pl. 4). A massive amphibolite unit, marble and calc-silicate marble are exposed in an old Bureau of Mines trench (16) (Byers, 1957, pl. 24) south of the main trench and will be referred to as YP-B16. The thinly interlayered character of various lithologies in the mine area, significantly different from the marble at Spruce Hen, has played an important role in the ore forming process and will be discussed in more detail in the section on alteration.

Other structural features at the mine include several large fault zones and many smaller shear zones that usually parallel the foliation. Dominant joint directions are east-west and north-south ± 15 degrees. Joint planes are common sites for quartz and calcite veins and, locally, thin felsic dikes; several dikes run subparallel to the main trench fold axis and several other dikes are exposed in the adit.

Compositionally, schists contain variable amounts of quartz, biotite, white mica, feldspar, and garnet, with minor tourmaline and opaque minerals. Metamorphic garnet is often retrograded to feldspar and biotite or chlorite. Feldspathic schist (with up to 50 percent feldspar and less than 10 percent biotite) and feldspathic quartzite (less than 15 percent feldspar) are common, especially in the main trench. Quartzite also contains up to 30 percent calcite. Contact metamorphism, expressed by biotite rosettes and tourmaline crystals oriented perpendicular to foliation, are common. Marble is moderately impure with fine-grained metamorphic quartz, plagioclase, garnet, and pyroxene interstitial to the calcite matrix. Impurities account for 10 to 80 percent of the rock and represent original siliceous argillaceous dolomitic limestone. Light colored, fine-grained metamorphic calc-silicate minerals (pyroxene, garnet, epidote-clinozoisite, plagioclase) form compositional bands within the marble. There are many one centimeter to one meter wide calc-silicate marble bands exposed in the adit that pinch and swell and have isoclinally folded metamorphic calc-silicate layers (figs. 16 + 17).

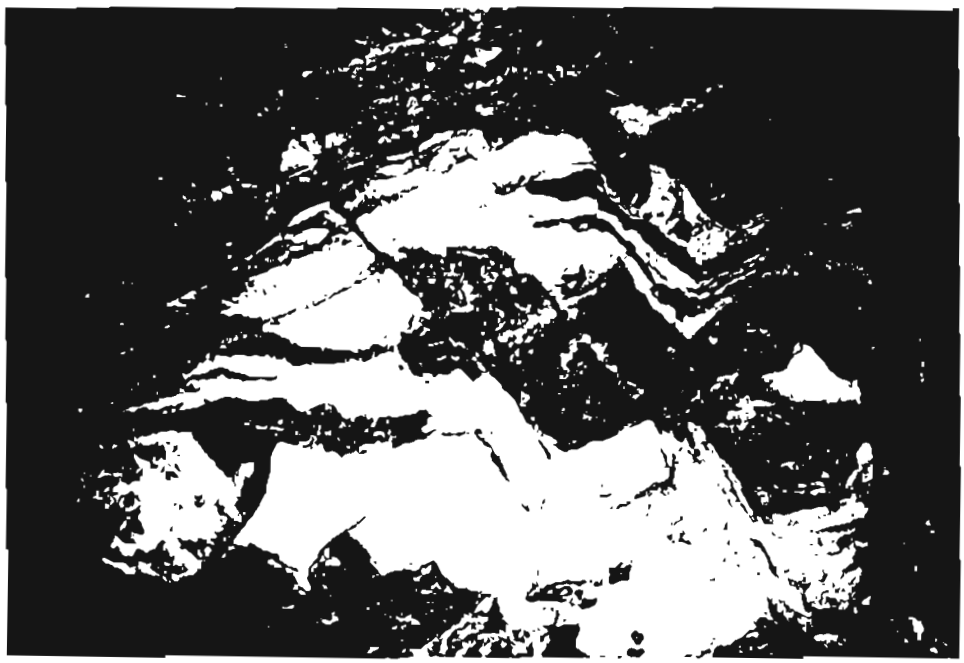

Figure 16. Light-colored, fine-grained calc-silicate marble layers interlayered in schist along the back drift, Yellow Pup adit. Large dark orange garnets (lower left) are metasomatic. Vertical dimension approximately 1 meter.

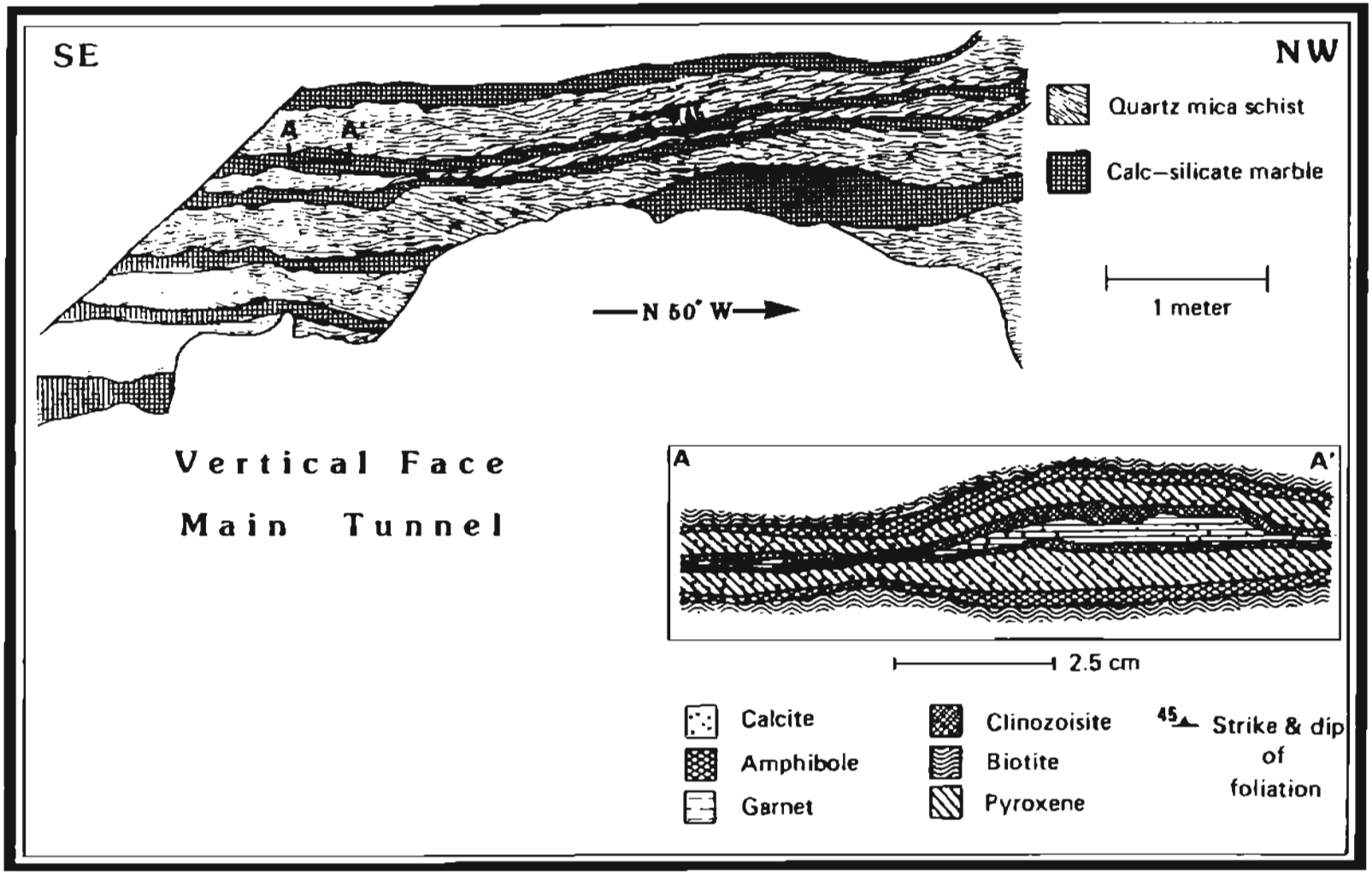

Figure 17. Map of vertical face of thin calc-silicate marble layers in schist exposed in the underground workings, main tunnel, Yellow Pup adit. Face orientation is N 50° W, layers trend approximately N 80° E dipping 45° N. Enlargement shows zoning of calc-silicate minerals in bimetasomatic layers between schist and marble.

These features presumably represent ductile deformation during regional metamorphism. Bimetasomatic layering occurs locally along the contacts between marble and schist (fig. 17).

Alteration and Mineralization

Higher grade scheelite is concentrated along the axis of the fold in the main trench (fig. 18) and in a pod-like area in the second drift underground (fig. 19); however, minor amounts of scheelite are scattered throughout the adit and general mine area (pls. 4 - 6). High grade zones occur as (1) fine-grained disseminated scheelite in the host rock (average grade 1.2 percent WO_3), (2) coarse-grained scheelite in cross-cutting quartz or calcite veins (grades up to 18.9 percent WO_3), and (3) fine- to coarse-grained stratiform scheelite (0.1 percent to 6.3 percent WO_3) within the main ore zone and emanating out from it. Scheelite in quartz veins and stratiform scheelite within thin layers several centimeters or less in thickness also occurs away from known zones of concentrated ore. These areas commonly contain less than 0.2 percent WO_3.

Accompanying the scheelite mineralization are various hydrothermal alteration effects which reflect the original rock type and the degree of exposure to hydrothermal fluids the rocks have experienced. Alteration assemblages at the Yellow Pup are more complex than those noted at the Spruce Hen property. This is due, in part, to the thinly interlayered nature of carbonate, schist, and quartzite units that experienced hydrothermal alteration and to the relatively high calcium content of many of the quartzites and schists. A distinction between early anhydrous and later hydrous alteration phases can be seen at Yellow Pup in the carbonate-rich horizons. This distinction, however, is not as easily discernible in the other altered units. Yet, from

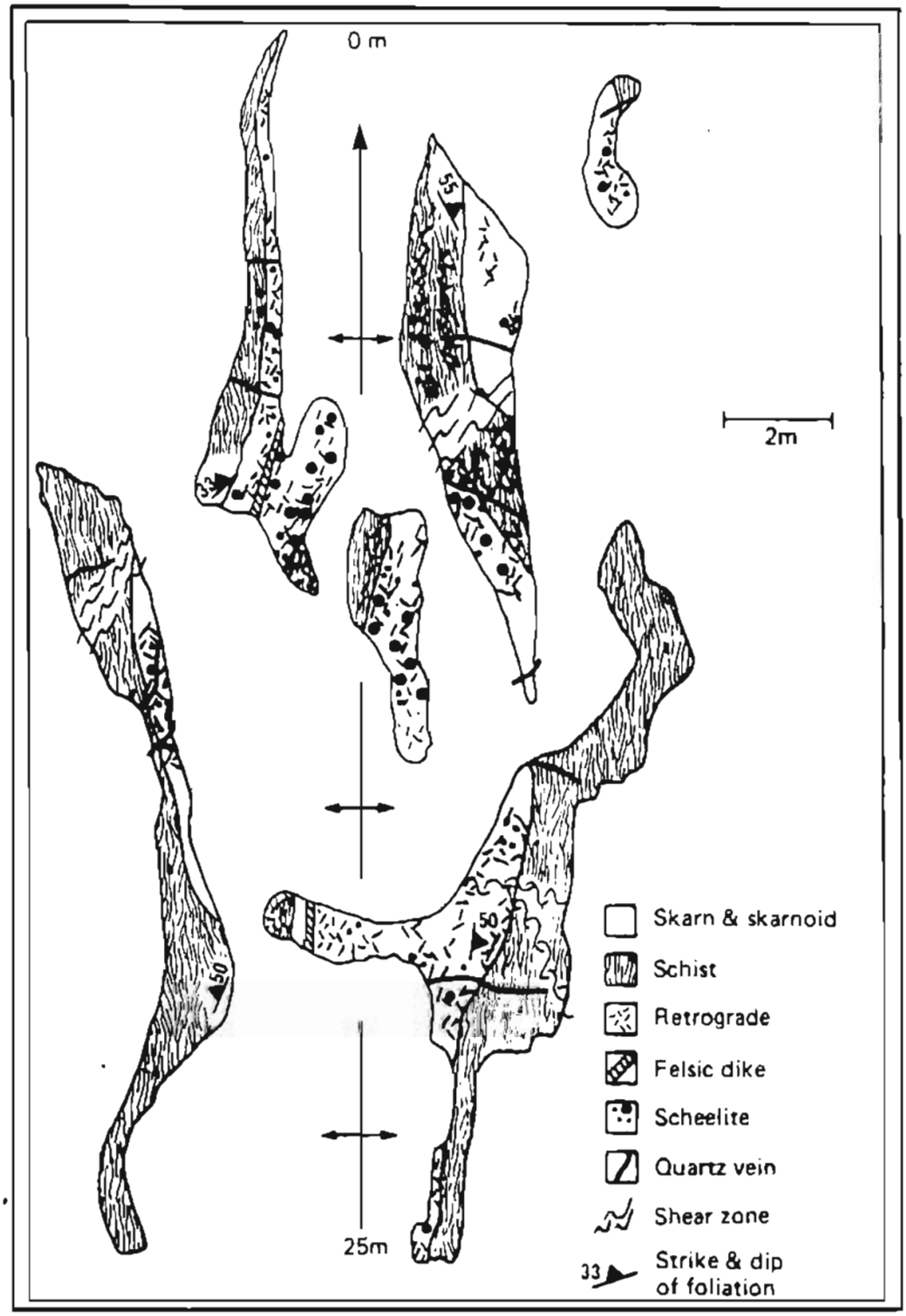

Figure 18. Generalized alteration map of the main trench at Yellow Pup. Most scheelite is localized along the axis of the antiformal structure in amphibole + calcite + quartz zones in skarnoid, skarn, and adjacent schist units.

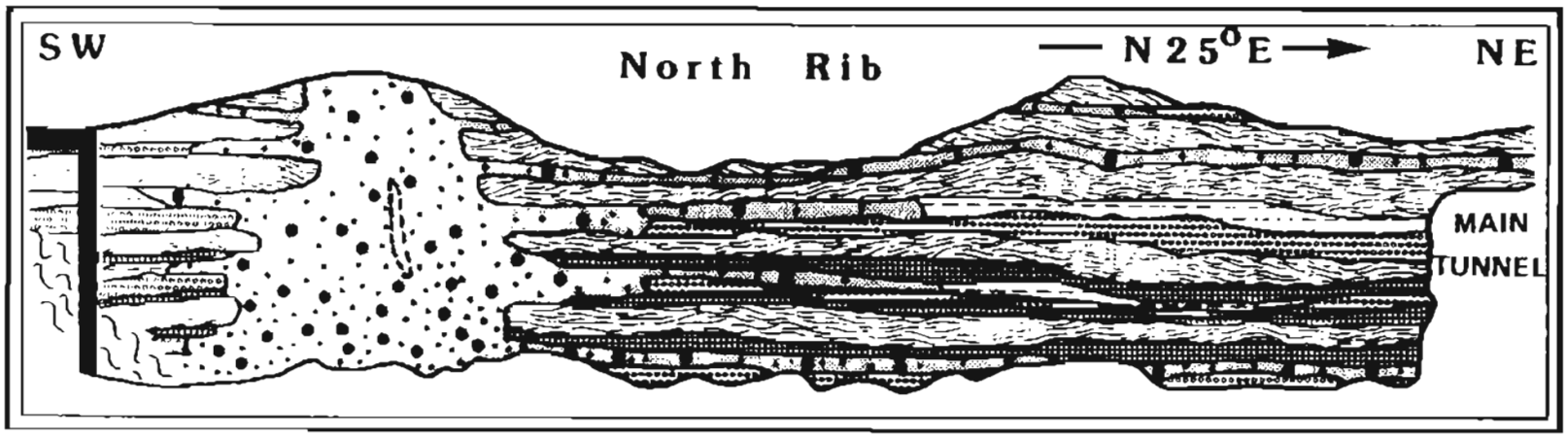

EXPLANATION

White mica, chlorite, biotite, calcite, quartz alteration

Scheelite

Calc–silicate marble

Marble

Quartzite

Schist

Altered felsite dike

Shear zone

1 meter

Figure 19. Vertical rib map of ore zone in the back drift of Yellow Pup adit. Phyllosilicate alteration and mineralization is localized in pod zone and in marble and calcareous quartzite layers extending out from the pod area. Several of the scheelite layers visibly terminate in outcrop against scheelite-free, unaltered marble and quartzite. A highly altered and difficult to trace felsic dike is present in the central part of the scheelite pod zone.

field and petrographic evidence described below, it appears likely that the hydrothermal alteration was caused dominantly by late stage hydrous fluids.

The most intense alteration is localized within two main areas, the main trench and in the rear drift of the subsurface workings (pls. 4 + 5, figs. 18 + 19). Smaller zones of alteration are present throughout the mine area. Field evidence shows the alteration to be localized along the axis of an antiform, around joints and fractures, along lithologic contacts and foliation planes, and around quartz veins and felsic dikes (fig. 20).

Exoskarn

Early Skarn Skarn is developed in numerous thin carbonate horizons in the main trench, in the adit near the entry shaft, and in massive marble in YP-B16 (pls. 4 + 5). As mentioned earlier, the carbonate contains variable amounts of metamorphic quartz, plagioclase, pyroxene, and garnet. Later, metasomatic garnet developed preferentially in quartz-bearing marble, resulting in massive garnetite with remnant metamorphic quartz. Metasomatic pyroxene or pyroxene + garnet, in contrast, occurs mostly in more calc-silicate-rich marble. Idocrase, minor wollastonite, and fluorite are present in garnet-pyroxene skarn along with small amounts of fine-grained, unembayed scheelite. Scheelite is not present in massive garnet skarn. Locally, the early skarn is banded with intermixed garnet, pyroxene $\pm$ garnet, and altered schist and quartzite layers that vary from centimeters to a meter thick, reflecting the original complexly interlayered lithologies. Textures and grain shapes of the metasomatic minerals are similar to those described at Spruce Hen though many of the individual grains are smaller in size and lighter in color (fig. 20). Although exoskarn zonation is poorly developed at Yellow Pup, in thin section a pattern can be observed along the

Figure 20. Joint controlled retrograde alteration of garnet-pyroxene skarnoid in the main trench at Yellow Pup.

contacts with other units. This is:

contact ---> garnet ---> garnet+pyroxene ---> pyroxene ---> marble.

The absence of well-developed zoning is probably due to the influence of fine layering and inhomogeneity of the host rocks, such that simple fluid compositional gradients could not be established or maintained.

Away from the main skarn zone, calc-silicate veins cut through otherwise unaltered marble; they show a zoning pattern of garnet cores with pyroxene selvages. Within the pyroxene-garnet skarn, dark orange garnet veins replace earlier formed skarn.

Late Skarn Hydrous retrograde alteration of early skarn is present along most skarn contacts and along many cross-cutting fractures (figs. 20 + 21), with as much as 40 to 50 percent replacement of early skarn by hydrous phases. Garnet is replaced by a fine-grained aggregate of clinozoisite $\pm$ calcite + quartz and pyroxene is replaced by large pseudomorphic amphibole + calcite + quartz. Sphene and apatite are nearly always present in retrograded zones. Coarse-grained aggregates of anhedral to subhedral scheelite are surrounded by randomly oriented amphibole needles, calcite, quartz, sphene, and remnant pyroxene (figs. 22 + 23). Retrograde scheelite zones form small cross-cutting, irregularly shaped to layered, higher grade zones within lower grade early skarn. Where early skarn formed in thin layers and was subsequently retrograded, scheelite grains and aggregates are concentrated in layers enriched in secondary randomly oriented amphibole $\pm$ chlorite $\pm$ clinozoisite + calcite + quartz. These layers appear fairly continuous within the main ore zone and up to tens of meters away from it, giving a stratiform appearance to the ore (fig. 24). This characteristic retrograde mineral assemblage also forms in previously unaltered carbonate layers, in which case amphibole needles either form randomly in the carbonate, along boundaries between

Figure 21. Retrograde alteration of thin garnet-pyroxene skarnoid layers in schist in the main trench at Yellow Pup.

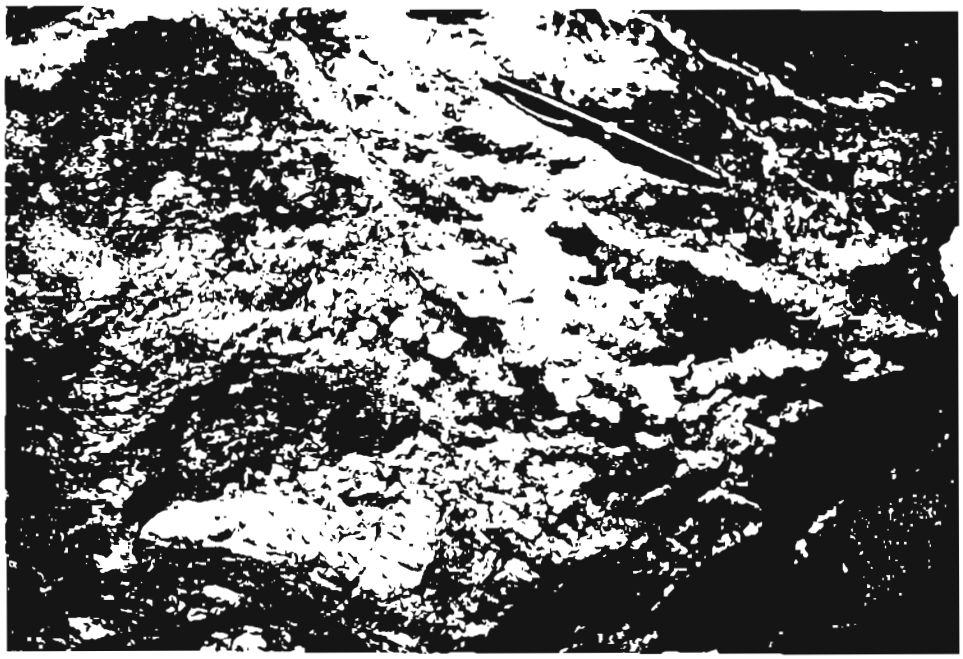

Figure 22. Large scheelite aggregates with amphibole + calcite + quartz in retrograded skarnoid and schist in the main trench at Yellow Pup.

Figure 23. Photomicrograph of retrograde alteration of skarnoid to green amphibole in thin needles and ragged masses + quartz (clear) + scheelite (high relief) from the main trench at Yellow Pup. Plain light, field of view 2.35 mm.

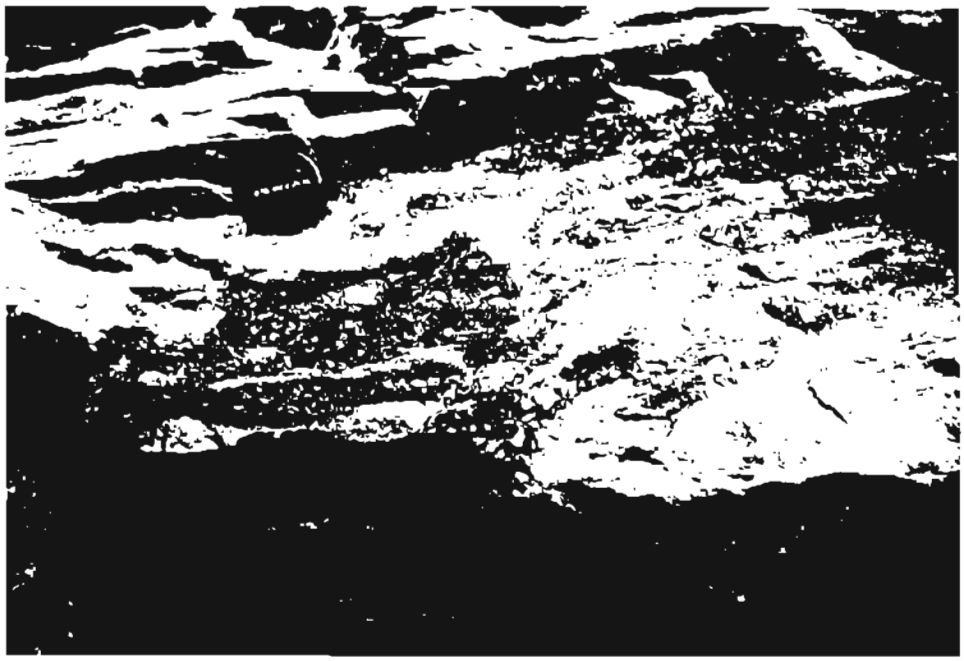

Figure 24. Thin layers of scheelite (white blebs) + amphibole + quartz + calcite (vugs created by weathering) retrograde alteration in the main trench at Yellow Pup.

calcite and metamorphic quartz grains in quartz-bearing marble, or replace metamorphic pyroxene and plagioclase in calc-silicate marble. Scheelite most typically is found as single euhedral grains within the carbonate or takes on the shape of the calcite grain being replaced. Sphene and apatite are present in appreciable amounts. Other minerals found in carbonate skarn retrograde zones are chlorite (after amphibole), fine-grained white mica (after clinozoisite and remnant metamorphic plagioclase), and iron oxides; these minerals replace anhydrous and hydrous minerals and, along with additional calcite and quartz, are the latest alteration event affecting the skarn texture.

Endoskarn and wallrock alteration

In contrast to Spruce Hen, alteration of schist and quartzite can be quite extensive whether near the main carbonate zone or in thinly interbedded intervals; this alteration can be seen in the main trench and in the rear drift underground (figs. 18 + 19). The high degree of alteration presumably is a result of numerous fluid pathways along lithologic contacts, the slight calcareous nature of many of the schists and quartzites, and the large volumes of fluid channeled through the area. The characteristic alteration mineral assemblages for the most common rock types are discussed below:

Feldspathic schist

feldspar (plagioclase) ---> clinozoisite, pyroxene

biotite ---> amphibole

feldspar + biotite ---> pyroxene

feldspar ---> fine-grained white mica ± calcite

feldspar ---> chlorite

Most feldspathic schist shows alteration to clinozoisite; however, adjacent to pyroxene-garnet skarn, thin layers of feldspathic schist have altered to pyroxene. Pyroxene, in turn, has retrograded to amphibole with remaining feldspar altered to fine-grained white mica. Whether the clinozoisite and white mica are entirely early or late stage phases is unclear; in general, white mica is associated with other retrograde minerals.

Quartz mica schist

biotite ---> amphibole or chlorite

white mica ---> fine-grained white mica

feldspar ---> clinozoisite, fine-grained white mica, or amphibole

garnet ---> chlorite, clinozoisite, sphene,

The reactivity of the quartz mica schist units appears dependent on the amount of plagioclase present and the proximity to carbonate horizons. This rock type is generally not as altered as feldspathic schist, although near and within the high grade mineralized zone in the rear drift of the adit, garnetiferous quartz mica schist is totally altered to calcite + coarse-grained white mica + chlorite + quartz + sphene + apatite + scheelite.

Feldspathic quartzite

feldspar ---> clinozoisite, fine-grained white mica, or garnet

Clinozoisite is the predominant alteration mineral in feldspathic quartzite. Garnet forms only in minor amounts along the contacts with carbonate skarns whereas, clinozoisite alteration extends further into the unit. Adjacent to carbonate skarn, pyroxene,

clinozoisite, and minor garnet are present. Complete replacement of feldspar by fine-grained white mica is more characteristic of the alteration seen underground in the rear drift.

Calcareous quartzite

calcite ---> garnet

calcite ---> fine-grained white mica, amphibole, pyroxene, chlorite, sphene, scheelite

A continuum of composition probably exists between calcareous quartzite and quartzose marble units. Garnet is present mainly in the carbonate skarn zone in the main trench and in the adit near the shaft. Underground in the rear drift (fig. 19), however, thin calcareous quartzite horizons contain significant amounts of large vermicular scheelite grains and aggregates along with white mica and chlorite - all replacements of calcite (fig. 25). Scheelite in these layers can be traced for at least 12 meters away from the main high grade zone.

Felsic Dike

feldspar ---> white mica, chlorite, biotite, quartz, calcite, sphene, apatite, scheelite

There are several dikes composed of quartz, plagioclase, and alkali feldspar within the mine area. At least two occur in the main trench area and are subparallel to the length of the trench. Several other dikes are exposed underground one of them is in the high grade pod. The dikes are not easily distinguished in hand sample from other altered rocks. In thin section, however, they show igneous textures such as interlocking equigranular grains, well developed plagioclase twinning, and lack of foliation. These dikes also have experienced alteration to various degrees. The characteristic alteration

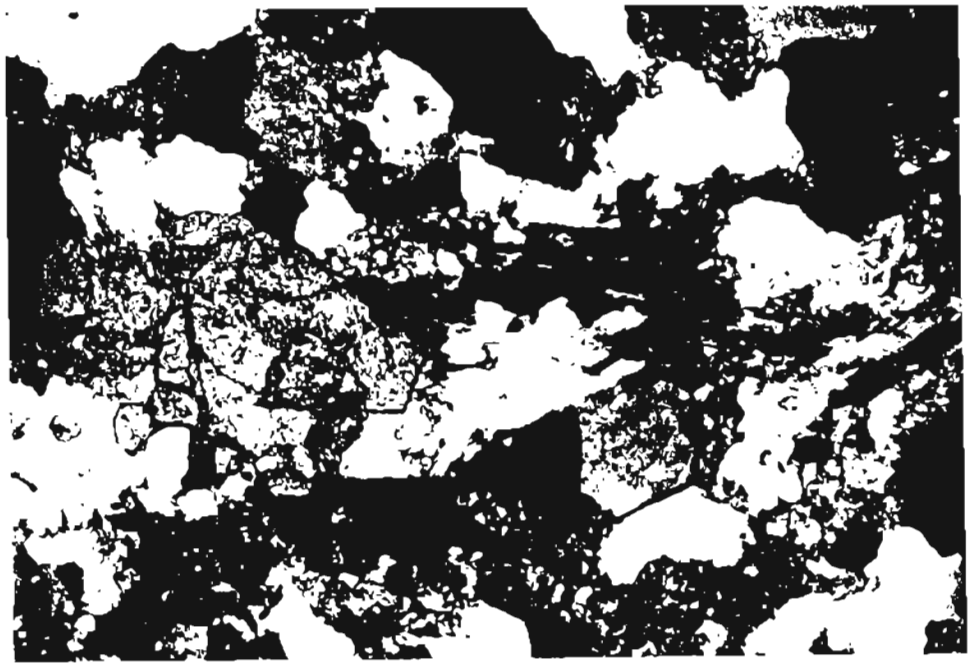

Figure 25. Photomicrograph of scheelite (yellow) + white mica (irregular masses) + amphibole (blades) + quartz + sphene (high relief) alteration in calcareous quartzite, Yellow Pup. Cross polars, field of view 2.35 mm.

assemblage is coarse-grained white mica + chlorite + biotite + calcite + quartz + sphene + apatite ± scheelite. Pyroxene and amphibole occur as replacement minerals near contacts with pyroxene-garnet skarn. Within the dikes scheelite forms fine- to coarse-grained, subhedral crystals and aggregates surrounded by white mica, chlorite, and plagioclase.

Timing of the scheelite mineralization in the dikes is unclear. However, where the dikes are in contact with garnet-pyroxene skarn, most of the scheelite appears to be associated with the later retrograding event. It is interesting to note in comparing the felsic dikes with the feldspathic schists, that little if any clinozoisite is present in the dikes and no scheelite is present in the unaltered schist.

The alteration assemblages listed above are generalized patterns. It is apparent that some alteration occurred early and some late in the skarn-forming system but details of the timing are largely indeterminate. In many instances zoning in altered schist and quartzite is present along the contact with calcareous units and along quartz veins. This zoning is:

pyroxene ± garnet ± clinozoisite	---->	amphibole + clinozoisite	---->	clinozoisite + chlorite	---->	clinozoisite + biotite

Pyroxene and garnet are subordinate to the more hydrous phases in most cases. This suggests the majority of fluids passing through the Yellow Pup area were of lower temperature than those present at Spruce Hen. The consistent association of scheelite ± sphene and apatite with other alteration phases implies that these minerals were metasomatically introduced into the rock units rather than being present as original constituents. The high degree of alteration present at Yellow Pup suggests significant quantities of hydrothermal fluid passed through the rocks in the mine area.

Ore Zones

Scheelite is concentrated in two main zones at the Yellow Pup: the main trench and underground in the rear drift (pls. 4 - 6). Both areas are within stratigraphic horizons that have appreciable carbonate material. The main trench ore zone includes garnet-pyroxene skarn, wallrock alteration and endoskarn, felsic dike alteration, and retrograde alteration of earlier formed minerals. Most scheelite is within both early and late stage carbonate skarn, but some is found also in altered calcareous quartzite and schist, quartz veins, and in altered felsic dikes.

At the ore zone underground in the rear drift, on the other hand, there is a distinct lack of garnet or pyroxene. Instead, the alteration assemblage present is coarse-grained white mica + chlorite + biotite + calcite + quartz + apatite + sphene $\pm$ scheelite (fig. 26). The ore zone in the drift is a pod-shaped area 3 meters in diameter that cuts vertically through compositional layering (fig. 19). Thin marble layers and calcareous quartzite are present in the ore zone, but the dominant lithology is garnetiferous feldspathic quartz biotite schist. Scheelite, concentrated in calcareous quartzite layers around the pod-like ore zone, gives a stratiform appearance to the ore. In these layers scheelite decreases in size and abundance with increasing distance from the ore zone. The conduit for the fluids is not clearly evident in the drift exposures, but the alteration and morphology of the zone suggest a cross-cutting felsic dike could have channeled the fluids into this zone. Petrographic study of highly altered rock in the mineralized zone confirms that an igneous dike was originally present.

Tungsten values are highest in the pod-like zone underground and in retrograded skarn but locally are also quite high in quartz veins (appendix IV). Scheelite is absent or present only in minor amounts in the garnet-rich skarn zone formed from calc-silicate marble in the main trench. Quartz veins also contain some

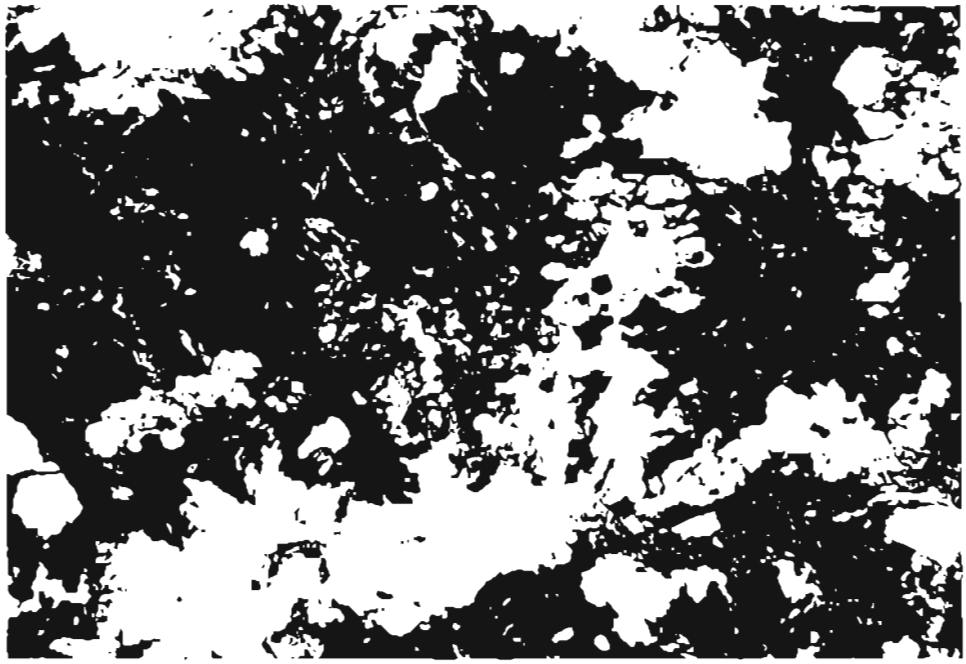

Figure 26. Photomicrograph of scheelite aggregate (grey, high relief) in white mica (highly birefringent fan) + chlorite (blue) + biotite (brown) + calcite alteration in pod-shaped ore zone in back drift of Yellow Pup adit. Cross polars, field of view 3.5 mm.

gold and silver. One pyrite- and stibnite-bearing vein underground also contains elevated concentrations of base metals.

In summary, scheelite at the Yellow Pup deposit is always accompanied by distinctive alteration mineral assemblages. These assemblages reflect the original host rock composition and the chemical properties of the hydrothermal fluids. In no instances was scheelite noted in a rock that did not show signs of hydrothermal alteration. Therefore, even though the scheelite may, in places, be stratiform in appearance, the origin of the scheelite is clearly epigenetic.

Ore grade scheelite zones at the Yellow Pup property are the result of hydrothermal fluids reacting with appropriate host rocks along structural conduits. Based on the extent of alteration in the mine area and the presence of several calcareous layers in the stratigraphic section, it appears likely that additional scheelite-bearing zones may be present. Additional ore zones will most likely occur near the intersection of calcareous horizons with faults, fractures, and dikes that have acted as fluid conduits. Thus, expected distribution of scheelite would be in pipe- or pod-like concentrations with some concentration in favorable beds around the fluid conduits.

Gil Property

Introduction

The Gil claim block staked by Resource Associates of Alaska (RAA) in 1981 is located four kilometers northeast of the Yellow Pup property (fig. 2). During the summer of 1982, RAA put in several north-south trending trenches that exposed 835 meters of continuous bedrock, creating some of the best exposure in the area. The

stratigraphic units trend from N. 45° E. to N. 60° E. and dip approximately 60° NW. The trenches cross-cut stratigraphy and expose approximately 525 meters of stratigraphic section.

General Geology

The rock sequence exposed along the trenches at Gil appears to include the Fairbanks schist and the Cleary sequence of Smith and others (1981) and Robinson and others (1982) (fig. 1). The Fairbanks schist occurs in the southern end of the trench (pl. 7, fig. 4) comprising about 150 to 200 stratigraphic meters. Overlying this is the Cleary sequence, totaling 280 to 300 meters, with Fairbanks schist above it at the northernmost section of trench. There is a possibility of structural thickening (Mark Hall, pers. comm.) or thinning as several large fault zones are present. The general geology of the trenches is discussed in the earlier section on regional geology.

Alteration and Mineralization

There is abundant evidence for hydrothermal alteration of the various units throughout the trench exposure. Marble horizons show the most intense alteration and contain most of the scheelite mineralization. Petrographic examination has shown that the amphibolite, quartzite, and schist units locally were also affected by altering hydrothermal fluids. This alteration ranges from thin selvages bordering quartz veins to larger zones of recrystallization or replacement. Most alteration appears to be localized near large quartz veins or shear zones and along foliation planes or lithologic contacts. Some of the altered metamorphic rocks also contain minor scheelite. It is important to note the restriction of scheelite to altered host rocks and the localization of the scheelite

in and near cross-cutting structural features. Alteration of the various units will be discussed below.

Exoskarn

Marble units at Gil have in part been altered to calc-silicate skarn. These skarns bear little resemblance to those seen at the Spruce Hen property, and in some cases are difficult to distinguish in hand specimen from dark green massive amphibolite. In comparison with the Spruce Hen, the most striking features of the skarns at Gil are the presence of large scheelite-bearing quartz veins that cut through the skarns (fig. 27), the lack of garnet, the abundance of quartz, and the very large elongate pyroxenes that resemble amphiboles in hand specimen. Early anhydrous and late hydrous mineral phases are both present at Gil, but their variety and abundance differ significantly from the Spruce Hen skarns.

Early Skarn Pyroxene is the dominant early anhydrous calc-silicate mineral in all the skarns at Gil. Grains are euhedral, extremely elongate (up to 1.0 cm), commonly twinned, light green, and slightly pleochroic (fig. 28). In contrast with metamorphic pyroxenes in the marble, the metasomatic pyroxenes are larger, more euhedral, and more iron-rich (as indicated by darker color and larger extinction angle). The unusually elongate morphology of the metasomatic pyroxenes has led to their mistaken identity as amphiboles in hand specimens.

Quartz, scheelite, and minor idocrase are also present with metasomatic pyroxene. Quartz accounts for up to 40 percent of the rock whereas idocrase, if present, forms less than 5 percent. Scheelite occurs as large (up to 1.0 cm diameter) anhedral to subhedral crystals and crystal aggregates. Remnant metamorphic

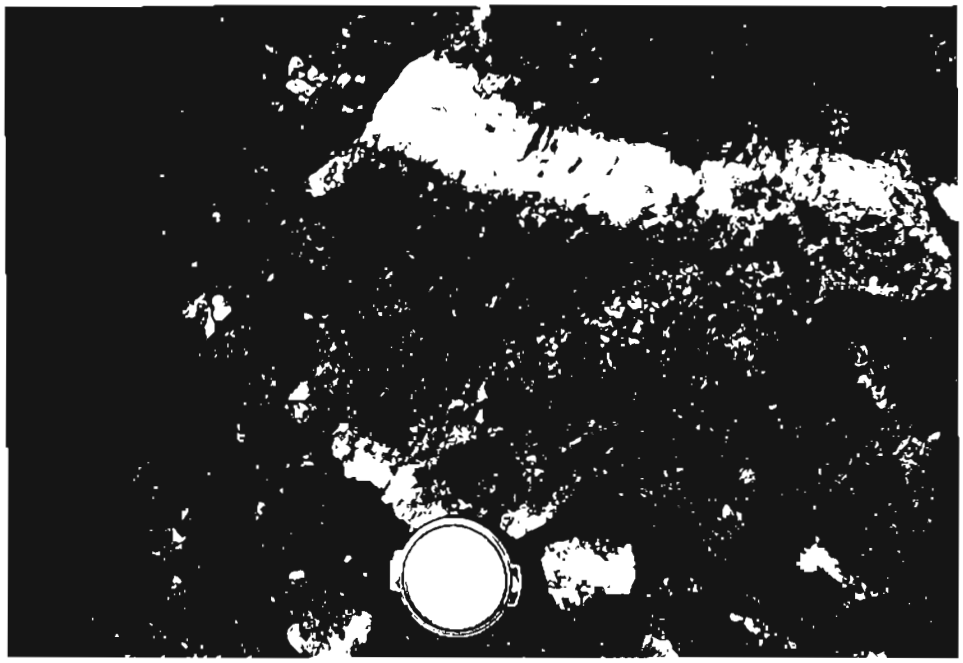

Figure 27. Quartz-cored pyroxene-scheelite high grade skarn at the Gil trenches.

Figure 28. Photomicrograph of large elongate pyroxene (blue, yellow) in skarn partially replaced by calcite + quartz + amphibole (dark blebs) at Gil. Cross polars, field of view 3.5 mm.

plagioclase, pyroxene, calcite, and quartz are variously present in some skarns, reflecting a range of composition in the impure marble protoliths.

Several of the skarns have the morphology of veins within the marble units (fig. 27). Skarn veins are cored by massive quartz with a pyroxene selvage, resulting in a zoning pattern of:

marble	<---	pyroxene + quartz + scheelite	<---	quartz	--->	pyroxene + quartz + scheelite. ---> marble

Scheelite-bearing, quartz-pyroxene veins in the marble can be traced into adjacent footwall schist where they are noticeably thinner, generally barren of scheelite, and lack wide pyroxene selvages. Smaller veins of quartz + pyroxene + calcite ± scheelite are common in marble units as well as in more siliceous units near marbles. These veins are crudely zoned with quartz ± calcite centers flanked by borders containing large euhedral pyroxene. Scheelite, where present, forms large (1.0 cm) euhedral crystals growing from the edge of the vein toward the center. Thin clinozoisite ± pyroxene selvages are present along veins within calcareous host rocks, whereas bleached selvages are often present surrounding veins in micaceous quartzite and schist.

Late Skarn Pyroxene destruction is common in skarn zones with retrograde replacement by quartz + amphibole + calcite ± chlorite. Quartz is usually the dominant replacement mineral (up to 60 percent of rock); amphibole (0-30 percent) is of lesser concentration. This results in sieve-textured amphibole pseudomorphs of pyroxene in a quartz groundmass where the quartz forms large (5 - 10 mm) grains with undulatory extinction, and amphibole forms thin needles or diamond shaped grains. Other minerals found in retrograded skarn are calcite, iron oxide, and clinozoisite. Retrograde zones

have a distinct lack of scheelite or have very high grades (up to 15 percent) of large scheelite aggregates intergrown with amphibole and quartz.

Endoskarn and vein alteration

Minor scheelite is present in micaceous quartzite layers where it is localized within or adjacent to quartz, quartz-pyroxene, or quartz-calcite veins (fig. 29). Alteration assemblages and mineral textures at Gil are similar to those in the quartzite and schist endoskarn at the Yellow Pup property, except that pyroxene is the dominant alteration phase present. Alteration consists of pyroxene replacement of plagioclase or calcite along vein selvages and foliation planes, with secondary clinozoisite, amphibole, fine-grained white mica, calcite, and sphene. Scheelite is irregularly shaped, of varying size and often encloses quartz, calcite, and fine-grained white mica. Scheelite-bearing endoskarn is formed in a quartzite in close proximity to a pyroxene skarn in marble. Endoskarn is along one of the quartz veins that core the pyroxene skarn (pl. 7, inset). All of the quartz-rich scheelite-bearing rocks examined at Gil show evidence that the scheelite was secondary in origin.

Petrographic study of the amphibolite units has revealed areas of recrystallization or alteration. These areas contain tiny amphibole needles at the edges of larger randomly oriented amphiboles and at angles to foliation in schistose units, epidote replacing amphibole, and concentrations of calcite, quartz, sphene, and opaque phases (fig. 30). Sphene often forms rims around ilmenite. The altered areas are found in the nonfoliated massively textured amphibolite which in some cases is surrounded by well foliated amphibolite schist (fig. 31). The massive character appears to be the result of recrystallization during or after regional metamorphism. Numerous calcite stringers and vuggy areas filled by calcite, quartz, and tiny needle-like amphibole grains are also

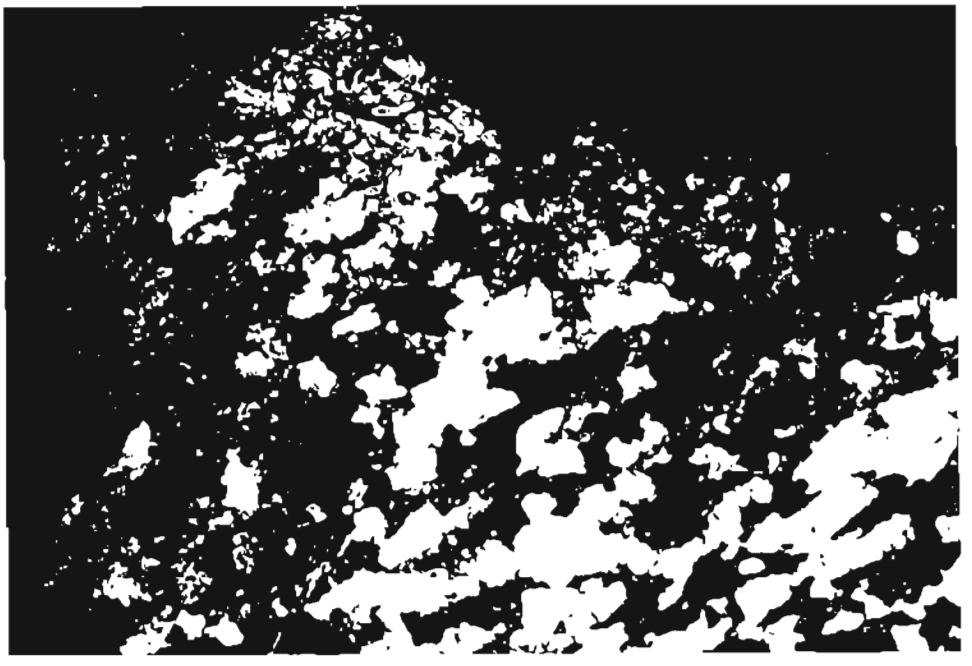

Figure 29. Photomicrograph of pyroxene endoskarn selvage in micaceous quartzite along edge of quartz vein. Scheelite (euhedral, brown, right side) and pyroxene (euhedral, light brown) grew along edge into the quartz vein (grey). Small pyroxene replace feldspar in quartzite. Cross polars, field of view 3.3 mm.

Figure 30. Photomicrograph of altered amphibolite. Amphibole needles (upper left) + quartz replace larger amphiboles (yellow to grey, lower right). Cross polars, field of view 1.25 mm.

Figure 31. Well foliated, relatively unaltered amphibolite with amphibole and minor epidote and sphene. Gil trenches, cross polars, field of view 2.35 mm.

common in the massive amphibolites. Scheelite was observed in one such area where petrographic examination revealed the scheelite to be in a quartz-rich groundmass with only remnant amphibole and chlorite. A possible explanation for the alteration is a wide shear zone a few meters away. Where a 2 cm wide quartz vein cuts through amphibolite, some amphiboles are larger in size and not foliated and there are a number of calcite stringers present. Scheelite in amphibolite was noted in the vicinity of the quartz vein. Analysis of the vein revealed it contained 1.8 ppm Au and 2 percent WO_3. Nowhere at Gil was scheelite observed in well foliated, unaltered amphibolite.

Another example of alteration of amphibolite can be seen in rocks from the ore dump next to a shaft at Stepovich. Amphibole + fine-grained plagioclase + ilmenite surrounded by sphene is altered to veins of coarse-grained pyroxene + plagioclase with centers of large bladed ilmenite. Joesting (1942) described a massive amphibolite unit directly below the ore horizon which probably is where this rock came from.

Ore Zones

Most of the scheelite and all of the higher grade scheelite at Gil is within the carbonate skarns. The width of the skarn zones range from a few centimeters to several meters thick. The extent of skarn formation is a function of the marble thickness and the amount of metasomatic fluid available to form the skarn minerals. The highest grades of scheelite are found in the thickest marble units that are cored by quartz veins. These skarns vary from 0.3 meters to 2.0 meters wide in the trench exposures, with average grades of 1.2 to 3.0 percent WO_3 (appendix IV, table 5). The lateral and downdip extent of skarn bodies is unknown, however the importance of veins in controlling development of the highest grade skarns suggest that the skarns at Gil may be discontinuous and sporadic, although the abundance of veins and alteration present

suggests mineralization of favorable marble horizons away from the trench is also quite likely.

There is a high density of large continuous quartz veins in the northern section of the trench where the Cleary sequence is exposed. The dominant orientations of the veins, including those in skarn are N. 15 - 25^{o} E., N. 25 - 30^{o} W. Thin irregular discontinuous veins parallel to foliation (N. 45 - 60^{o} E) are also present. Some of the larger veins veins are auriferous and argentiferous, and, in a few cases, the veins also contain significant amounts of tungsten. Skarns cored by quartz do not appear to contain gold or appreciable silver.

MINERAL COMPOSITIONS

Minerals selected as examples of the various rock and alteration types from the three prospects discussed as well as others from the Gilmore Dome area were analysed by electron microprobe techniques. The procedures for and representative examples of 309 analyses are given in appendix II. Electron microprobe analysis was used to establish compositions for metamorphic versus metasomatic minerals, to show zonation within a mineral, and to compare compositions with other tungsten skarns worldwide. Minerals analysed were garnet, pyroxene, amphibole, white mica, chlorite, biotite.

Garnet

Gilmore Dome garnet compositions are expressed as the three endmembers Grossularite (Gr) $Ca_3Al_2(SiO_4)$, Andradite (Ad) $Ca_3Fe_2(SiO_4)$, and Spessartine (Sp) $Mn_3Fe_2(SiO_4)_3$ + Almandine (Alm) $Fe_3Al_2(SiO_4)_3$ (fig. 32). The garnets display a wide range in composition and have been put into fields based upon petrographic and compositional data.

Metamorphic garnets in calc-silicate marble with compositions in the range of $Gr_{82-89}Ad_{9-14}Alm+Sp_{1-4}$ are light pink, fine-grained, and often present in layers which mimic sedimentary layering (figs. 16 + 17). In rocks where there has apparently been little introduction of fluids, compositions are more aluminous (Gr_{85-89}). Some calc-silicate rocks have garnets that are coarser-grained with core compositions of Gr_{85-89} and rims of Gr_{82} (figs. 20 + 21). These rocks, termed skarnoid by Zharikov (1970), have experienced some fluid metasomatism but they are predominantly metamorphic in origin.

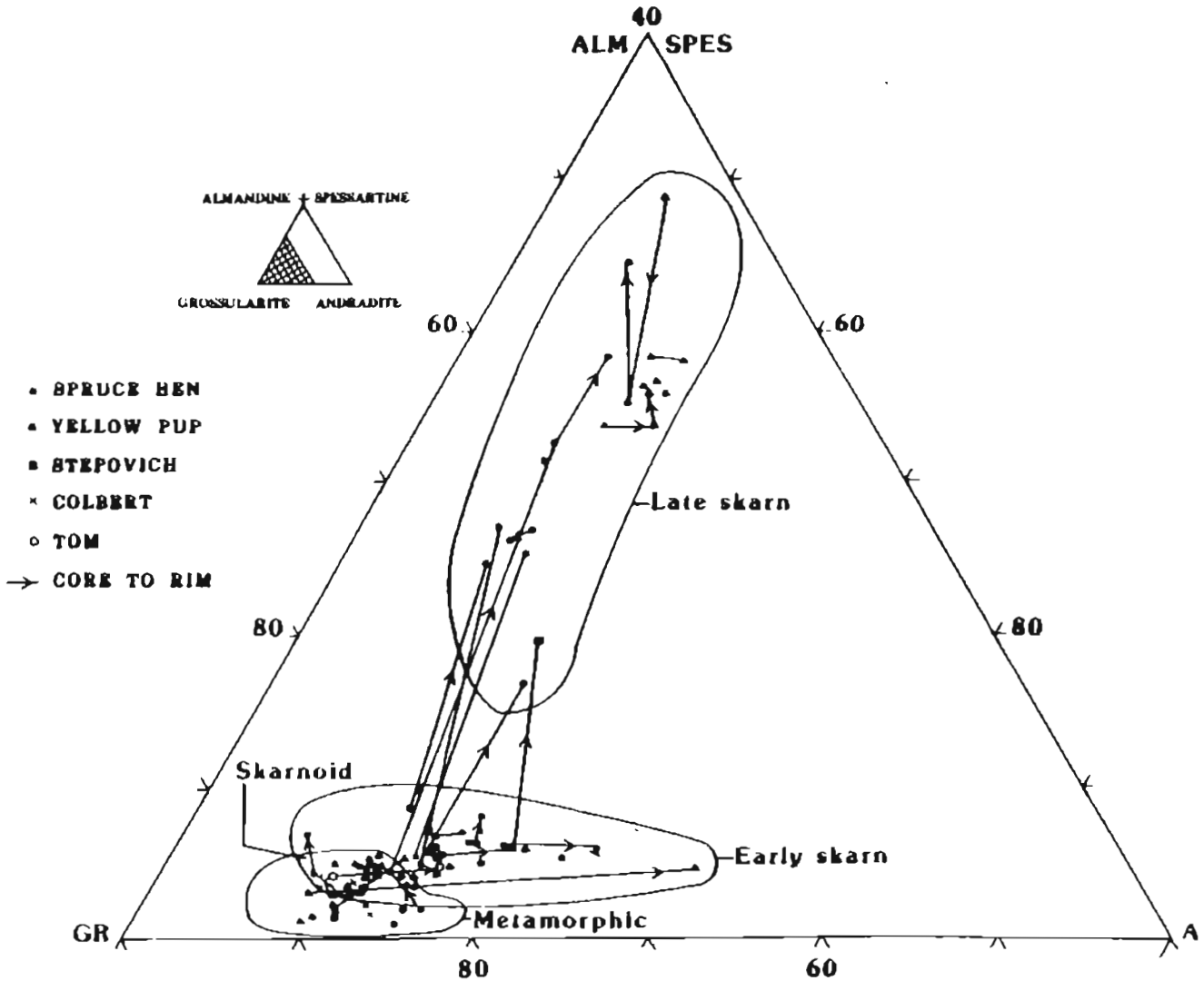

Figure 32. Compositions of garnets from Gilmore Dome.

Metamorphic garnets are also found as cores to garnets in exoskarn. In figure 32, core to rim compositions are connected by a line, the arrow pointing towards the rim composition. Early skarn garnets have compositions of $Gr_{65-81}Ad_{12-20}Alm+Sp_{3-10}$ with an average composition of $Gr_{79}Ad_{16}Alm+Sp_5$. Skarn garnets are higher in Fe^{3+} and Mn than metamorphic garnets although there is some overlap. Metasomatic zoning is common with rims generally enriched in Fe^{3+}. Early skarn garnets, ranging in color from orange to dark red and brown, are generally isotropic. At Spruce Hen the garnets are present in pyroxene-garnet skarn and as garnet veins in pyroxene dominant skarn (figs. 7 - 9). Their compositions are generally more andraditic than Yellow Pup garnets from the main trench. Most of the main trench garnets are of the skarnoid type. Garnets formed in marble in trench YP-B16 had rim compositions that were slightly more andraditic than at Spruce Hen. Also characteristic of Yellow Pup is a 3 cm thick predominantly unaltered marble layer within schist that contains both small pink garnets (Gr_{85}) and larger brown garnets (Gr_{79}) within millimeters of each other. In the rear drift of the adit, relatively unaltered marble with calc-silicate layers has small pods and bands of large dark orange garnets with compositions of $Gr_{77}Ad_{11}Alm+Sp_{10}$ (fig. 16).

Both Spruce Hen and Yellow Pup have late stage subcalcic garnets similar to those described by Newberry (1983). These garnets are darker in color, zoned, anisotropic to isotropic, and rim earlier formed garnet (fig. 11). They often have euhedral faces formed in vugs or in quartz or calcite.

At Spruce Hen subcalcic garnets are found as selvages on barren quartz veins, as zones along metamorphic idocrase bands, as centers of earlier formed garnet-pyroxene veins in marble, and as garnet veins in pyroxene garnet skarn. Much of the deposition of subcalcic garnet was along the same fluid pathways of early skarn. Subcalcic garnet formation was after the main pyroxene garnet skarn event but prior to retrograding.

Late stage garnets ($Gr_{59-68}Ad_{8-14}Alm+Sp_{3-17}$ with an average of $Gr_{65}Ad_{10}Alm_{20}Sp_5$) are enriched in Fe^{2+} and Mn with a Fe^{2+}/Mn (Alm/Sp) ratio of 4.

At Spruce Hen and Yellow Pup subcalcic garnet is associated with abundant fluorite, but fluorite is not ubiquitously found with subcalcic garnet.

Late garnets at Yellow Pup are found in the banded skarn zone near the shaft in the adit (pl. 5). Barren bands (4mm wide) of massive garnitite with remnant quartz ($Gr_{45-50}Ad_{6-13}Alm+Sp_{32-47}$) alternate with pyroxene-garnet endoskarn in narrow schist layers. The average composition of subcalcic garnet at Yellow Pup is $Gr_{51}Ad_{11}Alm_{26}Sp_{11}$ with an Fe^{2+}/Mn ratio of 2.4. The garnets are more enriched in Mn relative to Fe^{2+} than those at the Spruce Hen.

Pyroxene

Clinopyroxene compositions are based on mole percent Diopside (Di) $CaMgSi_2O_6$, Hedenbergite (Hd) $CaFeSi_2O_6$, and Johannsenite (Jo) $CaMnSi_2O_6$. Gilmore Dome pyroxene compositions, like garnets, vary with the type of rock and alteration present (fig. 33). Metamorphic pyroxenes in calc-silicate marble have compositions of $Hd_{36-46}Di_{50-60}Jo_{1-5}$. These salitic pyroxenes are light green, fine-grained and associated with metamorphic garnet (fig. 17). One sample from Yellow Pup that showed no signs of alteration had salitic pyroxene ($Hd_{36}Di_{60}Jo_4$) with grossularitic garnet ($Gr_{88}Ad_{10}Alm+Sp_2$). At Gil, fine-grained semi-foliated pyroxene in a siliceous dolomitic marble have compositions of $Hd_{50-55}Di_{42-48}Jo_{1-3}$. The sample is cut by a pyroxene skarn vein which may have affected the composition. Range of compositions for metamorphic pyroxene at Gilmore Dome falls predominantly into the skarnoid range for tungsten skarns in the Sierra Nevada (Newberry, 1980), and reflects, in part, the original composition of the impure marbles.

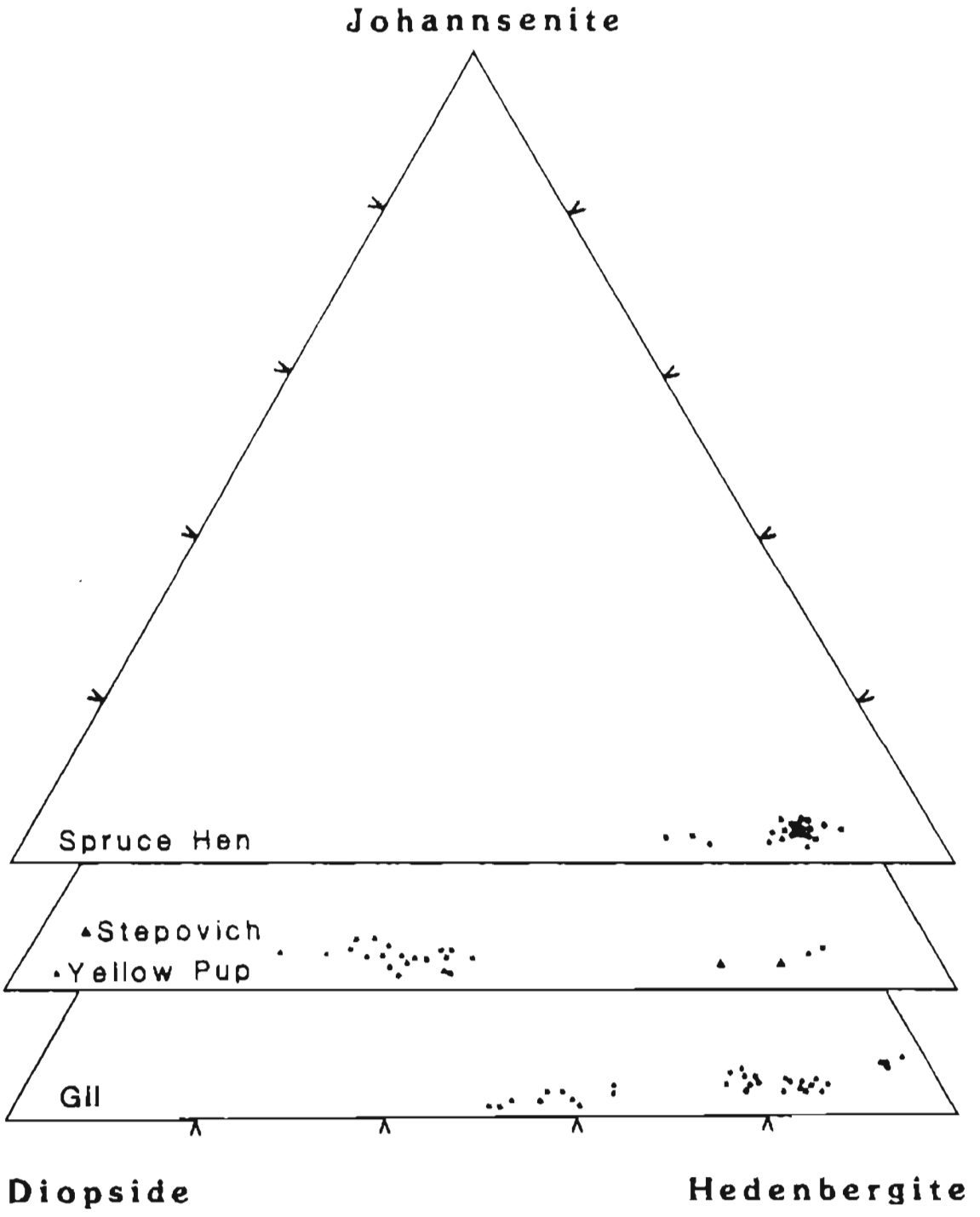

Figure 33. Compositions of pyroxenes from Gilmore Dome.

Pyroxenes in exoskarn have considerably more Fe^{2+}, are coarser-grained, and darker in color than metamorphic pyroxene. Hedenbergitic pyroxenes are common at Spruce Hen and Gil but rare at Yellow Pup except for pyroxenes from YP-B16, which are slightly more hedenbergitic than those at Spruce Hen. Pyroxene at Spruce Hen ($Hd_{78-85}Di_{10-18}Jo_{2-6}$) (fig. 10) shows slight core to rim zoning of Hd_{81} to Hd_{78} or Hd_{81} to Hd_{83}. Several pyroxenes have less hedenbergitic compositions ($Hd_{68-72}Di_{25-29}Jo_{3-4}$) and may be recrystallized metamorphic pyroxene (skarnoid). Pyroxenes associated with scheelite have compositions of $Hd_{79-82}Di_{13-17}Jo_{3-4}$.

Vein-controlled skarns at Gil have a wider range of compositions than those seen at Spruce Hen. In one example, pyroxene ($Hd_{80-81}Di_{14-15}Jo_{4-5}$) skarn formed in quartz-bearing marble is cut by a quartz-pyroxene vein. Skarn pyroxenes near the vein become more diopsidic along their rims. Within the vein, pyroxene along the edge are $Hd_{51-62}Di_{35-47}Jo_{2-3}$ but in the center of the vein the compositions are back to $Hd_{82-84}Di_{13-14}Jo_{3-5}$. At the highest grade skarn, pyroxene ($Hd_{89}Di_{4}Jo_{7}$) next to the quartz core is more Fe^{2+} and Mn enriched than pyroxene ($Hd_{77}Di_{20}Jo_{3}$) at the skarn/marble contact (fig. 27). Core pyroxenes are the most hedenbergitic for Gilmore Dome. The variability of compositions at Gil may reflect the degree to which fluids have interacted with country rocks. A crude trend is towards more hedenbergitic pyroxene closer to the fluid source within a given skarn prospect.

Pyroxenes are also present in endoskarn. At Yellow Pup large Mn enriched pyroxene ($Hd_{32-40}Di_{55-63}Jo_{4-8}$) associated with subcalcic garnet replace schist layers. At other localities, endoskarn pyroxenes associated with amphibole, biotite, and plagioclase are slightly more iron-rich ($Hd_{40-47}Di_{48-58}Jo_{1-4}$).

Amphibole

Amphiboles occur in both metamorphic and altered rocks. Figure 34 shows amphibole compositions plotted as a function of Si, Mg/Fe_{total}+Mn+Mg, and total alkalies, and by type of occurrence (after Leake, 1978). Massive amphibolite, rocks from thick mafic units of basaltic composition, are primarily tschermakitic hornblende and magnesio-hornblende (fig. 31). Some amphiboles are zoned with rims higher in Si, Ca, and Mg and lower in Al and Fe. This is shown on figure 34 where one rock contains points 1 through 5 with point 1 the core and point 2 the rim. Secondary needles around larger amphiboles are more Al-poor actinolitic hornblende and actinolite (pt. 3) (fig. 30). In some cases alteration of amphibolite was accompanied by scheelite deposition (pts. 4 + 5). In general, amphiboles associated with scheelite in mafic units are higher in Fe and Si and lower in Mg and Al than in the surrounding host. Amphiboles that showed abundant secondary needles corresponded to zones in mafic units that were nonfoliated and had an abundance of quartz and calcite veining. Well foliated mafic schists also show some zoning toward more actinolitic rims (pts. 6 + 7).

Amphiboles formed in pyroxene skarn during the retrograde event (fig. 13) are the lowest in Mg of all the amphiboles analysed. Most retrograde amphiboles at Spruce Hen and Gil are hastingsitic hornblende (pts. 8, 9, + 10). Actinolite is found in strongly retrograded skarn associated with quartz and scheelite at Spruce Hen (pt. 11). Retrograde alteration of pyroxene $\pm$ garnet endoskarn at Yellow Pup produces ferroactinolitic-hornblende and ferroactinolite (pts. 12 + 13). In the same rock, ferrohornblende forms as alteration products of pyroxene-plagioclase endoskarn in a schist layer (pts. 14 + 15). On a retrograded contact between pyroxene skarn and schist endoskarn, actinolitic hornblendes are associated with minor scheelite (pt. 16).

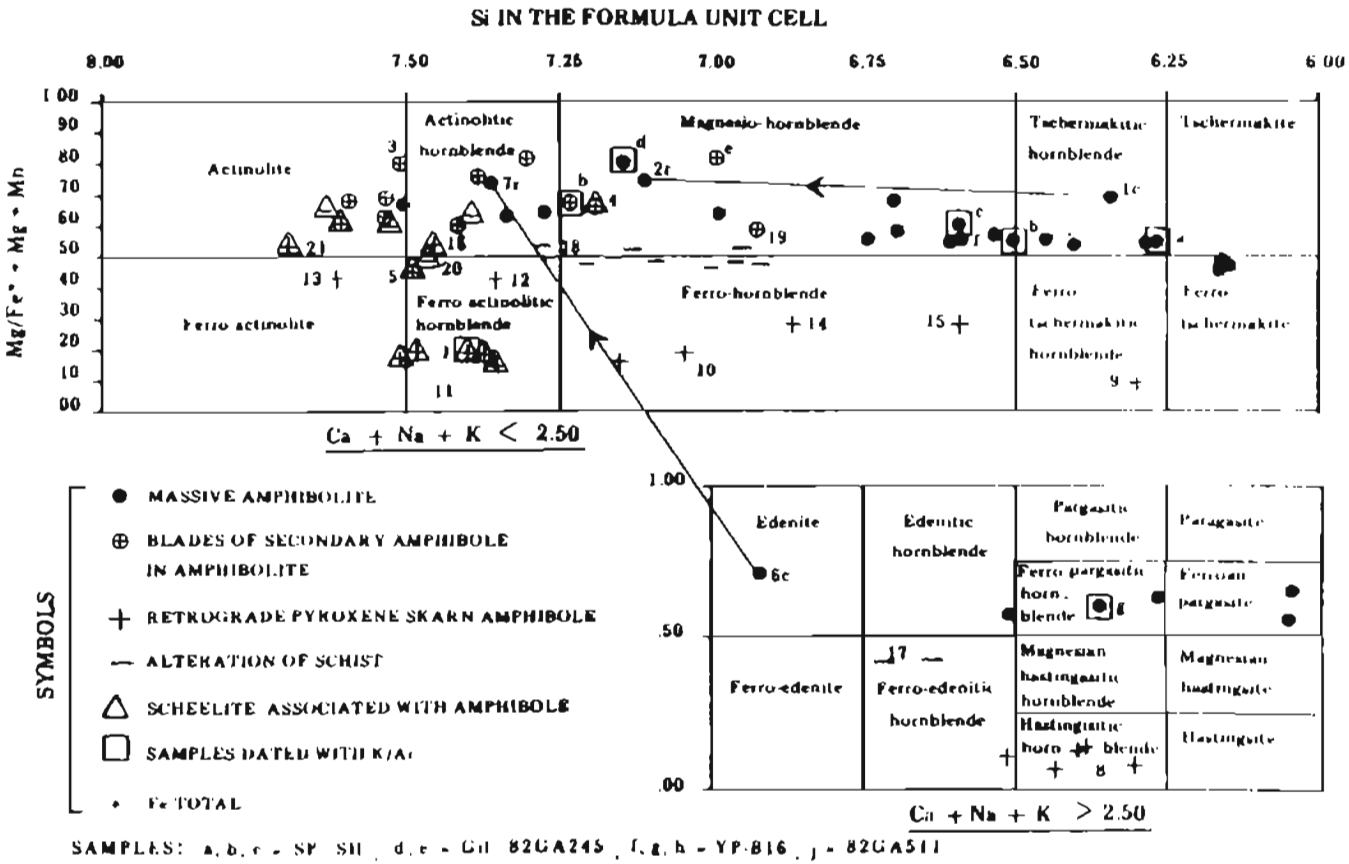

Figure 34. Compositions of amphiboles from Gilmore Dome (modified from Leake, 1978).

Amphiboles formed in schist (after biotite) next to the high grade zone in the back drift at Yellow Pup are dominantly hornblendes (pts. 17, 18, 19). Point 17 is furthest from the mineralized zone, 18 and 19 are closest to the white mica - chlorite - biotite - quartz alteration zone. Actinolite and actinolitic hornblende with scheelite forms in schist along a contact with pyroxene-garnet skarn (pts. 20 + 21).

In general, amphiboles can be distinguished by their composition which in altered rocks is a function of the mineral being replaced by the amphibole. Iron-rich pyroxenes alter to iron-rich amphiboles whereas replacement of more magnesian pyroxenes or schists produces magnesian amphiboles. Amphiboles associated with scheelite reflect the altered rock or mineral, but are in general more Al-poor than amphiboles not associated with scheelite.

Phyllosilicates

White micas form a solid solution series between muscovite ($K_2Al_4[Si_6Al_2]O_{20}[HO,F]_4$) and celadonite ($K_2[Mg,Fe]_6Si_8O_{20}[OH]_4$) with phengites being intermediate in composition (fig. 35). Low grade metamorphic white micas are celadonic in composition but with increasing metamorphic grade the muscovite component progressively increases (Laird and Albee, 1981). White micas form as the dominant alteration mineral primarily at Yellow Pup in the high grade pod in the back drift of the adit (fig. 26), in felsic dikes (fig. 15), and in schist in the main trench at Yellow Pup. Compositions of white micas from the Yellow Pup adit pod are muscovite-rich phengites. In partially altered schist adjacent to the pod the white mica is more celadonic.

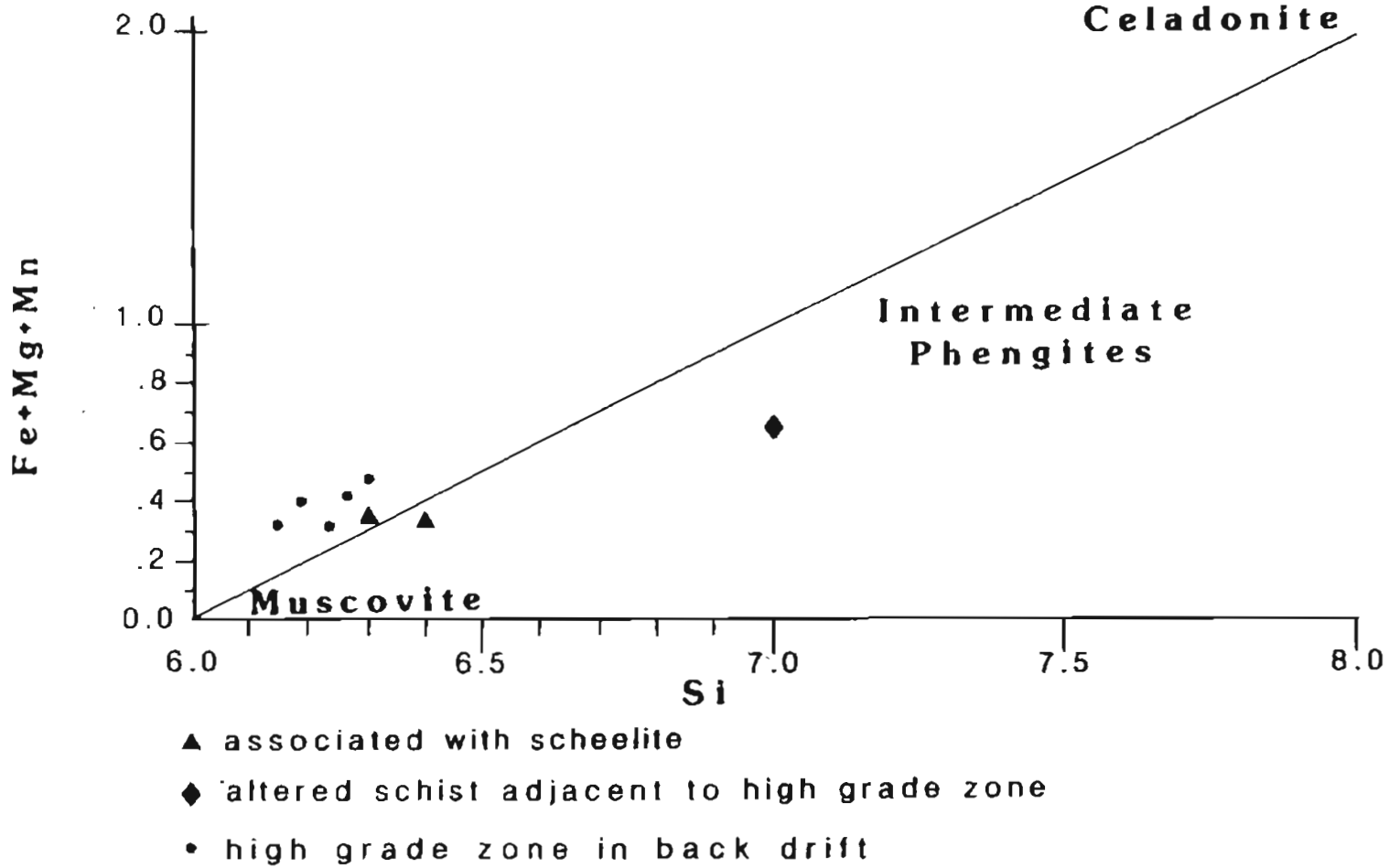

Figure 35. Compositions of white mica from Gilmore Dome (modified from Laird and Albee, 1981).

Chlorite and biotite are also important alteration minerals in the high grade pod at Yellow Pup (fig. 26) and as distal alteration phases in schist. Both chlorite and biotite associated with scheelite in the pod have more iron and less aluminum than those in less altered schist (figs. 36 + 37).

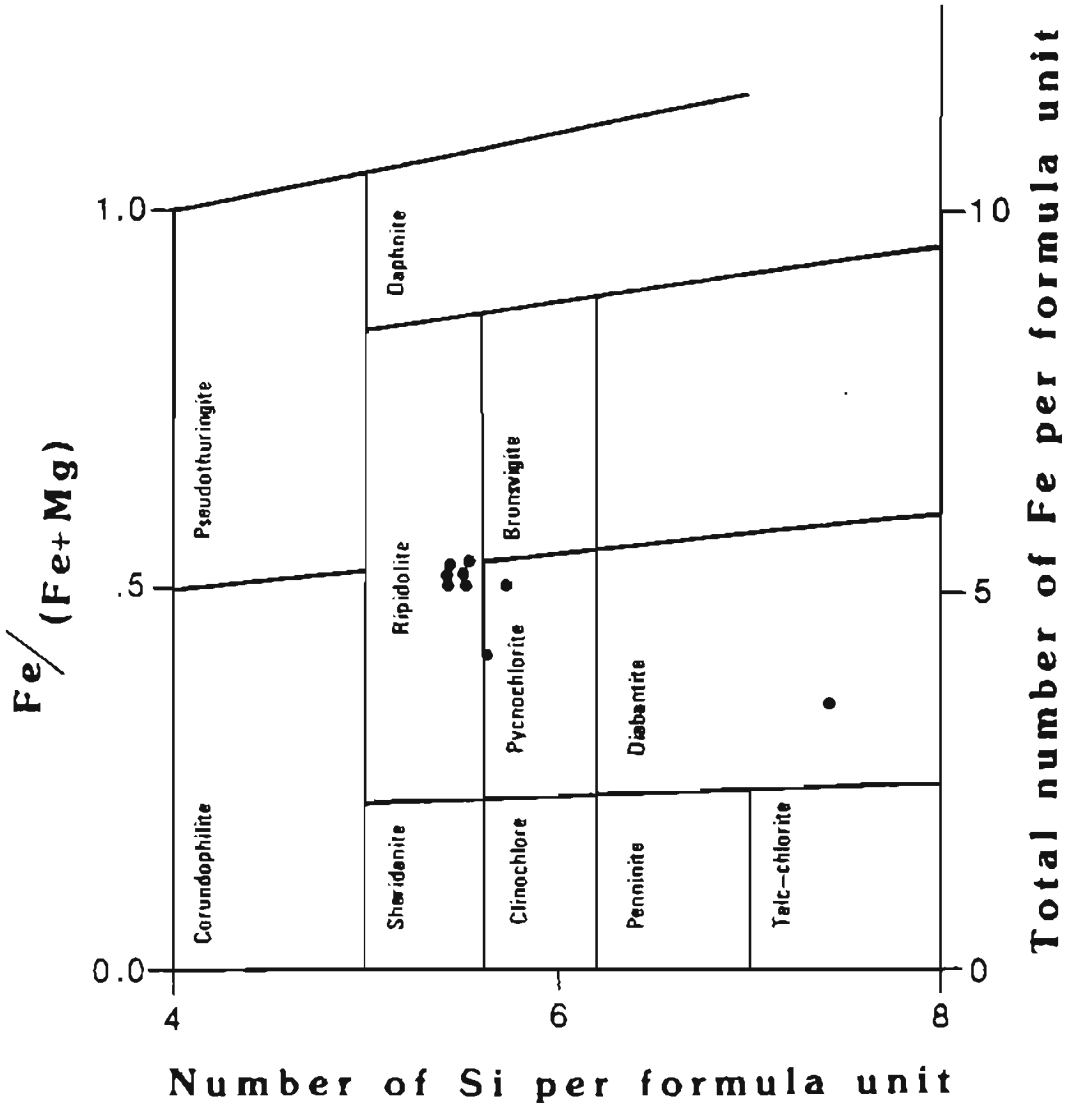

Figure 36. Compositions of chlorite from Gilmore Dome (after Hey, 1954).

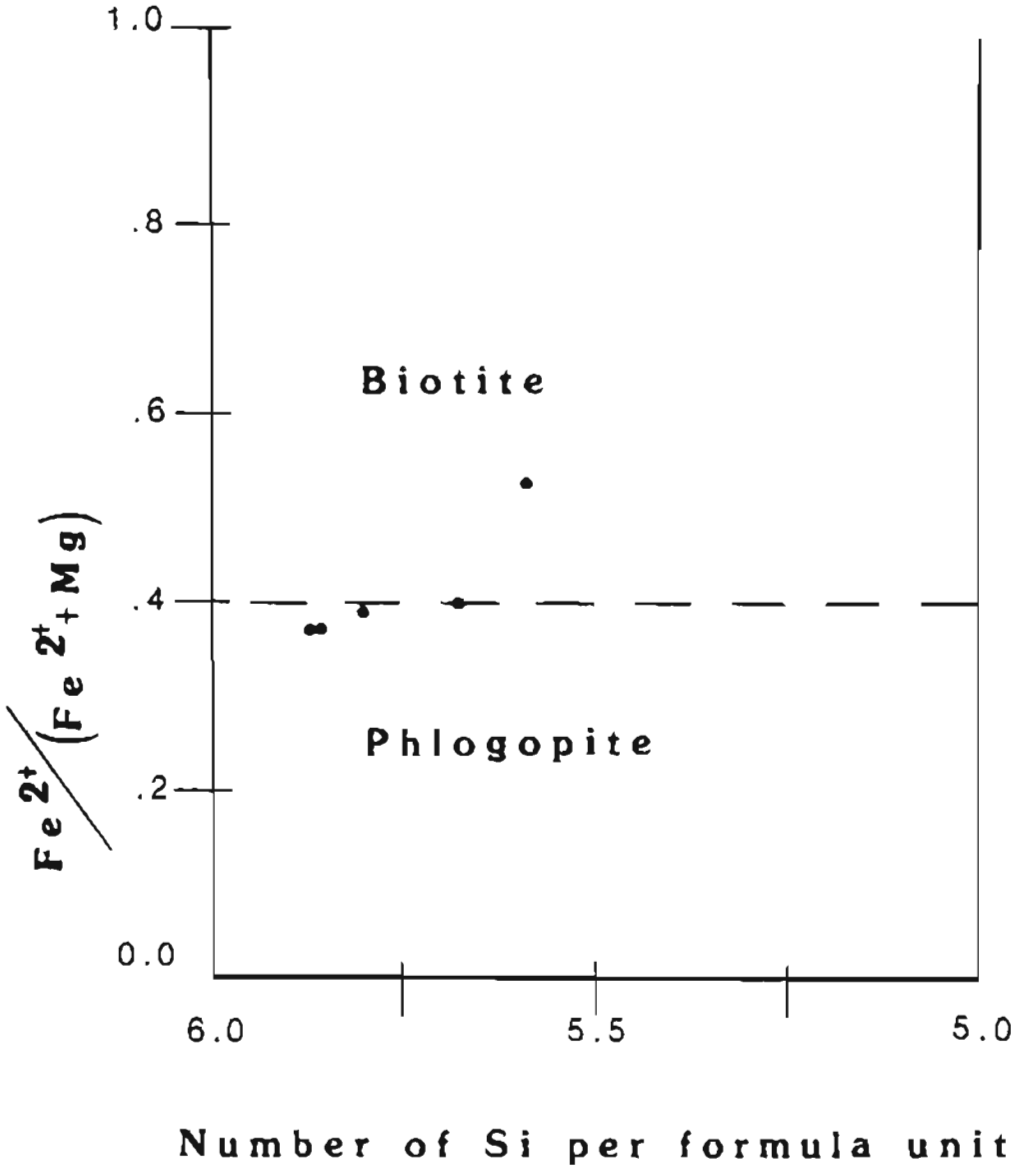

Figure 37. Compositions of biotite from Gilmore Dome (after Deer and others, 1966).

POTASSIUM-ARGON AGE DATES

Six samples were submitted for potassium-argon (K/Ar) dating to establish the timing of mineralization relative to regional and contact metamorphism. Amphiboles from retrograded pyroxene skarn at Spruce Hen and Gil, and white mica from Yellow Pup were selected as representative samples of the mineralized event. Amphiboles from large mafic units (amphibolites) at Spruce Hen, Yellow Pup, and Gil were selected based on their proximity to the main pluton, thickness of the units, and degree of alteration. Two samples of biotite from the Gilmore Dome pluton were also dated to establish K\Ar ages for the intrusive (appendix III).

Biotite located near the contact between a porphyritic granodiorite phase and the surrounding porphyritic granite gave an age of 89 $\pm$ 3 Ma (figs. 38 + 39). In the interior portions of the pluton another biotite sample had an age of 86 $\pm$ 3 Ma. These ages represent cooling ages of the intrusive and are in good agreement with an emplacement age of 91 $\pm$ 1 Ma derived from a Rb-Sr whole rock isochron of the Gilmore and Pedro Dome plutonic complex (Blum, 1983) and with hornblende from fine-grained granodiorite (93 $\pm$ 5 Ma) and biotite from porphyritic granite (95 $\pm$ 5 Ma) from the Pedro Dome plutonic complex (Forbes, 1982).

Amphibole ages from the mafic units range from 88 Ma to 196 Ma. The oldest age comes from the thickest mafic unit located in the Gil trenches. Here the well foliated amphibolite contains 85 percent magnesio-hornblende (fig. 34, pts. d + e) as large (0.4 mm) darker green crystals and smaller (0.05 mm) lighter colored needles, 5 - 7 percent biotite, 3 - 4 percent opaque phases, and minor quartz and calcite.

At Yellow Pup, the rock dated came from a massive mafic unit exposed in trench YP-B16. This rock has an age of 89 $\pm$ 3 Ma. Magnesio-hornblende and ferroan

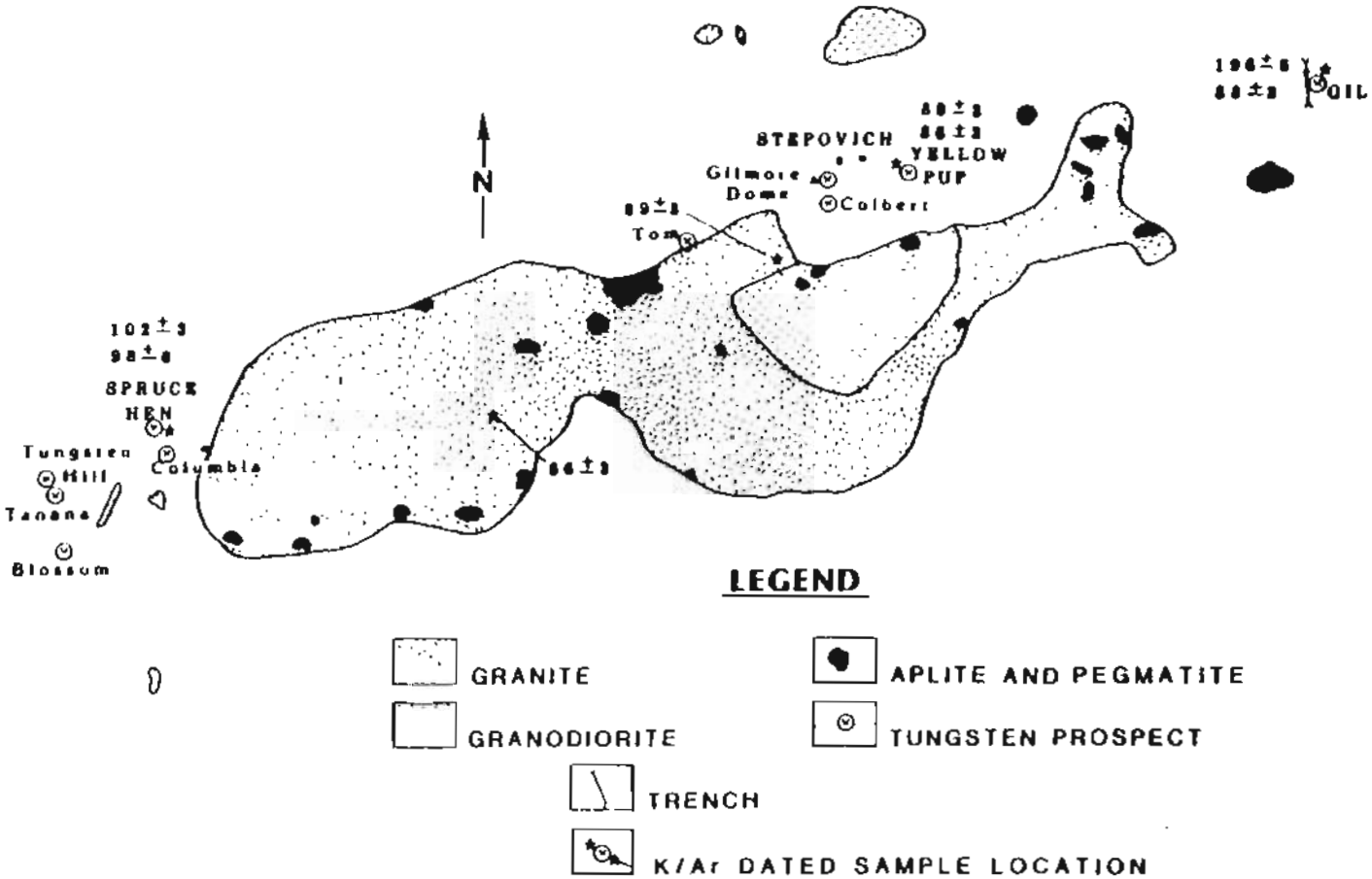

Figure 38. Location of potassium-argon dating samples from the Gilmore Dome area.

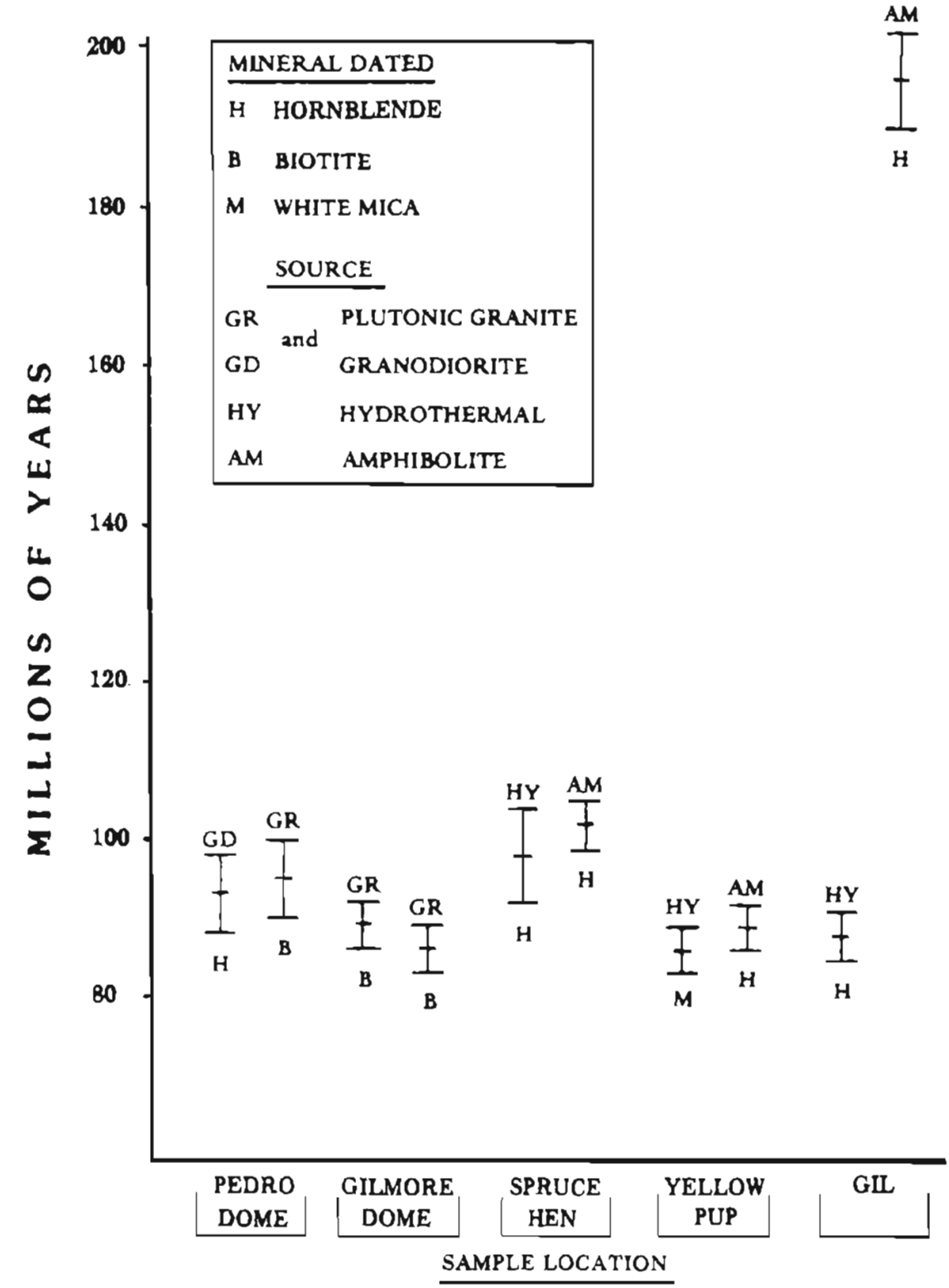

Figure 39. Ages of potassium-argon samples from the Fairbanks mining district.

pargasitic hornblende (fig. 34, pts. f, g, h) compose 90 percent of the rock and have an interlocking, nonfoliated texture with random small needles between larger irregularly shaped crystals. Sphene, quartz, epidote, and minor calcite, chlorite, apatite, and ilmenite are also present. Based on field and petrographic evidence the rock is considered recrystallized. Recrystallization could be due in part to hydrothermal activity expressed by several large, nearby, mineralized, cross-cutting quartz veins.

A large mafic unit exposed between the Spruce Hen pit and the pluton gave a minimum age of 102 ± 3 Ma. In thin section, this rock contains 90 percent tschermakitic hornblende and magnesio-hornblende (fig. 34. pts. a, b, c). Large irregular sections of interlocking amphiboles are separated by smaller more foliated amphiboles. Plagioclase, biotite, sphene, and opaque minerals are also present in small amounts. This rock appears less recrystallized than the one at Yellow Pup (figs. 38 + 39).

Ages from mineralized rocks range from 86 to 98 Ma. Retrograded pyroxene skarn amphiboles have compositions that range from hastingsitic hornblende to ferro-actinolite (fig. 34). At Gil the age of the amphibole in skarn is 88 ± 3 Ma. The skarn is approximately 180 meters south of the site of the 196 Ma date. At Spruce Hen amphibole from skarn gave an age of 98 ± 6 Ma. A phengitic white mica from the mineralized pod in the adit at Yellow Pup gave an age of 86 ± 3 Ma.

Wilson and others (1985) in their compilation of radiometric data from the Yukon Crystalline Terrane suggested that a widespread Early Jurassic regional metamorphic event occurred about 180 Ma ago and in the western part of the terrane there was a Mid-Cretaceous regional metamorphic event approximately 125 - 105 Ma ago. This event was followed by a terrane-wide plutonic event from 105 - 85 Ma.

Biotite ages from the pluton and Blum's (1983) Rb/Sr emplacement age fit into the Cretaceous plutonic event. The oldest amphibolite age of 196 Ma represents a

metamorphic age that has experienced the least, if any, resetting by the emplacement of the pluton. This age is in reasonable agreement with the data for a Jurassic metamorphic event. Ages of the amphibolites at Spruce Hen and Yellow Pup are much younger than at Gil and represent resetting by the plutonic event. The Yellow Pup age is contemporaneous with the biotite ages for the pluton. The Spruce Hen age is slightly older than the biotite cooling age and the K/Ar emplacement age but is concordant with biotite and hornblende ages from Pedro Dome (fig. 39).

Amphiboles are the most resistant mineral of all the K-bearing minerals to argon loss due to temperature increases. In amphiboles, resetting age by release of argon does not begin until the amphiboles have surpassed the minimum blocking temperature of approximately 500^{o}C (Harrison and McDougall, 1980). To measure the approximate thermal effects of the crystallization of the Gilmore Dome pluton on the surrounding metamorphic rocks Jaegar's (1957) method of calculating the extent of contact aureoles was used. Assuming the shape of the pluton as a vertical sheet with an average thickness of 1 km, temperature of the intrusion of 800^{o}C., depth of emplacement 5 km, and temperature of the country rock of 150^{o}C., the country rock would exceed the 500^{o}C. blocking temperature of amphibole for only 250 meters beyond the intrusive contact (Winkler, 1979).

On the surface, both Spruce Hen and Yellow Pup samples are from distances at least twice that far from known intrusive contacts. This leads to several possibilities for the ages seen in these rocks. First, it is not known whether the pluton underlies the mineralized areas to the north. Drilling at Spruce Hen to 34 meters and at Stepovich to 70 meters (C.R. Nauman, pers. comm., 1986) did not intercept the plutonic contact. Second, the calculations are for heat conductivity from crystallization of the magma assuming a dry system. Recrystallization of amphiboles and release of argon could be accomplished by the passage of hydrothermal fluids at temperatures considerably less

than 500°C. Petrographic examination of the two samples shows the Yellow Pup sample to be completely recrystallized whereas the Spruce Hen sample has areas of unrecrystallized foliated amphiboles. The Spruce Hen sample would then be expected to give an intermediate age between the regional and plutonic metamorphic events.

Based on the ages of amphibole and white mica from mineralized rocks, the ore-forming event was contemporaneous with the emplacement and cooling of the pluton. The amphibole age from Spruce Hen is slightly older than the other samples, but this age difference is within analytical uncertainty (fig. 39).

GEOCHEMISTRY

Samples of the mineralized rocks as well as some of the country rocks were collected for analysis of W, Au, Ag, Mo, Sn, F, As, Sb, Hg, Cu, Pb, and Zn (appendix IV, tables 1, 2, 3). In addition 38 representative samples were taken for major oxide analysis and the same trace element suite (appendix IV, table 4). Samples collected for trace elements were taken from rocks considered potentially ore-bearing, whereas major oxide samples were taken for their lack of alteration and weathering. Figures 40 and 41 summarize the trace element data. The mean values for each element at the three locations are plotted for altered rocks and quartz veins. The mean value for each element in the country rocks and amphibolites derived from the major oxide data is also plotted.

Altered rocks at Spruce Hen composed primarily of pyroxene-garnet skarn are enriched in Ag, Mo, Sn, F, Cu, Zn, As, Sb, and Hg compared with altered rocks from Yellow Pup and Gil (figs. 40 + 41). The rocks with the highest grade of W at Spruce Hen also have the highest values of Mo, Sn, and Au. Many of these samples are of retrograded pyroxene-garnet skarn. All of the higher grade W rocks contain F in amounts greater than 2 percent.

At Yellow Pup rocks with the highest grade W have the highest values in Mo and some elevated Au. Elevated Sn values are present in the main trench but not in the ore pod in the adit. Values of F are slightly higher in the main trench than in the adit. Elevated Au values are found in rocks from the adit ore zone and in quartz veins.

Gil samples, in most cases, have similar or lower mean values than Yellow Pup in altered rocks and quartz veins (figs. 40 + 41). Rocks at Gil that have the highest W grades also have the highest Mo values. Sn, if present, is in skarn. Compared with Spruce Hen and Yellow Pup, F is not appreciably enriched in skarn.

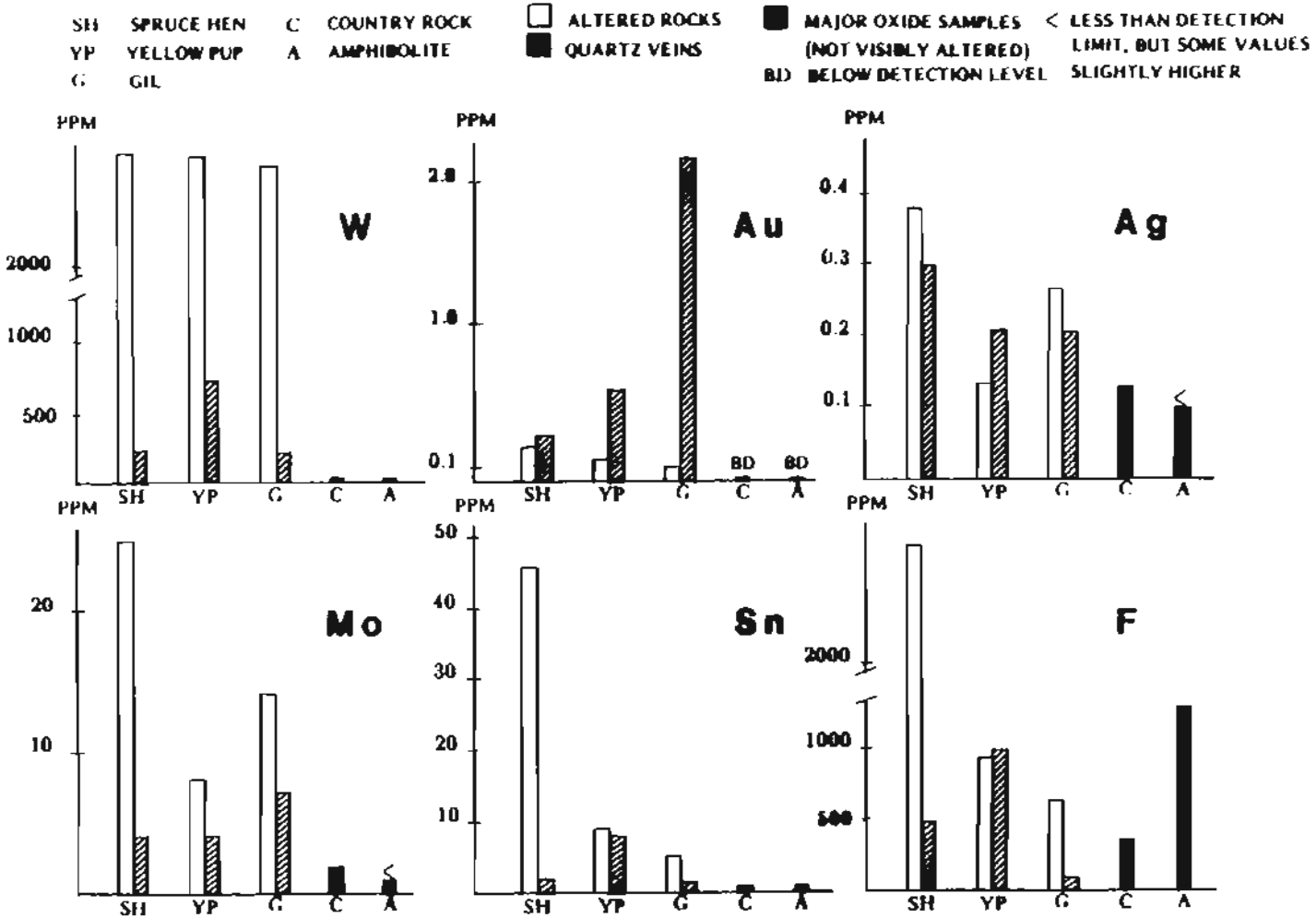

Figure 40. Mean values of trace elements from Gilmore Dome.

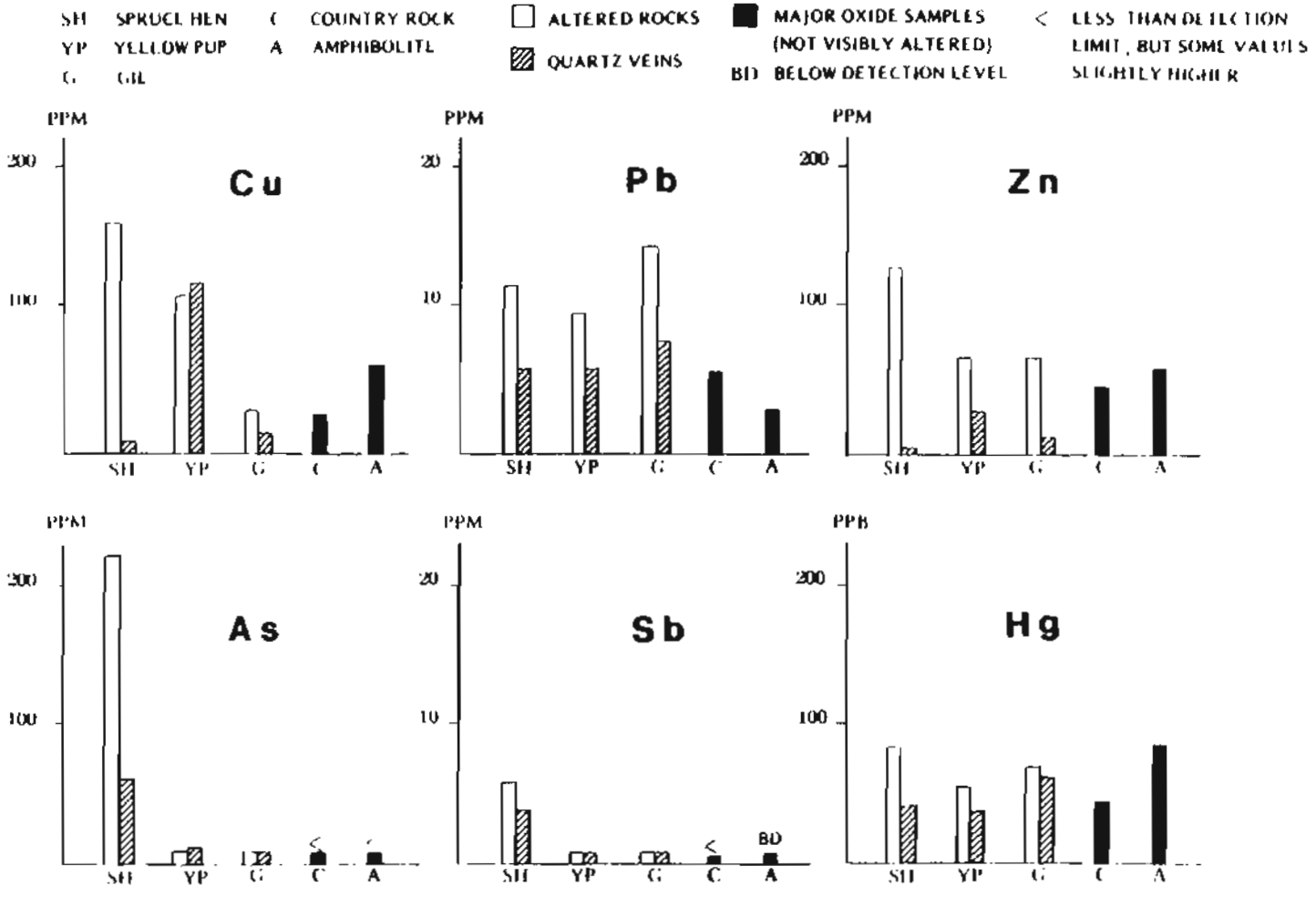

Figure 41. Mean values of trace elements from Gilmore Dome.

Figure 42 shows the ranges and means of W values in altered rocks for the three prospects. The mean values are almost identical for the three prospects but the range in values is not. Spruce Hen shows a smaller range than Yellow Pup (the highest) or Gil. Scheelite at Spruce Hen is mostly fine-grained and evenly distributed within pyroxene-garnet skarn whereas much of the scheelite at Yellow Pup is erratically concentrated as aggregates in late stage skarn zones. Scheelite at Gil is localized as large crystals in pyroxene-quartz skarn. Figure 42 implies that the amount of W in solution was similar at the three prospects, but the range in W values was a function of the type of skarn formed.

For Au, only samples with values at or above the detection limit were considered, thus the number of samples considered was substantially less than with the other elements. More data is needed to fully understand the variations in Au in the skarns. With this in mind, mean Au values show a decrease from Spruce Hen to Yellow Pup to Gil but show an increase in mean values in quartz veins from Spruce Hen to Gil (figs. 40 + 41). Au appears to be concentrated in rocks that have experienced late stage alteration (saprolitic zones at Spruce Hen and white mica - chlorite alteration in the adit ore zone at Yellow Pup).

Quartz veins are common at the prospects and may be enriched in both W and Au. Three types of veins have been noted: dominantly W-bearing veins, W and Au veins, and dominantly Au-bearing veins. Spruce Hen has W and W and Au vein types; Yellow Pup and Gil have all three types. The highest mean value of W in quartz veins is at Yellow Pup and the highest Au value is at Gil (fig. 40). Other than W and Au, veins at Spruce Hen are higher in Ag, As, and Sb, while Yellow Pup veins are enriched in Sn, F, Cu, and Zn. Veins at Gil are slightly enriched in Mo, Pb, and Hg. Quartz veins cross-cut earlier formed skarn or country rock except those at Gil that core pyroxene skarn.

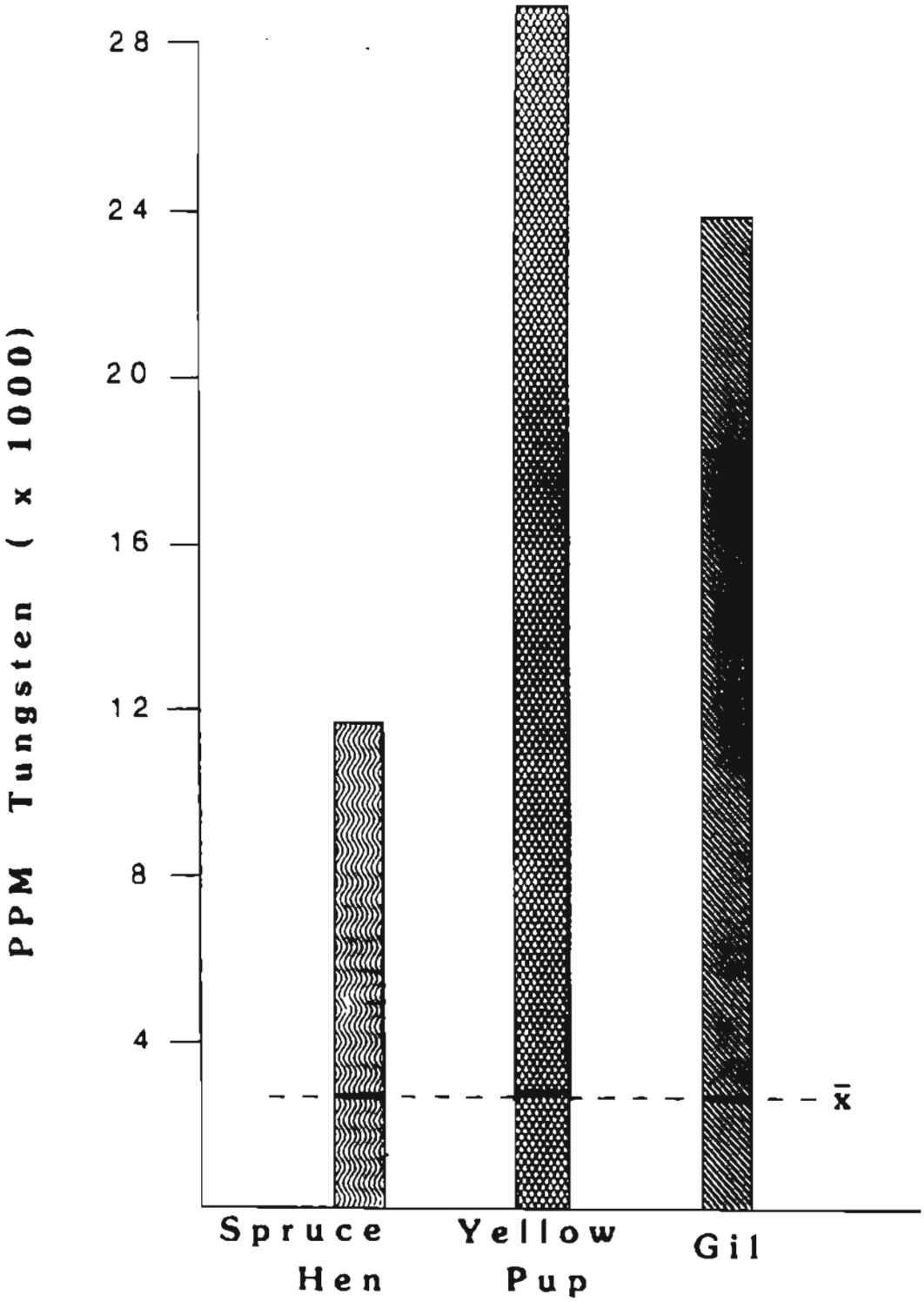

Figure 42. Ranges and means of tungsten values for Spruce Hen, Yellow Pup, and Gil.

The mean values for trace elements in the amphibolites and country rocks are low compared with the altered rocks and the quartz veins. These values are within average abundances stated in Levinson (1974) (appendix IV, table 8).

In general, skarn rocks have elevated values of W, Mo, Sn, F, and occasionally Cu, Zn, Au, and Ag. Except at Spruce Hen, Sb, Hg, and As are not noticeably higher in skarn. Some felsic dikes at Spruce Hen are very high in all the elements analysed and especially in As, Sb, Hg, Ag, and Pb. Bi has been noted in the Stepovich mineralized zones (Byers, 1957).

To further evaluate the geochemical data, Pearson correlation coefficients for the data were derived using a SAS CORR procedure (appendix IV, table 6 + 7). The rocks were broken into two groups: altered and relatively unaltered. Altered rocks include skarns and adjacent wallrocks whereas unaltered rocks include country rocks, many of them considered questionable in rock type or presence of alteration or mineralization. A correlation coefficient of +0.5 or greater was used to distinguish correlations between elements. The element sets for each type are listed below:

altered rocks:	Zn - F - Sn
	Mo - Sn - W
	Sn - F - Zn - Mo
	W - Mo
unaltered rocks:	Sb - As

This suggests there is no elemental relationship between the two groups. Values for Au and Ag were not considered because the majority of analyses were below the detection level of 0.1 ppm used in the analysis.

Tungsten skarns worldwide contain a variety of metals in addition to the common association of W, Mo, Cu, and Zn. The association of W, Mo, and Sn was noted as statistically significant in Black Rock tungsten-bearing skarns versus barren skarnoid (Elliott, 1971). Tungsten skarn at Tem Piute, Nevada is noted for the variety

of elements present including W, Fe, Mo, Zn, Pb, Bi, Cu, Ag, and F (Buseck, 1967). The metal association of W, Mo, Sn, Bi, Cu, Pb, and Zn is present in skarn in Bulgaria (Zhelyaskova-Panajotova, 1972). Mineralized quartz vein swarms in Greenland that are distal (1 - 3 km) from tungsten skarn (W, F, Be, Sn, Bi) contain W, As, Pb, Bi, Ag, Sb, Cu, Zn, and Au (Hallenstein and Pederson, 1983). Thus, Gilmore Dome skarns have many similarities with other tungsten skarns in the trace metals present in skarn.

Trace element analysis of the major oxide samples was conducted in hopes of establishing background values to use as a comparison with the mineralized rocks. It is probable that the rocks exposed in the Gil trenches, though distal to the main intrusive mass, are still within the metamorphic/metasomatic contact aureole. Many of the rocks have been erratically exposed to various degrees of hydrothermal alteration. A study of the Kellhauni tin deposits, Bolivia (Lehman, 1985) showed that large hydrothermal alteration halos (up to approximately 6 kms) with elevated Sn values developed in quartzites and shales surrounding granites with associated tin mineralization. Similarily, a hydrothermal alteration halo with elevated W values around granites with nearby tungsten mineralization was noted by Deere and others (1985). Thus, it appears elemental background values around mineralized plutons can be enriched in country rocks without noticable alteration effects, and to get accurate background values the rocks have to be out of the alteration halo. Therefore, it is not recommended that the trace element values of major oxide samples taken for this study be considered representative of the Fairbanks schist or Cleary sequence rocks. Additional work on rocks collected further from the plutonic complex must be carried out to clearly establish unaffected background values.

DISCUSSION

The Gilmore Dome mineralization is a result of the intrusion of the Cretaceous pluton into a complexly interlayered sequence of metamorphosed sedimentary and lesser volcanic rocks. The fortuitous emplacement of magma along the axis of an antiformal structure with calcareous units trending the length of the pluton was instrumental in the formation of mineralized skarn horizons extending over 16 kilometers. Variability present in skarn mineralization can be accounted for by differences in host rock stratigraphy, time of formation, and distance from the pluton. Localization within host rocks and extent of skarn ore replacement was a function of structural conduits and amount of fluid present.

Host rock control

Calcareous rocks are most receptive to skarn formation with the amount of calcite available for calc-silicate formation and ore deposition determining the type of skarn formed. In relatively thick marbles with lesser amounts of impurities (such as at Spruce Hen and Stepovich), Fe-rich pyroxene and garnet with lesser idocrase and wollastonite form (figs. 32 + 33). Zoning of calc-silicate minerals within the skarn is usually present to some degree. Zoning similar to that at Spruce Hen was noted in skarn from Stepovich. Moderate grade, fairly uniform scheelite development favors the pyroxene zones and is best developed in relatively pure marble skarns (pl. 2). Other tungsten skarns with these characteristics are Cantung (Zaw, 1976), MacTung (Dick, 1976), Strawberry, (Nockleberg, 1981), Pine Creek (Newberry, 1982). Impure marbles with large amounts of metamorphic calc-silicate phases (such as the main trench at Yellow Pup) have less free calcium to react with metasomatic fluids and thus have

poorer development of Fe-rich phases, zoning, and scheelite deposition. Skarn and skarnoid mineralogy reflects the more Mg and Al enriched impurities (figs. 32 + 33). King Island (Kwak, 1978) and Black Rock (Newberry, 1980) are examples of tungsten skarns formed in calc-silicate dominated rocks.

The thickness of calcareous units has a strong control on skarn morphology along Gilmore Dome. Thickness varies considerably within the area from one centimeter to at least three or four meters. Where thick marbles exist, skarn development is concentrated more in the marble than surrounding country rock (pl. 1). In thinly interlayered sequences like at Yellow Pup, endoskarn and wallrock alteration may be quite extensive (pl. 4). Thin units have more avenues for fluid migration and subsequent interaction of components between units, therefore show a wider range of alteration types and compositions of minerals (figs. 32 + 33). Kwak (1978) noted at King Island that within zones of thinly interbedded marble and hornfels, fluids migrated along units but did not cross impermeable boundaries such as hornfels units even on the centimeter scale. This is the case at Gilmore Dome especially in calcareous quartzite and thin marble (fig. 24). The type of units interlayered with marble will have an effect on the type of alteration minerals formed (such as garnet in calcareous or feldspathic quartzite, pyroxene ± garnet in quartz mica schist, or white mica - chlorite - calcite - scheelite in quartz mica schist). Similar alteration of marble and schist layers has been noted in Greenland (Hallenstein and Pederson, 1983) where scheelite occurs with clinozoisite - pyroxene - quartz - fluorite in marble and clinozoisite - biotite in schist.

Deposition of scheelite appears to be controlled primarily by host rock calcium activity, thus marble is a more favorable host than calc-silicate rock, and calcareous quartzite is a better host than non-calcareous quartzite (fig. 25). Permeability of units also appears to be a controlling factor in fluid mobility and skarn ore formation. High

permeability and high calcium content would account for the presence of scheelite in thin calcareous quartzite units most notably present in the adit at Yellow Pup (fig. 19) but also present at Gil.

Thus, the morphology of the tungsten skarns reflects that of the replaced unit and in a sense these deposits are not only stratiform, but also strata-bound (figs. 19, 21, 24). In Maucher's model of strata-bound W-Hg-Sb, scheelite is also limited to certain units but the tungsten is considered syngenetic in origin. The use of the word strata-bound is thus somewhat misleading because it is applicable to both types of tungsten ore and can be a source of confusion. As has been shown here, scheelite-bearing skarn can be strata-bound and quite extensive along strike locally and within a district, characteristics described for syngenetic strata-bound tungsten. Therefore, the strata-bound or stratiform character of an ore zone in itself does not distinguish the genesis of tungsten ores.

Scheelite deposition is not limited to noticeably calcareous rocks as shown by scheelite in schist and amphibolite units. The presence of scheelite in rocks other than marbles could be taken as evidence that scheelite was syngenetic. Features which can help distinguish between skarn and syngenetic strata-bound ore include mineral assemblages associated with ore, textural fabrics of gangue and ore minerals, presence or absence of zoning, compositions of gangue minerals, cross-cutting features, and age of mineralization. As has been previously shown skarn formation in non-carbonate rocks has been documented at the Sansano copper mine, Japan (Shimazaki, 1982) and for iron skarns in volcanic host rocks (Einaudi and others, 1981).

In a similar fashion a detailed study of tungsten-bearing calc-silicate quartzites in Portugal (Derre and others, 1982) was conducted to evaluate the possibility of a synsedimentary origin for the tungsten. That study showed calc-silicate quartzites were limited to the contact aureole, scheelite was limited to calc-silicate quartzites near

wolframite veins, and the background W level increased two times within the contact zone. Scheelite-bearing calc-silicate quartzites contained randomly oriented amphibole, epidote, chlorite, biotite, plagioclase, calcite, fluorite, sphene, apatite, and sulfides. Derre and others (1982) concluded that the scheelite and calc-silicate mineral formation were related to the plutonic hydrothermal event, the source of W could not be the surrounding metamorphic rocks, and the calcic quartzites acted as traps for tungsten due to their chemical composition and mechanical properties.

Along Gilmore Dome host rocks have affected the type and composition of gangue mineralogy, the grade of mineralization, and the morphology of the ore zone.

Temporal relationships

The mineralizing system can also be viewed as a function of time. K/Ar ages along with mineral compositions, textures, and assemblages have shown the mineralizing event was preceded by regional and contact metamorphism. Al and Mg-rich calc-silicate minerals formed as layers in marble, as entire units, and as bimetasomatic layers between units during metamorphism (figs. 16 + 17). For prospecting purposes the distinction between metamorphic and skarn calc-silicate rocks is important as unaltered metamorphic calc-silicate rocks are invariably devoid of any scheelite.

During the cooling of the pluton several phases of skarn development and mineralization occurred. An early higher temperature phase resulted in Fe and Mn enriched pyroxene-garnet-idocrase-wollastonite exoskarn (figs. 7 + 8), pyroxene $\pm$ garnet $\pm$ plagioclase endoskarn (fig. 7), skarnoid (figs. 20 + 21), fine-grained evenly distributed scheelite of moderate grade, and minor deposition of Mo, Sn, F. Recent work (Allegro, 1986) has shown Au deposition is in part contemporary with pyroxene skarn formation in relatively pure marble at the Stepovich property. With evolution of

the system, pyroxene and garnet became more enriched in Fe and Mn (figs. 32 + 33). Subcalcic garnet was the latest and most evolved garnet to form. Presence of subcalcic garnet is considered characteristic of tungsten skarns associated with reduced plutons or wallrocks or formed at great depths (Newberry, 1983). Compositional trends of pyroxene and garnet are similar to those present at MacTung (Dick and Hodgson, 1982) (fig. 43) and are considered representative of a reduced oxidation state trend for tungsten skarns (Newberry, 1982). Similar enrichment trends have been noted in many skarn deposits (Zharikov, 1970; Guy, 1979; Einaudi and others, 1981). Stability relations in Ca-Fe-Si-C-O-H systems (Burt, 1972; Einaudi and others, 1981) show that early skarn formation occurs over a range of temperatures (approx. 650^{o}C. to 400^{o}C.) and oxidation states.

As the magmatic and hydrothermal system cooled the stability of calc-silicate minerals changed as a function of temperature. Hydrous assemblages became stable and replaced preexisting phases in skarn and endoskarn or formed in previously unaltered rocks. Amphibole $\pm$ calcite + quartz replacement of pyroxene characterizes this retrograde phase along with lesser clinozoisite, chlorite, and sphene (figs. 13, 20 - 24, 28). Compositions of amphiboles reflect the compositions of the mineral being replaced (fig. 34). Amphibole assemblage alteration zones have been noted at many tungsten skarns such as Tem Piute (Buseck, 1967), Maikhura (Zharikov and Vlasova, 1972), MacTung (Dick, 1976), and Pine Creek (Newberry, 1982).

A rock composed dominantly of amphibole need not be an igneous mafic rock but could be formed from a variety of rocks through hydrothermal alteration. Characteristics to distinguish between the two types of rocks are mineral assemblages, textures, spatial distribution, and mineral composition. Also, the presence of scheelite within a mafic igneous rock does not in itself show a syngenetic depositional

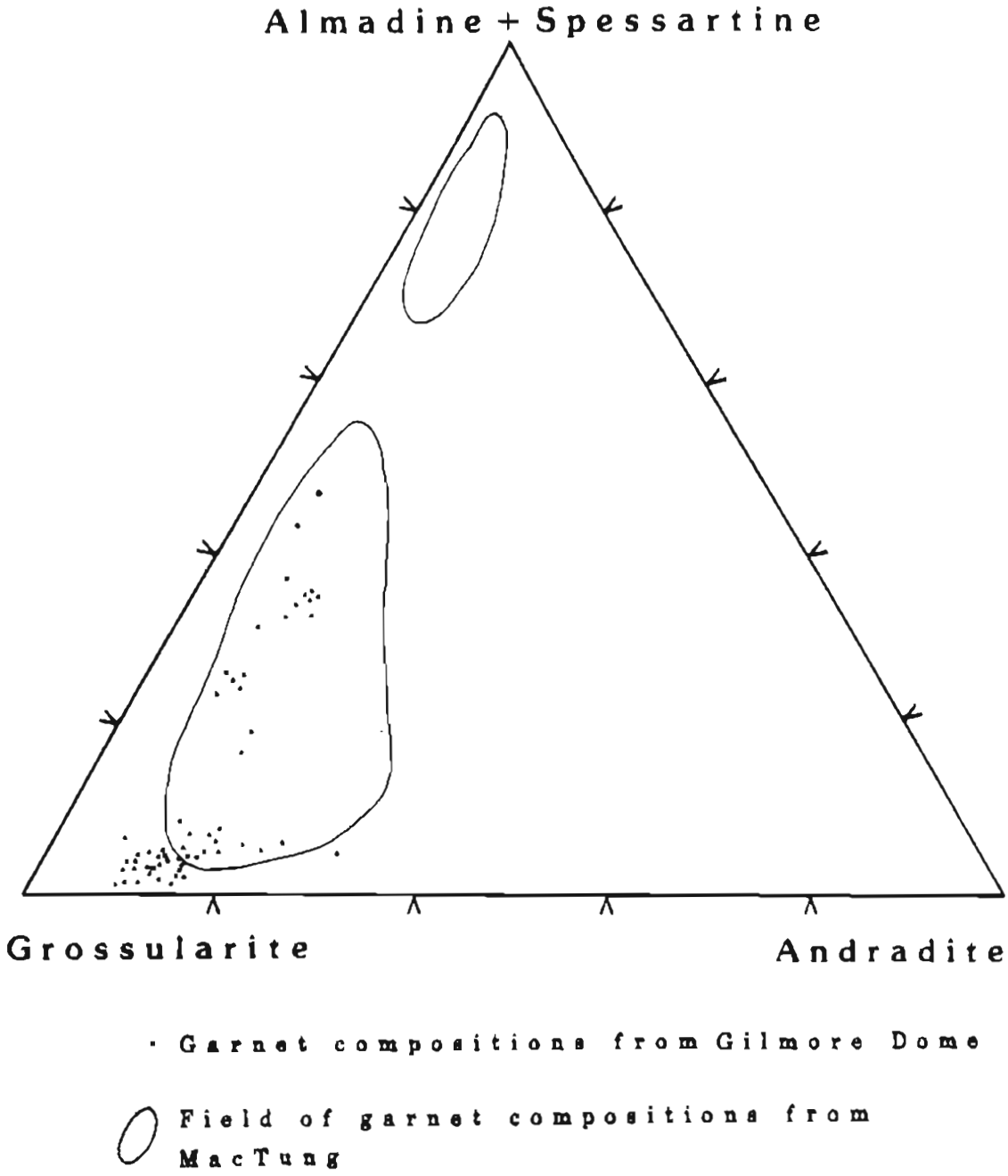

Figure 43. Trend of garnet compositions from MacTung tungsten skarn (after Dick and Hodgson, 1982).

relationship. Criteria noted above can be used to distinguish between syngenetic and introduced scheelite.

Phengitic white mica, chlorite, biotite, quartz and calcite alteration of interlayered schist and carbonate and of felsic dikes is also common during the later stage of anhydrous skarn destruction and may contain significant high grade ore (figs. 15, 25, 26). The presence of a quartz - calcite - white mica - chlorite vein in marble at Stepovich containing pyrrhotite, chalcopyrite, pyrite, and argentite suggests sulfide deposition occured during this lower temperature alteration phase. This phyllosilicate mineral assemblage has been noted at Sangdong, South Korea (Kim, 1971), and at the Max mine, British Columbia (Dawson and Dick, 1978). Minor biotite and chlorite alteration of amphibole in pyroxene-garnet skarn suggests these minerals are stable at lower temperatures than amphibole and formed at a later time.

Ore grades in retrograde zones along Gilmore Dome are usually very low or much higher than in early skarn. This is seen petrographically at Spruce Hen where scheelite in early skarn is remobilized locally during retrograding (scheelite absent retrograde zones) and redeposited in high grade pockets as large aggregates and crystals (figs. 13 + 22). Scheelite-bearing quartz veins, some containing retrograde minerals (amphibole, chlorite, white mica), cut through skarn and country rock and may contain significant tungsten (pls. 1 + 4). Cu and Zn values are also higher at Yellow Pup in the main trench in schist around a quartz vein. Gold deposition may become more prevalent during this phase in retrograde zones as well as in quartz veins. Gold occurred in rocks from retrograde zones in pyroxene-garnet skarn and saprolitic zones at Spruce Hen and in the ore pod in the adit at Yellow Pup as well as in highly retrograded pyroxene skarn at Stepovich (Allegro, 1986). Relative timing of W and Au-bearing quartz veins is not clear. The geochemical data is too limited to delineate definite relationships, but it appears that W $\pm$ Au in veins and retrograde zones

preceded Au-bearing veins. Mertie (1918) noted Au-bearing quartz veins cross-cut scheelite lodes at the Tanana, Columbia, and Tungsten Hill group claims. This was also the case at Spruce Hen, Yellow Pup, and Gil as observed in this study. The timing of some gold deposition is concurrent with the later lower temperature phyllosilicate alteration based on elevated gold values in the Yellow Pup adit ore zone from which the white mica age date of 86 Ma came from. A secondary or later hydrothermal stage of quartz veins in tungsten skarn has been noted at Sangdong, Korea (Farrar and others, 1978).

In a general sense, the evolution of the mineralizing system is a result of declining temperature as the plutonic system cools. This progression is reflected in the hydrous mineralogy and ore deposition. It is also possible that some of these features are a result of fluids cooling as they traveled further from the plutonic heat source.

Spatial relationships

A standard model for skarns shows a pluton intruding marble and skarn being formed at the intrusive/marble contact. In re-evaluating tungsten deposits the argument has been used that intrusive rocks are not in the immediate area therefore the deposit is not associated with an intrusive event (e.g. Tweto, 1960; So, 1968; Maucher, 1976; Stumpfl, 1977). However, skarn development 100's of meters from intrusive contacts has already been recognized by numerous workers (Sangdong, Korea, John, 1963; Seven Rila Lakes, Bulgaria, Zhelyaskova-Panajotova and others, 1972; Northern Cordillera, Canada, Dawson and Dick, 1978; MacTung, Canada, Dick and Hodgson, 1982; Cananea, Mexico, Meinert, 1982; and Central East Greenland, Hallenstein and Pederson, 1983).

The whole question of skarn distance from the Gilmore Dome pluton is somewhat speculative as there is no data on how extensive the pluton is below the

current erosion level. The occurrence of pegmatitic and aplitic dikes at all the skarn prospects suggests some nearby intrusive mass. For the discussion of spatial relationships distances from the surface contact of the main intrusive mass to the different occurrences will be used; these are clearly maximum distances. Spruce Hen is approximately 600 meters away from the intrusive, Yellow Pup is 800 meters away, and Gil is 2000 meters away from the main plutonic body. Other evidence suggesting Spruce Hen is closer to the intrusive is the abundance of layers of large idocrase crystals and lesser wollastonite in otherwise unaltered marble. This was also seen in marble adjacent to the pluton. Using this framework it appears that the mineralizing system changed with increasing distance from the pluton.

Pyroxene and garnet compositions not only change with time in an individual skarn but also with distance. Pyroxene formed in marble (as opposed to dominantly calc-silicate rocks) shows an enrichment trend in Fe and Mn with increasing distance from the pluton (fig. 33). This relationship is also present when considering skarn pyroxenes from the Stepovich (approximately 600 m from the pluton) which are similar in composition to the Spruce Hen. Pyroxenes from the quartz-cored skarn at Gil are the most Fe and Mn enriched. This type of enrichment trend was noted at the Cananea copper skarns by Meinert (1980).

Early garnet compositions at Spruce Hen and Stepovich are also similar and show the same later subcalcic compositions (fig. 32). Yellow Pup garnets, however, have rims that are more andraditic in early skarn and subcalcic garnets that contain more Mn. This would imply that with increasing distance garnet, like pyroxene, becomes enriched in Fe and Mn.

No garnets are present in skarns at Gil, but in a few cases very minor idocrase is present. Gil skarns also have an abundance of quartz. Experimental work by Hochella and others (1982) on the stability of idocrase shows the assemblage idocrase-

quartz-pyroxene is stable at temperatures lower than 400^{o}C. at 2 kb with a low XCO_2 fluid phase. This would be below garnet stability and could account for the lack of garnet in skarns at Gil.

The abundance of retrograde alteration near intrusive contacts has been noted in numerous skarns (Einaudi and others, 1981). Along Gilmore Dome, retrograde or later lower temperature formation of skarn and endoskarn is more predominant than early skarn formation at Yellow Pup than Spruce Hen or Gil. There are several possible explanations for this: 1) the fluids cooled as they traveled away from the fluid source, or 2) most higher temperature fluids were not channeled to Yellow Pup but later cooler fluids were.

In retrograde zones the dominant phases are: Spruce Hen - amphibole + quartz $\pm$ calcite, Yellow Pup - amphibole or white mica + quartz $\pm$ calcite, Gil - quartz + amphibole $\pm$ calcite. The proportion of quartz and calcite to amphibole increases with increasing distance suggesting retrograde alteration is dominanted by fluids less saturated in Al and possibly Fe and Mg.

The size of skarn zones appears to decrease as distance from plutonic contacts increases. Skarn at Spruce Hen is relatively continuous along strike for 50 meters (pl. 3). Skarn at Yellow Pup in the trench is continuous for approximately 25 meters and less than 5 meters in the adit ore zone (pls. 4 + 5). At Gil, skarn appears to be much more limited in size (2 - 3 meters) even though strike exposure is poor (pl. 7, inset).

The trace element concentrations also reflect proximity to the pluton. Spruce Hen has higher values in altered rocks in most of the elements analysed, especially in Mo, Sn, F, As, Cu, Zn, and Ag (figs. 40 + 41). Though average W grades are similar for the three areas, the range in values is highest at Yellow Pup and Gil (fig. 42). This in part reflects the enrichment of grade during retrograding at Yellow Pup and scheelite

solubility decreasing with the high activity of Ca (in pure marble) and lower temperatures of pyroxene skarn formation at Gil.

Abundance of quartz veins and the concentrations of elements in the veins also change with distance. From Spruce Hen to Gil there are 1, 3, and 5 Au-bearing veins (= or >0.1 ppm) and 5, 6, and 13 W-bearing veins (>20 ppm) . At Yellow Pup and Gil veins with both Au and W are present. The highest Au values are at Gil. Thus, mineralized vein density and Au values increase with increasing distance while W values increase then decrease with distance. This type of zoning from W dominant to Au dominant veins with distance from intrusive was recorded by Foster (1975) at Richardson's Kop deposit, Rhodesia.

Moderate to relatively high grade W values in Au-bearing quartz veins have been reported by Byers (1957) for a number of mines and prospects in the Pedro Dome area. Scheelite occurs at the Wackwitz, Mizpah, Cleary Hill, Leslie, Egan, Johnson, Tolovana, and Rainbow properties. Many of these areas are at least three kilometers to the northeast of the main plutonic complex but in an area with numerous granitic dikes (Byers, 1957).

Quartz veins containing elevated values of other trace elements also show a zonation pattern. Spruce Hen veins have elevated Ag, As, and Sb (similar to the altered rocks and felsic dikes), Yellow Pup has Sn, F, Cu, and Zn, and Gil has Mo (reflecting the vein-controlled skarns) and minor Pb and Hg.

The general spatial characteristics shown by the properties studied for this report are not present everywhere along Gilmore Dome. For example, the Tom property, directly on the intrusive contact, is reported to have experienced only very minor low temperature alteration with elevated Au values (C.R. Nauman, pers. comm., 1986). In addition, the Colbert property, located between the intrusive and the very high grade Stepovich property, has experienced alteration similar to the Yellow Pup in most places

but is generally lower in grade and extent (Byers, 1957; this study). The lack of significant ore in potential host rocks at these prospects emphasizes the importance of structural control in skarn formation, particularly at large distances from an intrusive.

Structural control

Local concentrations of tungsten have occurred along the axis of an antiform and around faults, quartz veins, and aplitic and pegmatitic dikes. The main trench at Yellow Pup is along an antiform that appears to have acted as a trapping mechanism for fluids channeled to the area by dikes or faults that are exposed in the trench. A number of NNW and NNE striking faults have been detected by geophysical methods by Resources Associates of Alaska in the eastern section of the mineralized belt along Gilmore Dome (C.R. Nauman, pers. comm., 1986). This is also the dominant direction for mineralized quartz veins at Gil.

The association of aplitic and pegmatitic dikes in mineralized zones was first noted by Mertie (1918) when numerous prospect pits and trenches were excavated on Gilmore Dome. All three occurrences studied and the Stepovich property have granitic dikes within mineralized rocks. Spruce Hen has a very high grade altered dike next to skarn and in the pit to the south a dike has high values in a number of elements. Dikes are present along the axis of the main trench at Yellow Pup and within the ore pod in the adit. At Gil, a pegmatitic dike 3 meters from pyroxene skarn is surrounded by rocks enriched in W and Sn. These dikes have undoubtably served as conduits for some of the mineralizing solutions.

Locally, fluid flow away from the main conduit is along lithologic contacts, permeable units, and joint planes. This is well illustrated by zoning at Spruce Hen along metamorphic idocrase layers in marble, thin scheelite-bearing quartzite units

emanating out from the ore pod in the Yellow Pup adit (fig. 19), and irregular alteration of schist along joints in the main trench at Yellow Pup (fig. 20). Einaudi and Burt (1982) note that endoskarn can be widespread where fluid flow is along lithologic contacts. This would especially be the case with thinly interlayered units. And as previously shown, repeated use of the same conduit over time creates complex mineralogy, zoning patterns, and ore grade patterns.

Fluid distribution

A further parameter that will effect the size of the ore zone is the amount of fluid passed through the host rocks. Two areas along Gilmore Dome apparently received the bulk of the fluid: the northwest end around Tungsten Hill and the northeastern end around Gilmore Dome (fig. 2). The area of Gilmore Dome (Stepovich, Yellow Pup, and Colbert) has the most extensive and highest grade mineralization. Tungsten Hill has enriched values of Ag, Sn, F, As, Sb, and Hg in skarn and felsic dikes. Localization of fluids along the eastern end of the pluton near Gilmore Dome may be due in part to fluids migrating along the contact between the presumably earlier granodiorite mass (north and south of Yellow Pup) and the surrounding granite. In magmatic systems with multiple intrusions, tungsten skarns are usually associated with the most felsic stage (Newberry and Swanson, 1986). Newberry and Swanson also showed evidence for alteration along the western contact of granite and granodiorite (fig. 2). Northerly trending faults and dikes intercepting this contact zone could have channeled fluids to the two distinct marble horizons in the area. This would explain the lack of skarn formation along the contact further to the west (Tom prospect). It is of interest to note that the majority of tungsten in Au lodes near Pedro Dome are NNW of

the Gilmore Dome pluton in the Cleary Creek area (see Byers, 1957, pl. 23). The most felsic plutonic mass (Blum, 1983) is nearest this area of W mineralization.

On the far western end of the pluton there are numerous aplitic dikes exposed around the nose of the pluton. This indicates a water-rich phase was present during crystallization and may have been responsible for some skarn formation. The enrichment in elements in altered rocks and dikes could be accounted for by a closer proximity to the intrusive or by a difference in the composition of the exsolved fluids from the intrusive. The lack of notable skarn development along the central portions of the pluton and the availability of receptive host rocks in the area would suggest that skarn formation was not solely the result of thermal convection of fluids leaching material from the country rocks but was in part controlled by the release of fluids from the intrusive.

Summary

This study confirms that tungsten concentrations are in metasomatic skarns spatially and genetically associated with the Gilmore Dome pluton. Several parameters influencing ore deposition were the type of calcareous host rock, the evolution of the system with time, the location of the host rocks from the pluton, the structural conduits the fluids used, and the amount of fluid present.

Most characteristics of the Gilmore Dome skarns are similar to other tungsten skarns worldwide. The association of gold in tungsten skarns as found at Gilmore Dome is not as common, but has been reported in other tungsten skarns (Pine Creek mine, Bateman, 1956; Scheelore mine, Sierra Nevada, Rinehart and Ross, 1964; Monte Cristo, Nevada, Sonnevil, 1979; Dublin Gulch tungsten skarns, Keno Hill district, Yukon, Gleeson and Boyle, 1980) and in quartz veins near tungsten skarns (West Tower,

Casa Diablo Mountain Quadrangle, Rinehart and Ross, 1956; Sangdong, Korea, Farrar and others, 1978). An example of a plutonic hydrothermal W-Au system similar to that at Gilmore Dome is the Getchell gold deposit in Humbolt County, Nevada (Silberman, and others, 1974). At Getchell, K/Ar dating has confirmed the emplacement of a granodiorite pluton and subsequent alteration and mineralization were all part of a magmatic thermal event approximately 90 m.y. ago. Alteration and mineralization consisted of tungsten skarn formation along plutonic contacts and later disseminated gold deposition along the Getchell fault in altered granodiorite and sedimentary rocks (Silberman, and others, 1974).

Additional studies of the Gilmore Dome gold system are needed to show the timing relationships with tungsten deposition. There is evidence of alteration of intrusive rocks (Newberry and Swanson, 1986) and gold breccia zones near the intrusive contact to suggest a system similar to Getchell may have been operative during the cooling of the magmatic event.

Economic Conclusions

Estimation of the grade and tonnage potential of the skarns in the Fairbanks mining district is somewhat speculative due to the lack of outcrop, complex structure, and the highly erratic and lenticular deposition of ore. With this in mind general resource estimates can be obtained from Bureau of Mines work (Byers, 1957), unpublished industry sources (Allegro, 1986), and the data derived from this study. The parameters to consider are a mineralized tungsten trend with a strike length of at least 16 kilometers, individual ore zones 3 to 30 meters in length with a majority of them less than 15 meters, average thicknesses of ore horizons of 0.5 to 1.0 meters, and a tungsten grade that varies from 0.1 to 20 percent WO_3. Average grade at Stepovich is

3.0 percent WO_3 while elsewhere along Gilmore Dome grade averages between 0.5 to 1.0 percent WO_3. Currently the Stepovich property has ore zones of higher grade and greater extent than the rest of the Gilmore Dome skarns.

Bureau of Mines work in the 1940's (Byers, 1957) outlined approximately 22,400 tons of 3.2 percent WO_3 on the Stepovich property. Further exploration has shown that there are other skarn occurrences similar to the Stepovich beyond the area examined by the Bureau of Mines which add to the tonnage estimate for that property. Grade and tonnage of skarns elsewhere along the Gilmore Dome pluton are significantly less than those seen at the Stepovich property. An absolute minimum tonnage for the lower grade skarns (0.5 to 1.0 percent) based on current exposure as well as speculated occurrences in covered areas is 10,000 tons. Although the Stepovich property is the most appealing area, the lower grade skarns are the most prevalent, and must be considered more representative when presenting grade and tonnage potential for the district. It can be reasonably projected that the skarns in the Gilmore Dome area contain a minimum of 35,000 tons of 0.75 percent WO_3.

This data can be compared with a compilation of data from tungsten skarn deposits worldwide (Cox and Singer, 1986). Grade and tonnage values from economic tungsten skarns were plotted (figs. 44 + 45) along with the probability a skarn will contain a specific grade and tonnage. The data base includes skarns in a district rather than single occurrences and has a specific bias towards larger economic deposits. However, the resulting curves can be used to evaluate a skarn in relation to other known skarns and is also a way to evaluate the amount of tungsten put into the rocks by a plutonic system. From the placement of data from the Gilmore Dome area on the curve it is apparent that the tungsten skarns are typical of other skarns though they are on the low end for tonnage. It is also apparent from this graph that the Stepovich property is a very high grade though low tonnage skarn.

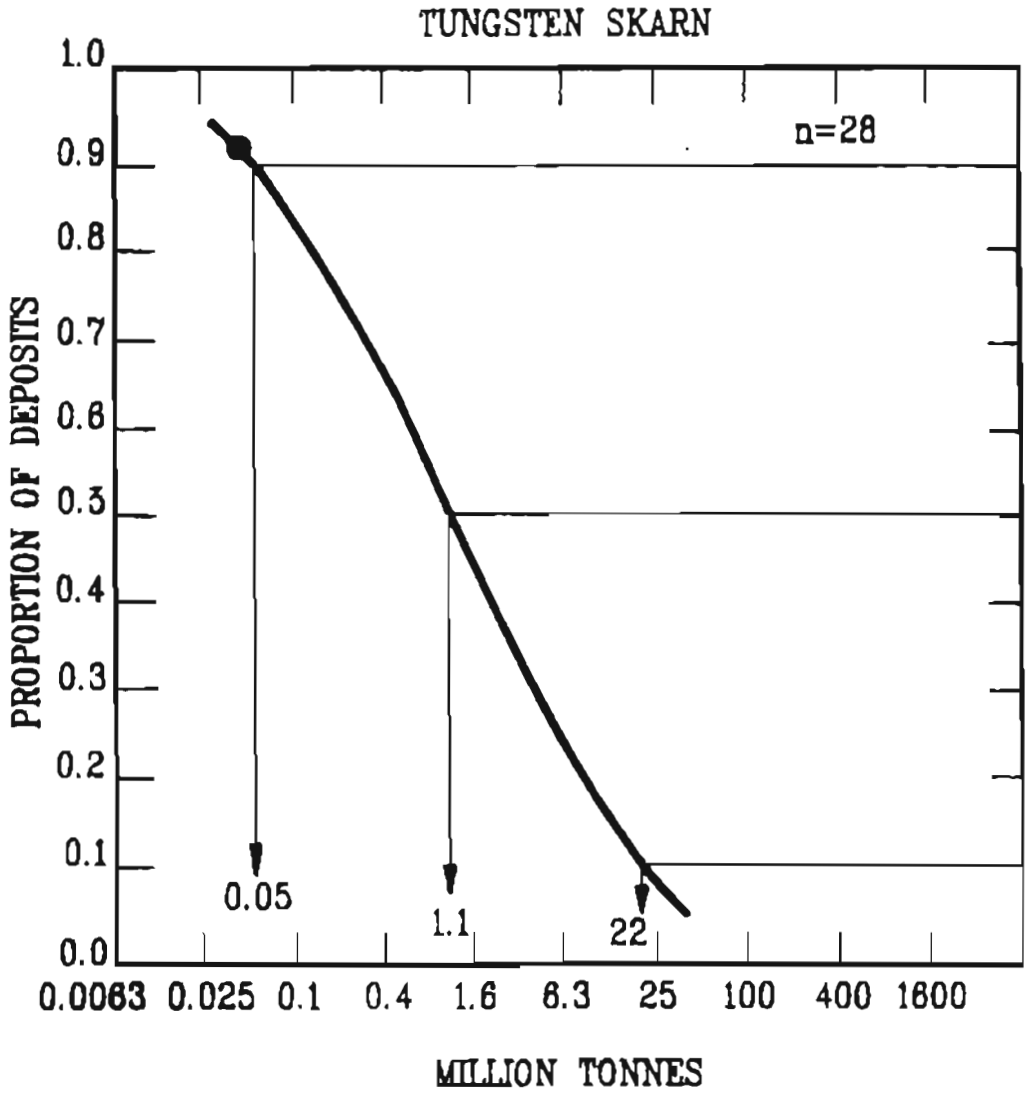

Figure 44. Tonnages of tungsten skarn deposits worldwide. Data for Gilmore Dome skarns: ● = characteristic Gilmore Dome skarns. Curve from Cox and Singer, 1986.

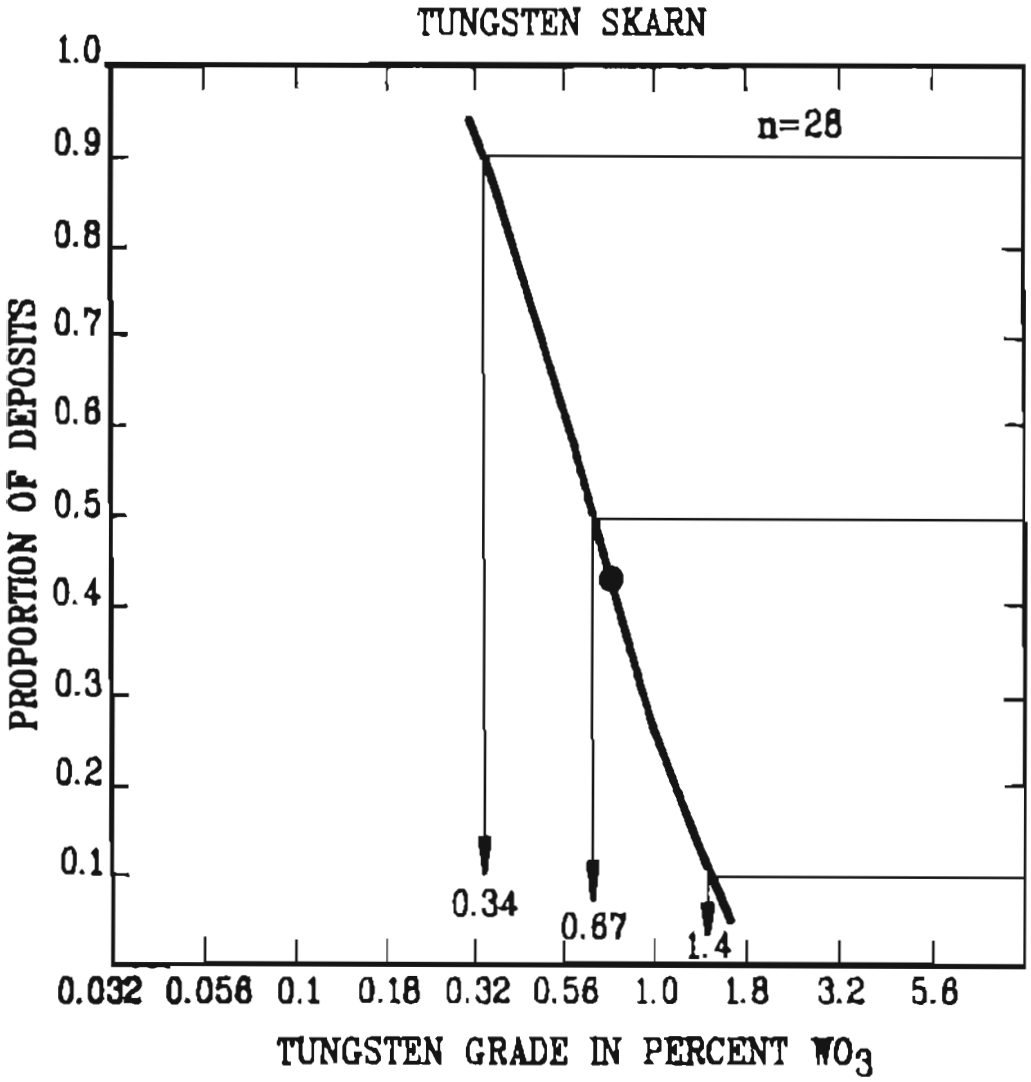

Figure 45. Tungsten grades of tungsten skarn deposits worldwide. Data for Gilmore Dome skarns: ● = characteristic Gilmore Dome skarns. Curve from Cox and Singer, 1986.

During years of low tungsten prices the skarns may not be economically feasible to mine for tungsten, however their gold content makes these skarns attractive when gold prices are relatively high. Gold is found in some of the Gilmore Dome skarns but most notably at Stepovich in pyroxene skarns formed in pure marble (Allegro, 1986). Further work in this area is needed to define the extent of these gold-bearing tungsten skarns. At present, the gold content of the skarns is what makes the Gilmore Dome area worthy of continuing exploration.

REFERENCES CITED

Allegro, G.L., 1986, Fairbanks district annual report, 1986: unpublished report, Resource Associates of Alaska, 35 p.

Bateman, P.C., 1956, Economic geology of the Bishop tungsten district, California: California Dept. Nat. Resources, Div. Mines Spec. Rept. 47, 87 p.

Blum, J.D., 1983, Petrology, geochemistry, and isotope geochronology of the Gilmore Dome and Pedro Dome plutons, Fairbanks mining district, Alaska: Alaska Div. of Geol.and Geophys. Surveys Report of Investigations 83-2, 59 p.

Blum, J.D., 1985, A petrologic and Rb-Sr isotopic study of intrusive rocks near Fairbanks, Alaska: Can. J. Earth Sci., v. 22, p. 1314-1321.

Brooks, A.H., and others, 1916, Mineral resources of Alaska: U.S. Geol. Survey Bull. 642, 279 p.

Burt, D.M., 1972, Mineralogy and geochemistry of Ca-Fe-Si skarn deposits: Unpubl. Ph.D thesis, Harvard Univ., 256 p.

Buseck, P.R., 1967, Contact metasomatism and ore deposition, Tem Piute, Nevada: Econ. Geol., v. 62, p. 334-353.

Byers, F.M., Jr., 1957, Tungsten deposits in the Fairbanks district, Alaska: U.S. Geol. Survey Bull. 1024-I, D178-D218.

Chapin, T., and Harrington, G.L., 1919, Mining in Fairbanks, Ruby, Hot Springs, and Tolstoi district: U.S. Geol. Survey Bull. 692, p. 321-353.

Cox, D.P., and Singer, D.A., 1986, Mineral deposit models: U.S. Geol. Survey Bull. 1693, p. 55-57.

Cunningham, W.B., Holl, R., and Taupitz, K.C., 1973, Two new tungsten bearing horizons in the older Precambrian of Rhodesia: Mineral. Deposita, v.8, p. 200-203.

Dawson, K.M. and Dick, L.A., 1978, Regional metallogeny of the Northern Cordillera: Tungsten and base-metal bearing skarns in southeastern Yukon and southwestern Mackensie: Canada Geol. Survey, Current Research, Pt. A, paper 78-1A, p. 287-292.

Deer, W.A., Howie, R.A., and Zussman, J., 1966, An introduction to the rock forming minerals: Longman, 528 p.

Derre, C., Lecolle, M., and Roger, G., 1982, Les Quartzites a silicates calciques et scheelite: Pre concentrations familieres ou pieges pour un tungstine etranger lie a l'hydrothermalisme perigranitique? Exemple du Nord-Est Transmontain (Portugal): Mineral. Deposita, v. 17, p. 363-385.

Dick, L.A., 1976, Metamorphism and metasomatism at the MacMillian Pass tungsten deposit, Yukon and District of MacKensie, Canada : M.S. thesis, Queens Univ., Kingston, 226 p.

Dick, L.A., and Hodgson, C.J., 1982, The MacTung W-Cu (Zn) contact metasomatic and related deposits of the northeastern Canadian Cordillera: Econ. Geol., v. 77, p. 845-868.

Einaudi, M.T., 1981, Skarns associated with porphyry plutons. I. Descriptions of deposits, southwestern North America, II. General features and origin, in Titley, S.R., ed., Advances in the geology; Geology of the porphyry copper deposits of southwestern North America: Tuscon, Univ. Arizona Press p. 139-183.

Einaudi, M.T., Meinert, L.D., and Newberry, R.J., 1981, Skarn deposits: Econ. Geol., 75th Anniversary volume, p. 317-391.

Einaudi, M.T., and Burt, D.M., 1982, Introduction-terminology, classification, and composition of skarn deposits: Econ. Geol., v. 77, p. 745-754.

Elliot, J.E., 1971, The mineralogy and geochemistry of the tungsten deposits of the Black Rock Mine area, Mono County, California: Unpubl. Ph.D. thesis, Stanford Univ., 131 p.

Farrar, E.F., Clark, A.H., and Kim, O.J., 1978, Age of the Sangdong tungsten deposit, Republic of Korea, and its bearing on the metallogeny of the southern Korean Peninsula: Econ. Geol., v. 73, p. 547-566.

Forbes, R.B., 1982, Bedrock geology and petrology of the Fairbanks mining district, Alaska: Alaska Div. of Geol. and Geophys. Surveys Open-file Report 169, 68 p.

Forbes, R.B., and Weber, F.R., 1982, Bedrock geologic map of the Fairbanks mining district, Alaska: Alaska Div. of Geol. and Geophys. Surveys Open-file Report 170, 2 sheets.

Foster, R.P., Mann, A.G., Armin, T., and Burmeister, B.B., 1975, Richardson's Kop Wolframite Deposit, Rhodesia: A geochemical model for the hydrothermal behavior of tungsten. in Mineralization in Metamorphic Terranes, Verwoerd ed., p. 107-128.

Foster, H.L., Weber, F.R., Forbes, R.B., and Brabb, E.E., 1973, Regional geology of Yukon-Tanana Uplands, Alaska: Am. Assoc. Pet. Geol., Memoir no. 19, p. 388-395.

Gleeson, C.F., and Boyle, R.W., 1980, The lithogeochemistry of the Keno Hill district, Yukon Territory: Geol. Survey Can. Paper 77-31, 19 p.

Guy, B., 1979, Petrology and isotope geochemistry of the scheelite-bearing skarns at Costabonne, Eastern Pyrenees, France: Unpubl. Ph.D. thesis, L'Ecole Natl. Superieure Mines, Pans, 238 p.

Hallenstein, C.P. and Pederson, J.L., 1983, Scheelite mineralization in Central East Greenland: Mineral. Deposita, v. 18, p. 315-333.

Harrison, T.M., and McDougall, A., 1980, Investigations of an intrusive contact, northwest Nelson, New Zealand - I. Thermal, chronological and isotope constraints: Geochemica et Cosmochemica Acta, v.44, p. 1985-2004.

Hey, M.H., 1954, A new review of the chlorites: Min. Mag., v. 30, p. 277.

Hill, J.M., 1933, Lode deposits of the Fairbanks district, Alaska: U.S. Geol. Survey Bull. 849B, p. 24-163.

Hochella, M.F. Jr., Liou, J.G., Keskinen, M.J., and Kim, H.S., 1982, Synthesis and stability relations of magnesium idocrase: Econ. Geol., v. 77, p. 798-808.

Holl, R., 1977, Earl Paleozoic ore deposits of the Sb-W-Hg formation in the eastern Alps and their genetic interpretations, in Klemm, D.D., and Sneider, H.J., eds., Time and strata-bound ore deposits: Berlin, Springer-Verlag, p. 169-198.

Holl, R., and Maucher, A., 1972, Synsedimentary-diagenetic ore fabrics in the strata- and time-bound scheelite deposits of Kleinarltal and Felbertal in the eastern Alps: Mineral. Deposita, v. 7, p. 217-226.

Gill, J.B., 1981, Orogenic andesites and plate tectonics: Springer-Verlag, Berlin, 390 p.

Joesting, H.R., 1942, Antimony and tungsten deposits in the Fairbanks and adjacent districts: Territory of Depart. of Mines Pamphlet no. 1, 22 p.

John, Y.W., 1963, Geology and origin of Sangdong tungsten mine, Republic of Korea: Econ. Geol., v. 58, p. 1285-1300.

Kerrick, D.M., 1977, The genesis of zoned skarns in the Sierra Nevada, California, Jour. Petrology, v. 18, p. 144-181.

Kim, O.J., 1971, Geologic structure and ore deposits of Sangdong scheelite mine: Soc. Mining Geologists Japan Spec. Issue 3, p. 144-149.

Kwak, T.A.P., 1978, The conditions of formation of the King Island scheelite contact skarn, King Island, Tasmania, Australia: Econ. Geol., v. 76, p. 439-467.

Laird, J. and Albee, A.L., 1981, Pressure, temperature, and time indicators in mafic schist: their application to reconstructing the polymetamorphic history of Vermont: Amer. Jour. Sci., v. 281, p. 127-175.

Leake, B.E., 1978, Nomenclature of amphiboles: Am. Mineralogist v. 63, p. 1023-1052.

Lehmann, B., 1985, Formation of the strata-bound Kellhauni tin deposits, Bolivia: Mineral. Deposita, v. 20, p. 169-176.

Levison, A.A., 1974, Introduction to exploration geochemistry: Applied Publishing Ltd., Calgary, 612 p.

Maiden, K.J., 1981, A discussion of the paper by I.R. Plimer "Exhalative Sn and W deposits associated with mafic volcanism as precursors to Sn and W deposits associated with granites": Mineral. Deposita, v. 16, p. 455-456.

Maucher, A., 1976, The strata-bound cinnabar-stibnite-scheelite deposits, in Wolf, K.H. (ed.), Handbook of strata-bound and stratiform ore deposits, v. 10: Elsevier, Scientific Publishing Co., New York, 1976, p. 477-503.

Meinert, L.D., 1980, Skarn, manto, and breccia pipe formation in sedimentary rocks in the Cananea District, Sonora, Mexico: Unpubl. Ph.D. thesis, Stanford Univ., 232 p.

Meinert, L.D., 1982, Skarn, manto, and breccia pipe formation in sedimentary rocks of the Cananea Mining District, Sonora, Mexico: Econ. Geol., v. 77, p. 919-949.

Mertie, J.B., Jr., 1918, Lode mining in the Fairbanks district: U.S. Geol. Survey Bull. 662, p. 403-424.

Mertie, J.B., Jr., and Overstreet, W.C., 1942, Tungsten deposits of the Fairbanks district, Alaska: U.S. Geol. Survey, unpubl. war report, 23 p.

Metz, P.A., 1977, Comparison of the mercury-antimony-tungsten mineralization of Alaska with strata-bound cinnabar-stibnite-scheelite deposits of the Circum-Pacific and Mediterranean regions, in Short Notes on Alaskan Geology - 1977: Alaska Div. of Geol. and Geophys. Surveys Geologic Report 55, p. 39-41.

Metz, P.A., and Robinson, M.S., 1980, Investigation of mercury-antimony-tungsten metal provinces of Alaska II: unpubl. report submitted to U.S. Depart.of Interior, Office of Surface Mining, Grant No. G5184001, p. 153-188.

Miyashiro, A., 1974, Volcanic rock series in island arcs and active continental margins: Am. J. Sci. v. 274, p. 321-355.

Newberry, R.J., 1980, The geology and chemistry of skarn formation and tungsten deposition in the central Sierra Nevada, California: Unpubl. Ph.D. thesis, Stanford University, 325 p.

Newberry, R.J., 1982, Tungsten-bearing skarns of the Sierra Nevada. I. the Pine Creek Mine, California: Econ. Geol., v. 77, p. 823-844.

Newberry, R.J. and Swanson, S.E., in press, Scheelite skarn granitoids: an evaluation of the roles of magmatic source and process: J. Ore Deposit Reviews.

Nockelberg, W.J., 1981, Geologic setting, petrology and geochemistry of zoned tungsten-bearing skarns at the Strawberry mine, Central Sierra Nevada, California: Econ. Geol., v. 76, p. 111-133.

Ohlsson, L., 1979, Tungsten occurrances in Central Sweden: Econ. Geol., v. 74, p. 1012-1034.

Perfit, M.R., Gust, D.A., Bence, A.E., Arculus, R.J., and Taylor, S.R., 1980, Chemical characteristics of island-arc basalts: Implications for mantle sources: Chem. Geol., v. 30, p. 227-256.

Plimer, I.R., 1980, Exhalative Sn and W deposits associated with mafic volcanism as precursors to Sn and W deposits associated with granites: Mineral. Deposita, v. 15, p. 275-289.

Rinehart, C.D., and Ross, D.C., 1956, Economic geology of the Casa Diablo Mountain quadrangle, California: California Div. Mines Spec. Rept. 48, 17 p.

------- 1964, Geology and mineral deposits of the Mount Morrison quadrangle, Sierra Nevada, California: U. S. Geol. Survey Prof. Paper 385, 106 p.

Robinson, M.S., 1981, Geology and ground magnetometer survey of the Yellow Pup tungsten deposit, Gilmore Dome, Fairbanks mining district, Alaska: Alaska Div. of Geol. and Geophys. Surveys Open-file Report 137, 9 p., 1 pl. scale 1 in. = 100 ft.

Robinson, M.S., Smith, T.E., and Bundtzen T.K., 1982, Cleary sequence of the Fairbanks mining district, primary stratigraphic control of lode gold/antimony mineralization (abs.): Abstracts with programs, Geol. Soc. of Am. Cordilleran Section Meeting, Anaheim, California.

Shimazaki, H., 1982, The Sansano hastingsite-bearing copper skarn deposit formed in the aluminous sediment, at the Yoshioka Mine, Japan: Econ. Geol., v. 77, p. 868-876.

Silberman, M.L., Berger, B.R., Koski, R.A., 1974, K-Ar Age relations of granodiorite emplacement and tungsten and gold mineralization near the Getchell Mine, Humbolt County, Nevada: Econ. Geol., v. 69, p. 646-656.

Smith, T.E., Robinson, M.S., Bundtzen, T.K., and Metz, P.A., 1981, Fairbanks mining district in 1981: New look at an old mineral province [abs.]: The Alaska Miner, v. 9, no. 11, Nov. 1981.

So, C.S., 1968, Die Scheelit-Lagerstatte Sangdong: Unpubl. Doct. thesis, Univ. Munich, 71 p.

Sonnevil, R.A., 1979, Evolution of skarn at Monte Cristo, Nevada: Unpubl. M.S. thesis, Stanford Univ., 81 p.

Stumpfl, E.F., 1977, Sediments, ores and metamorphism: new aspects: Phil. Trans. R. Soc. Lond. A., v. 286, p. 507-525.

Tempelman-Kluit, D.J., 1976, The Yukon crystalline terrane: Enigma in the Canadian Cordillera: Geol. Soc. of Am. Bull., v. 87, p. 1343-1357.

Thorne, R.L., and others, 1948, Tungsten deposits in Alaska: U.S. Bureau of Mines Reports of Investigations 4174, 51 p.

Tweto, O., 1960, Scheelite in the Precambrian gneisses of Colorado: Econ. Geol., v. 55, p. 1406-1428.

Wilson, F.H., Smith, J.G., and Shew, N., 1985, Reviews of radiometric data from the Yukon Crystalline Terrane, Alaska and Yukon Territory: Can. Jour. Earth Sci., v. 22 p. 525-537.

Winkler, H.G.F., 1979, Petrogenesis of Metamorphic Rocks: Springer-Verlag, Berlin, 348 p.

Zaw, U.K., 1976, The Cantung E-zone ore body, Tungsten, Northwest Territories - A major scheelite skarn deposit: Unpubl. M.S. thesis, Queens Univ., Kingston, Ont., 327 p.

Zharikov, V.A., 1970, Skarns: Internat. Geology Rev., v.12, p. 541-559, 619-647, 760-775.

Zharikov, V.A. and Vlasova, D.K., 1972, Alteration and ore mineralization in the skarns of the Maikhura deposit, in 24th Internat. Geol. Cong., Sect. 4, p. 509-518.

Zhelyaskova-Panajotova, M., Petrussenko, Sv., and Illev, Z., 1972, Tungsten and bismuth-bearing skarns of the Sangdong type from the region of the Seven Rila Lakes in Bulgaria, in 24th Internat. Geol. Cong., Sect. 4, p. 519-522.

APPENDICES

Appendix I

Abbreviations used in text and plates

alm	almandine	$Fe_3Al_2Si_3O_{12}$
amph	amphibole	$X_{2-3}Y_5Z_8O_{22}(OH)_2$
ad	andradite	$Ca_3Fe_2Si_3O_{12}$
bio	biotite	$K(Mg,Fe)_3(AlSi_3O_{10})(OH)_2$
chl	chlorite	$(Mg,Fe)_3(Si,Al)_4O_{10}(OH)_2$ $(Mg,Fe)_3(OH)_6$
clz	clinozoisite	$Ca_2Al_3O(SiO_4)Si_2O_7(OH)$
cc	calcite	$CaCO_3$
di	diopside	$CaMgSi_2O_6$
garn	garnet	$A_3B_2(SiO_4)_3$
gr	grossularite	$Ca_3Al_2Si_3O_{12}$
hd	hedenbergite	$CaFeSi_2O_6$
ido	idocrase	$Ca_{10}(Mg,Fe)_2Al_4(SiO_4)_5$ $(Si_2O_7)_2(OH)_4$
jo	johannsenite	$CaMnSi_2O_6$
pl	plagioclase	$NaAlSi_3O_8$-$CaAl_2Si_2O_8$
po	pyrrhotite	$Fe_{1-x}S$
pyr	pyrite	FeS_2
pyx	pyroxene	XYZ_2O_6
qtz	quartz	SiO_2
sch	scheelite	$CaWO_4$
sp	spessartine	$Mn_3Al_2Si_3O_{12}$

sph	sphene	$CaTiO(SiO_4)$
wm	white mica	$(K,Na)Al_2(AlSi_3O_{10})(OH)_2$
wo	wollastonite	$CaSiO_3$
altd	altered	
endo	endoskarn	
mb	marble	
skn	skarn	
G	Gil	
SH	Spruce Hen	
Step	Stepovich	
YP	Yellow Pup	

Appendix II

Mineral Analysis

Minerals selected as examples of the various rock and alteration types from the three skarn prospects discussed as well as other skarns from the Gilmore Dome area were analysed by electron microprobe techniques. Analyses of 309 samples were derived using a Cameca Electron Microprobe at Washington State University in Pullman, Washington. The samples were analysed using a 15 KV beam current, a beam diameter of 2um, and a 10 second counting time. Standards employed included well-characterized spessartine, diopside, orthoclase, albite, amd olivine samples. Most of the data reduction was done by computer programs at Washington State University.

Calculation of garnet molecular end members was based on the distribution of Ca, Mn, Fe^{2+}, Fe^{3+}, and Al for 16 cations. Total Fe was distributed between Fe^{2+} and Fe^{3+} assuming ideal stoichiometery; the trivalent site was filled with Al^{3+} and enough Fe to satisfy the site requirements of two cations. The andradite component was then calculated as the ratio of Fe^{3+} to Al + Fe^{3+} and the Al to Al + Fe^{3+} ratio represents the grossular + spessartine + almandine + pyrope component. The grossular component of the grossular + spessartine + almandine garnet component was calculated as the ratio of Ca to Ca + Mn + Fe^{2+} + Mg. Spessartine and

almandine are assumed to compose the remainder of the garnet.

Clinopyroxene compositions were calculated based on the distribution of Fe, Mn, and Mg per 4 oxygen. The hedenbergite component is represented by the ratio of Fe to Fe + Mg + Mn, the diopside component as the ratio of Mg to Fe + Mg + Mn, and the ratio of Mn to Fe + Mg + Mn as the johannsenite component. Molecular end members for all other minerals were calculated using standard techniques (Deer et al., 1966).

Table 1. Metamorphic garnet compositions from Gilmore Dome. Representative samples listed.

Sample Number	SH-8 3-79r	SH-8 3-80c	YP-B16 3-91	CB-1 4-23	YPM 7-3	CB-2 4-21
Location	SH	SH	YP	YP	YP	YP
Weight Percent						
SiO_2	38.93	39.11	38.65	38.60	38.56	38.78
CaO	35.90	35.61	35.88	35.57	34.78	35.18
Al_2O_3	19.87	18.94	19.97	19.32	19.72	20.01
TiO_2	0.46	0.91	1.35	1.49	0.49	1.39
MgO	0.15	0.09	0.08	0.07	0.10	0.10
MnO	0.00	0.04	0.75	0.65	1.17	0.71
Na_2O	0.05	0.00	0.03	0.06	0.00	0.00
FeO*	4.57	5.54	2.92	4.70	5.57	4.10
K_2O	0.02	0.01	0.00	0.00	0.00	0.00
Total	99.92	100.25	99.63	100.46	100.37	100.27
Mole Percent						
Gr	87.2	84.4	89.5	85.2	83.1	87.2
Ad	10.8	14.0	9.5	12.8	12.0	9.7
Alm & Sp	2.0	1.6	1.0	2.0	4.9	3.1

* Total iron as FeO

Table 2. Early skarn garnet compositions from Gilmore Dome. Representative samples listed.

Sample Number	SH-7 3-75c	SH-7 3-74r	YP-B16 4-8	SH-12 3-59	Step 12 4-12c	Step 12 4-13r
Location	SH	Sh	YP	SH	Step	Step
Weight Percent						
SiO_2	38.11	37.81	37.74	38.11	38.19	37.46
CaO	34.03	33.43	34.49	34.40	34.74	33.90
Al_2O_3	18.03	16.81	18.48	19.06	18.97	17.88
TiO_2	0.17	0.21	0.32	0.23	0.12	0.13
MgO	0.00	0.01	0.04	0.01	0.05	0.00
MnO	1.76	1.07	1.05	0.71	1.39	1.13
Na_2O	0.00	0.04	0.07	0.05	0.03	0.00
FeO*	8.11	9.56	7.00	6.86	6.77	8.93
K_2O	0.00	0.00	0.00	0.01	0.02	0.00
Total	100.21	98.94	99.19	99.45	100.28	99.43
Mole Percent						
Gr	75.3	72.4	79.2	80.9	79.6	74.7
Ad	18.9	22.5	16.4	14.0	15.4	19.4
Alm & Sp	5.8	5.1	4.4	5.1	5.0	5.9

* Total iron as FeO

Table 3. Late skarn garnet conpositions from Gilmore Dome. Representative samples listed.

Sample Number	82GA526 10-10	82GA526 10-15	SH-12 3-57	82GA207 10-57	82GA207 10-30	82GA207 10-51
Location	SH	SH	SH	YP	YP	YP
Weight Percent						
SiO_2	36.99	37.32	38.13	37.21	37.29	36.90
CaO	24.99	22.54	25.96	16.93	20.72	19.49
Al_2O_3	19.23	19.52	19.56	19.78	18.59	18.71
TiO_2	0.19	0.19	0.14	0.30	0.37	0.50
MgO	0.05	0.11	0.04	0.26	0.14	0.61
MnO	2.30	3.61	2.48	6.39	6.04	5.24
NaO_2	0.02	0.00	0.02	0.02	0.00	0.08
FeO*	14.25	14.89	13.85	18.17	16.54	17.66
K_2O	0.00	0.01	0.00	0.01	0.00	0.00
Total	98.02	98.19	100.18	99.07	99.69	99.19
Mole Percent						
Gr	63.5	59.3	64.6	45.9	51.4	49.8
Ad	10.1	8.2	10.5	6.5	13.1	12.4
Alm & Sp	26.4	32.5	24.9	47.6	35.5	37.8

*Total iron as FeO

Table 4. Metamorphic pyroxene compositions from Gilmore Dome. Representative samples listed.

Sample Number	YPM 5-8	YPB-16 5-7	YPM 8-29	82GA609 11-9	82GA263 10-58	82GA263 10-68
Location	YP	YP	YP	YP	G	G
Weight Percent						
SiO_2	52.50	52.20	53.26	50.03	50.17	49.64
CaO	24.53	24.62	24.74	24.17	24.05	23.10
Al_2O_3	0.58	0.33	0.19	0.27	0.25	0.48
TiO_2	0.02	0.04	0.03	0.10	0.02	0.09
MgO	10.55	10.13	11.95	9.03	8.40	7.33
MnO	1.36	0.78	1.55	0.85	0.43	0.61
Na_2O	0.12	0.05	0.00	0.09	0.14	0.20
FeO*	11.40	12.43	8.65	14.04	15.52	16.73
K_2O	0.00	0.00	0.00	0.00	0.01	0.01
Total	101.06	100.58	100.37	98.58	98.99	98.19
Mole Percent						
Hd	42.8	36.1	26.9	45.3	50.2	55.0
Di	53.1	59.5	68.2	51.9	48.4	43.0
Jo	4.1	4.4	4.9	2.8	1.4	2.0

*Total iron as FeO

Table 5. Skarn pyroxene compositions from Gilmore Dome. Representative samples listed.

Sample Number	SH-11 5-4	82GA546 5-5	Step 2 5-16	GT1 5-19	82GA263 10-65	82GA526 10-49
Location	SH	SH	Step	G	G	SH
Weight Percent						
SiO_2	49.29	49.79	50.41	49.04	47.84	50.97
CaO	22.89	22.90	23.33	22.46	23.40	24.46
Al_2O_3	0.33	0.23	0.29	0.26	0.39	0.34
TiO_2	0.05	0.00	0.00	0.05	0.11	0.01
MgO	1.75	2.40	3.89	0.44	2.50	10.07
MnO	1.18	1.26	1.25	1.97	1.25	1.62
Na_2O	0.06	0.08	0.13	0.13	0.16	0.06
FeO*	25.08	24.57	21.76	26.72	22.62	11.45
K_2O	0.01	0.02	0.01	0.00	0.04	0.02
Total	100.63	101.25	101.06	101.07	98.30	99.01
Mole Percent						
Hd	85.3	81.6	72.6	90.6	79.8	70.4
Di	10.6	14.2	23.2	2.7	15.7	26.1
Jo	4.1	4.2	4.2	6.7	4.5	3.5

*Total iron as FeO

Table 6. Amphibole compositions from Gilmore Dome. Representative samples listed.

Sample Number	82GA293 1-12	82GA293 1-15	82GA289 1-22	82GA546 14-8	82GA546 14-15	82GA151 14-20
Location	G	G	G	SH	SH	YP
Weight Percent						
SiO_2	39.05	48.18	45.87	46.94	39.83	52.22
CaO	2.09	12.02	12.39	11.60	11.50	11.61
Al_2O_3	13.78	6.10	9.01	5.60	12.36	1.35
TiO_2	0.83	0.19	0.37	0.10	0.34	0.00
MgO	14.23	14.82	11.98	3.40	2.05	10.57
MnO	0.14	0.25	0.35	0.76	0.66	1.00
Na_2O	0.23	1.25	0.12	0.69	1.02	0.13
FeO*	11.34	13.12	15.18	28.34	28.80	19.64
K_2O	6.91	0.25	0.26	0.26	1.54	0.07
Total	100.24	99.21	98.60	99.62	99.99	98.59
Mole Percent						
mg	0.69	0.66	0.58	0.17	0.11	0,48
Si	6.35	7.20	6.89	7.36	6.36	7.88
rock type	amphi-bolite	amphi-bolite w/ sch	amphi-bolite	skn w/ sch	skn w/ pyx	endoskn

*Total iron as FeO

Table 7. Phyllosilicate compositions from Gilmore Dome. Representative samples listed.

Sample Number	82GA214 11-6	82GA609 11-15	82GA716 9-13	82GA716 9-15	82GA716 9-10	82GA716 9-21
Location	YP	YP	YP	YP	YP	YP
Type	WM	WM	WM	CHL	CHL	BIO
Weight Percent						
SiO_2	46.63	47.24	48.33	25.38	26.05	36.06
CaO	0.04	0.00	0.07	0.03	0.03	0.02
Al_2O_3	33.19	29.62	33.83	21.67	21.36	16.94
TiO_2	0.29	0.34	0.02	0.06	0.08	1.65
MgO	1.46	1.96	1.19	13.21	13.15	8.96
MnO	0.00	0.03	0.03	0.51	0.43	0.31
Na_2O	0.53	0.31	0.33	0.05	0.07	0.02
FeO*	1.45	2.56	0.79	26.89	26.42	20.59
K_2O	10.02	10.83	10.30	0.02	0 01	9.14
Total	98.05	97.26	99.42	99.22	98.90	98.57
Mole Percent						
Fe+Mg +Mn	.4594	.7017	.3254			
Fe/ Fe+Mg				.53	.53	.54

*Total iron as FeO

Appendix III

Potassium-Argon data for Gilmore Dome.

Sample Number	K_2O (wt.%)	Mineral	Sample Weight (g)	$^{40}Ar_{rad}$ / (mol/g) $\times 10^{-11}$	$^{40}Ar_{rad}$ / $^{40}K \times 10^{-3}$	$^{40}Ar_{rad}$ / $^{40}Ar_{total}$	Age ± 1σ (m.y.)
82GA511	0.353		0.0424	5.17	5.86	32.61	98.12±5.7
SH	0.356	amph					
pyx	0.360						
skarn	X=0.356						
SH-SP	0.690		0.8318	10.45	6.11	73.4	102.20±3.1
SP	0.690	amph					MINIMUM AGE
amphb	0.690						
	X=0.690						
YP-M-BD	9.350		0.942	118.07	5.10	66.3	85.7±2.6
YP	9.340	wm					
mica	X=9.345						
skarn							
YP-B-16	0.620		0.9162	8.19	5.29	70.3	88.80±2.7
YP	0.630	amph					
amphb	X=0.625						
82GA339	0.630		0.7043	8.22	5.22	0.634	87.7±2.6
Gil	0.637	amph					
pyx	0.640						
skarn	X=0.636						
2359	0.550		1.0085	16.6	12.0	0.737	196.2±5.9
Gil	0.560	amph					
amphb	X=0.555						
81JB131	7.843		0.195	102.33	5.29	86.5	88.90±2.7
Gilmore	7.763	bio					
granite	X=7.803						
81JB149	7.236		0.1196	90.73	5.105	91.27	85.79±2.6
Gilmore	7.112	bio					
granite	X=7.174						

Note: rad = radiogenic, σ = standard deviation, x = mean,

$\epsilon + \epsilon = 0.581 \times 10^{-10}\ yr^{-1}$, $\beta = 4.962 \times 10^{-10}\ yr^{-1}$,

$^{40}K/K_{total} = 1.167 \times 10^{-4}$ mol/mol

minimum age : sample does not meet petrographic criteria for a reliable age (UAF Geochronology Laboratory comment and criteria)

Analyses by J.D. Blum (UAF-ADGGS Geochronology Laboratory)

Appendix IV

Geochemistry

Gilmore Dome rock samples were analysed by the State of Alaska Division of Geological and Geophysical Survey lab in Fairbanks, Alaska. Lead, gold, silver, molybdenum, antimony, and arsenic were analysed by atomic-absorbtion spectrophotometry on aqua-regia digests. Copper, zinc, cobalt, nickel, chromium, iron, manganese, and cadmium were analyzed by inductively coupled plasma atomic-emission spectrophotometry on aqua-regia digests. Lower limits of detection were 1 ppm for lead, antimony, molybdenum, copper, zinc, and cadmium: 10 ppm for arsenic, cobalt, nickel, chromium, iron, and manganese; and 0.1 ppm for gold and silver. Tin, tungsten, and mercury were analyzed by Bondar-Clegg & Company Ltd., Vancouver, B.C. Tungsten was analyzed by colorimetry with a lower detection limit of 2 ppm. Mercury was analysed by cold-vapor atomic-absorbtion spectrophotometry with a lower detection limit of 5 ppb. Tin was analyzed by X-ray fluorescence with a lower detection limit of 5 ppm.

Ten major oxides were identified using X-ray fluorescence spectrometry of fused rock pellets, and FeO was determined by volumetric chemical analysis. The X-ray

fluorescence spectrometer was calibrated using a combination of 19 Canadian and American whole-rock standards.

Table 1. Trace element rock analysis for Spruce Hen rocks.

Field no.	Cu	Pb	Zn	Au	Ag	Mo	Sb	Sn	W	Hg	As	F	Sample type	Description
2277	27	21	67	-0.1	0.1	6	5	-5	11	60	14	230	rc	Iron-stained silver muscovite schist.
2278	14	17	33	-0.1	0.2	5	7	-5	8	65	630	1400	rc	Iron-stained light-gray altered zone.
2279	21	8	17	-0.1	0.2	5	12	-5	8	80	276	380	rc	Iron- and manganese-filled stockwork fractured quartzite.
2280	29	7	65	-0.1	0.1	7	-1	-5	45	55	216	780	rc	Iron-stained silvery quartz schist.
2281	15	214	23	-0.1	0.3	29	140	12	43	35	453	670	rc	Felsic dike cutting quartzite.
2281	29	12	222	0.3	-0.1	112	1	125	1.17%	70	92	+2%	rc	Pyroxene skarn.
2283	28	7	23	0.1	-0.1	10	1	5	125	55	28	1100	rc	Dark green fine-grained schist endoskarn.
2284	51	35	58	0.1	1.1	21	6	18	170	65	1300	2700	rc	Altered mica schist.
2285	22	13	64	0.1	0.2	16	-1	20	340	295	752	3600	rc	Orange saprolitic zone with iron and manganese concretions.
2286	1530	11	136	0.2	0.7	30	46	35	0.19%	120	280	+2%	rc	Bright orange saprolitic zone.
2287	66	13	249	0.4	0.1	23	-1	110	0.55%	75	26	+2%	3'cc	Retrograde zone along edge of skarn unit.
2288	48	10	109	-0.1	-0.1	1	-1	1	1	80	20	810	rc	Muscovite-biotite-quartz schist and micaceous quartzite.
2289	37	8	62	-0.1	-0.1	1	-1	1	1	50	-10	520	rc	Crenulated biotite-muscovite-quartz schist.
2291	32	11	94	-0.1	-0.1	1	-1	2	1	40	-10	440	rc	Quartz-mica schist.
2292	43	8	90	-0.1	-0.1	1	-1	1	1	40	-10	650	rc	Biotite-quartz schist.
2293	18	8	92	-0.1	-0.1	2	-1	1	3	60	-10	1400	rc	Quartz-biotite schist.
2294	9	31	3	-0.1	0.1	10	-1	1	5	40	-10	210	rc	Felsic dike.
2295	157	4460	3050	0.1	23.4	184	440	60	+2000	255	9360	2200	15'rc	South pit, fine-grained felsic dike with pyrite boxworks.
2296	45	26	53	0.1	0.1	12	-1	10	38	60	18	1100	rc	South pit, felsic dike.
2357	7	5	6	0.1	0.1	1	1	1	13	40	82	170	rc	White micaceous quartzite.
2420	6	4	-1	-0.1	-0.1	3	1	5	190	40	-10	170	rc	Iron-stained quartz vein in marble.
2421	1	8	127	-0.1	-0.1	15	6	80	880	75	-10	1.6%	4'cc	Idocrase marble with pyroxene and garnet skarn zones.
2422	831	13	174	-0.1	0.8	13	1	30	1010	70	546	+2%	8'cc	Orange stained marble with felsic layers.
2423	23	9	50	-0.1	-0.1	9	1	8	675	55	23	2800	2'cc	Schist endoskarn, very silic with remnant schist layers.
2424	53	19	108	-0.1	-0.1	8	14	10	270	80	652	2400	4'cc	Strongly ironed-stained schist cut by felsic dike.
2425	19	13	140	-0.1	-0.1	10	7	32	920	80	834	9000	6'cc	Dark brown manganese-stained saprolitic zone with remnant idocrase.
2426	15	13	126	-0.1	-0.1	42	5	60	0.27%	55	220	+2%	5'cc	Pyroxene-garnet skarn separated by schist layers.
2427	2	10	260	-0.1	-0.1	29	1	35	0.39%	55	246	+2%	10'cc	Pyroxene-garnet skarn.
2428	5	3	2	-0.1	-0.1	4	1	5	170	30	-10	550	rc	Quartz-feldspar vein.
2429	7	14	107	-0.1	-0.1	4	1	5	73	40	-10	3200	rc	Dark blue-gray quartz-biotite schist with quartz veinlets.
2430	57	3	62	-0.1	-0.1	1	1	1	5	280	10	3800	rc	Dark green foliated, dense, amphibole endoskarn.
2431	4	12	216	0.3	-0.1	126	5	140	1.15%	65	29	+2%	4'cc	Retrograded pyroxene skarn.
2432	2	10	252	-0.1	-0.1	38	3	65	0.64%	65	-10	+2%	rc	Pyroxene-garnet-idocrase skarn.
2433	1	8	139	0.1	-0.1	25	4	80	1350	40	-10	+2%	rc	Retrograded pyroxene skarn.
2434	213	10	308	0.1	-0.1	47	1	60	0.23%	40	-10	+2%	rc	Pyroxene-garnet-idocrase skarn.
2435	3	10	173	0.8	0.1	64	12	160	0.57%	55	-10	+2%	rc	Pyroxene-garnet-idocrase skarn.
2436	13	17	3	-0.1	0.5	6	9	-5	120	40	241	1500	rc	Strongly iron-stained quartz vein.
2437	2	8	160	-0.1	-0.1	13	4	37	765	45	-10	1.6%	2'cc	Dark green fine-grained pyroxene skarn.
2438	5	12	9	-0.1	-0.1	9	5	-5	18	50	-10	600	rc	Felsic dike parallel to foliation.
2439	5	3	1	0.3	-0.1	5	4	-5	630	35	-10	430	rc	Iron-stained quartz vein.
2440	14	18	9	0.1	-0.1	47	2	-5	380	70	-10	410	rc	Felsic dike.
2441	22	4	43	-0.1	-0.1	1	1	1	1	90	-10	1400	rc	South of main pit, dark green coarse-grained amphibolite.
2442	1	10	76	-0.1	-0.1	11	10	30	1420	60	-10	1.8%	2'cc	Wollastonite skarn and marble.
2443	13	10	252	0.2	-0.1	6	-1	120	800	55	-10	+2%	rc	Contact between dark green skarn and schist endoskarn.

rc = random chip sample
cc = chip channel sample
+ = greater than
- = less than
Hg in ppb, all others in ppm unless noted

Field no.	Cu	Pb	Zn	Au	Ag	Mo	Sb	Sn	W	Hg	As	F	Sample type	Description
2444	136	15	33	5.5	0.5	9	<1	20	1.07%	75	135	830	rc	Altered felsic dike, with visible scheelite.
2445	56	28	67	<0.1	0.1	3	<1	<5	20	50	<10	2100	rc	Silicified schist.
2446	1310	31	159	<0.1	0.4	9	<1	10	0.27%	80	82	>2%	rc	Contact between retrograded skarn and amphibolite-rich endo-skarn with sulfides.
2447	331	9	140	<0.1	0.1	7	2	<5	1125	75	<10	>2%	rc	Along contact with skarn and schist.
2448	8	3	7	<0.1	0.1	6	6	<5	32	50	18	150	rc	Iron-stained quartz vein.
2449	16	4	57	<0.1	0.2	12	11	5	90	80	323	640	rc	Altered quartz schist.
2450	18	12	58	<0.1	0.1	10	3	5	19	60	80	200	rc	Iron-stained silver quartz-muscovite schist.
4630	139	3	38	<0.1	0.1	1	1	1	1	150	<10	660	rc	South pit, massive amphibolite.

Table 2. Trace element rock analysis for Yellow Pup rocks.

Field no.	Cu	Pb	Zn	Au	Ag	Mo	Sb	Sn	W	Hg	As	B	Be	F	Sample type	Description
2230	26	9	63	<0.1	<0.1	3	<1	5	610	20	<10	130	720	630	2' cc	Altered quartz mica schist with scheelite.
2231	13	29	108	<0.1	0.2	24	<1	5	0.71%	35	<10	95	600	1100	1' cc	Scheelite in altered zone.
2232	110	8	8	<0.1	0.1	2	<1	5	8	70	36	925	360	540	1½ cc	Pyrite and stibnite vein.
2233	26	12	59	<0.1	<0.1	1	<1	5	8	15	<10	165	450	590	rc	Iron oxide zone in high grade scheelite pod.
2234	3	12	65	0.3	0.1	2	<1	5	4	10	<10	215	2080	800	3' cc	Scheelite high grade pod zone.
2235	13	8	47	0.2	0.2	18	<1	5	1.60%	30	<10	75	670	1200	3' cc	Scheelite high grade pod zone below iron oxide zone.
2236	4	9	42	<0.3	0.1	5	<1	5	900	20	<10	90	300	570	2' cc	Scheelite in calc-silicate marble skarn.
2237	25	6	19	<0.1	0.1	2	<1	5	8	20	<10	30	90	240	rc	Quartz vein.
2238	2	21	69	0.5	0.1	3	<1	5	96	20	<10	45	680	980	3' cc	Quartz and garnet zone in calc-silicate marble.
2239	714	16	59	<0.5	0.3	3	<1	5	9	25	<10	215	350	630	2' cc	Quartz vein with copper staining.
2240	4	2	54	<0.5	0.1	3	<1	5	2	20	<10	150	690	1050	2' cc	Calc-silicate layer within marble.
2241	23	18	78	<0.1	0.1	3	<1	5	3	40	<10	75	540	760	2' cc	Calcareous schist with many veinlets.
2242	132	99	205	0.3	0.2	3	<1	5	15	15	96	135	420	470	2' cc	Stibnite vein.
2243	27	17	58	<0.1	0.1	2	<1	5	3	55	<10	235	490	850	2' cc	Quartz-scheelite vein in weathered marble zone.
2244	2	8	89	<0.1	0.1	2	<1	5	3	25	<10	265	650	850	2' cc	Disseminated scheelite zone.
2246	32	8	65	<0.5	0.5	2	<1	5	6	10	<10	250	700	800	4' cc	Quartz mica schist.
2247	2	5	60	<0.5	<0.1	1	<1	5	3	20	<10	370	780	760	2' cc	Quartz mica schist.
2248	53	5	30	<0.1	0.2	2	<1	5	3	20	<10	45	70	310	2' cc	Quartz vein.
2249	25	2	16	<0.1	0.1	1	<1	5	6	10	<10	150	4040	760	2' cc	Micaceous quartzite.
2250	4	7	52	0.1	<0.1	3	<1	5	380	10	<10	150	490	730	4' cc	Layered calc-silicate.
2251	29	ND	42	ND	ND	ND	ND	5	3	10	ND	40	300	490	2' cc	Manganese rich zone.
2252	19	23	71	<0.1	<0.1	2	<1	5	33	20	<10	335	710	730	2' cc	Near scheelite pod zone, quartz mica schist.
2253	28	3	55	0.2	<0.1	55	<1	5	2.89%	10	<10	65	410	980	3' cc	Near scheelite pod zone, high grade.
2255	25	9	59	<0.3	0.2	3	<1	5	?	10	<10	110	670	690	2' cc	Scheelite in calc-silicate layers.
2256	8	1	4	<0.1	0.1	3	<1	5	9	30	<10	20	20	80	rc	Quartz vein.
2257	15	4	70	0.1	0.2	2	<1	5	3	15	<10	170	550	690	rc	Fault intersection.
2260	ND	4	ND	0.6	0.1	6	<1	5	0.31%	10	32	35	320	5600	2' cc	Amphibole-white mica-chlorite-scheelite-quartz vein along joint face.
2261	ND	7	ND	<0.1	<0.1	2	<1	6	22	20	<10	165	740	2000	rc	Stepovich Dump, massive amphibolite.
2262	ND	4	ND	<0.5	<0.1	3	<1	5	5	215	<10	30	270	1500	rc	Stepovich Dump, massive amphibolite.
2263	1	2	60	0.1	<0.1	3	<1	5	3	140	<10	20	90	1100	rc	Stepovich Dump, massive amphibolite.
2264	ND	3	ND	<0.5	<0.1	8	<1	5	0.28%	50	<10	15	80	270	4' cc	Scheelite in quartz vein.
2265	ND	8	ND	0.5	<0.5	7	<1	10	0.21%	110	ND	30	610	850	3' cc	Retrograded layered calc-silicate marble.
2266	ND	7	ND	0.1	<0.1	6	<1	19	1800	60	ND	30	520	1200	3' cc	Retrograded layered calc-silicate marble.
2267	ND	6	ND	0.1	<0.1	7	<1	10	0.24%	25	ND	30	440	1100	1' cc	Scheelite in feldspar-chlorite rich rock.
2268	ND	3	ND	0.1	<0.1	6	<1	27	0.24%	15	ND	25	450	1700	2' cc	Pyroxene-garnet-idocrase-quartz.
2269	ND	4	ND	0.1	<0.1	6	<1	38	0.33%	20	ND	30	210	1500	3' cc	Scheelite in retrograded skarn.
2250	27	2	111	<0.1	<0.1	3	<1	5	3	15	<10	220	750	580	rc	Quartz mica schist.
2251	ND	6	ND	0.1	<0.1	3	<1	26	900	90	<10	45	570	1500	2' cc	Calc-silicate marble skarn.

rc = composite chip sample
cc = chip channel sample
> = greater than
< = less than
ND = Not determined
Hg in ppb, all others in ppm unless noted

Field no.	Cu	Pb	Zn	Au	Ag	Mo	Sb	Sn	W	Mg	As	B	Be	F	Sample type	Description
2257	ND	7	ND	0.1	-0.1	3	1	15	59	240	-10	45	550	1050	1' cc	Shear zone.
2253	ND	4	ND	-0.1	-0.1	4	1	13	1125	25	-10	55	440	1150	2' cc	Amphibole-chlorite-white mica-quartz retrograde zone.
2254	ND	6	ND	0.1	-0.1	8	1	24	0.26%	40	-10	25	260	1150	2' cc	Amphibole-clinozoicite-quartz retrograde zone.
2255	ND	5	ND	-0.1	0.1	3	1	9	85	95	-10	35	730	1100	2' cc	Garnet skarn with quartz and amphibole.
2256	ND	6	ND	-0.1	-0.1	10	1	16	0.26%	15	-10	25	180	1050	2' cc	Quartz vein along joint in calc-silicate marble.
2257	3510	ND	116	ND	ND	ND	ND	-5	4	10	ND	25	610	480	rc	Copper-stained quartz mica schist.
2258	8	8	59	-0.1	-0.1	14	1	6	0.51%	20	-10	25	380	750	rc	Amphibole-clinozoisite-quartz skarn.
2259	7	33	69	0.1	-0.1	4	1	-5	24	75	-10	30	770	750	rc	Vuggy, limonitic layers in skarn retrograded.
2260	163	3	104	0.1	0.2	3	1	-5	3	75	-10	115	780	720	rc	Altered quartz mica schist.
2261	ND	ND	ND	ND		ND	ND	8	21	100	ND	30	580	1150	2' cc	Retrograded skarn.
2262	ND	9	ND	-0.1	-0.1	5	1	5	1400	30	-10	25	290	720	2' cc	Retrograded skarn at fold hinge.
2263	ND	12	ND	-0.1	-0.1	8	1	6	0.26%	110	-10	35	730	680	2' cc	Layered amphibole-chlorite-pyroxene skarn.
2264	ND	8	ND	-0.1	-0.1	9	1	10	0.31%	130	-10	25	730	800	2' cc	Layered amphibole-chlorite-pyroxene skarn.
2265	ND	6	ND	0.2	0.1	25	1	6	1.06%	140	-10	30	200	970	3' cc	Skarn retrograded to quartz-amphibole-scheelite
2266	5	8	58	-0.1	-0.1	2	1	-5	10	140	-10	155	490	480	1' cc	Quartz-amphibole-feldspar vein.
2269	19	14	73	0.1	-0.1	3	1	-5	80	45	-10	ND	ND	1400	1' cc	Disseminated scheelite in granular weathered zone.
2270	1820	31	129	-0.1	-0.1	2	1	-5	2	50	-10	ND	ND	530	2' cc	Copper-stained quartz mica schist.
2271	362	3	73	0.8	0.5	3	1	5	160	25	-10	ND	ND	930	1' cc	Quartz vein near copper-stained schist.
2272	65	15	78	-0.1	-0.1	2	1	-5	3	40	-10	ND	ND	720	2' cc	Shear zone.
2273	12	27	62	-0.1	-0.1	3	2	5	170	30	19	ND	ND	690	2' cc	Scheelite in skarned calc-silicate layers.
2274	5	6	39	-0.1	-0.1	3	1	-5	495	35	-10	ND	ND	550	1' cc	Scheelite in skarned calc-silicate layers.
2275	45	8	93	-0.1	-0.1	3	2	-5	9	35	-10	ND	ND	550	2' cc	Disseminated scheelite in altered schist.
2276	9	4	10	-0.1	-0.1	2	4	-5	2	20	-10	ND	ND	75	1' cc	Quartz vein with copper-staining.
2339	1	2	44	-0.1	-0.1	4	1	50	19	40	-10	ND	ND	2200	12'	Iron-stained quartz vein in YB-B16 trench.
2340	7	1	6	0.2	-0.1	4	1	-5	40	35	-10	ND	ND	70	11'	Quartz vein in amphibolite in YB-B16 trench.

Table 3. Trace element rock analysis for Gil rocks.

Field no.	Cu	Pb	Zn	Au	Ag	Mo	Sb	Sn	W	Hg	As	F	Sample type	Description
2299	3	9	83	-0.1	-0.1	34	-1	6	1.60%	35	-10	440	4' rc	Dark brown altered zone in marble with quartz vein.
2300	22	52	88	-0.1	0.3	9	-1	-5	20	55	-10	510	5' cc	Limonitic altered quartz mica schist.
2301	27	86	94	-0.1	0.6	6	-1	-5	28	50	-10	400	5' cc	Iron-stained light gray quartz mica schist.
2302	20	33	74	-0.1	0.2	5	-1	-5	16	55	-10	460	5' cc	Iron-stained light gray to green chloritic mica schist.
2303	44	61	90	-0.1	0.3	4	-1	-5	21	50	-10	360	4' cc	Strongly iron-stained mica schist with quartz vein.
2304	24	30	96	-0.1	0.1	4	-1	-5	4	40	-10	510	4' cc	Manganese-stained micaceous quartzite.
2305	24	26	60	-0.1	0.1	3	-1	-5	6	45	-10	320	2' cc	Manganese- and iron-stained micaceous quartzite.
2306	48	18	24	1.8	0.3	5	-1	-5	0.25%	20	-10	310	1' cc	Quartz vein amphibolite.
2307	45	19	82	-0.1	0.2	3	-1	-5	15	30	-10	510	5' cc	Manganese-stained fine-grained quartzite.
2308	23	20	67	-0.1	-0.1	3	-1	-5	21	50	-10	440	5' cc	Iron- and manganese-stained interlayered schist and quartzite.
2309	56	21	76	-0.1	-0.1	5	-1	-5	18	50	-10	630	5' cc	Iron-stained quartz muscovite schist.
2310	43	23	47	-0.1	-0.1	5	-1	-5	24	35	-10	310	5' cc	Bleached schist and quartzite.
2311	38	16	76	-0.1	-0.1	3	-1	-5	7	35	-10	490	5' cc	Iron-stained quartz muscovite schist with chlorite.
2312	34	12	91	-0.1	-0.1	4	-1	-5	290	40	-10	800	5' cc	Dark brown gossan zone above marble.
2313	37	8	57	-0.1	-0.1	1	-1	-5	18	40	-10	1550	10' rc	Dark green foliated amphibolite.
2314	64	8	50	-0.1	-0.1	2	-1	-5	6	30	-10	830	10' rc	Dark green amphibolite.
2315	82	9	87	-0.1	-0.1	2	-1	-5	23	40	-10	1400	10' rc	Dark green foliated grading into lighter green massive amphibolite.
2316	34	16	17	0.4	0.1	4	-1	-5	1150	30	-10	210	1' rc	Quartz vein cross-cutting foliation.
2317	36	14	54	-0.1	0.1	4	-1	-5	5	45	-10	460	1' cc	Muscovite-biotite quartz schist.
2318	61	12	79	-0.1	-0.1	2	-1	-5	8	35	-10	1550	9' rc	Green slightly foliated biotite-amphibolite.
2319	51	22	43	-0.1	-0.1	2	3	-5	16	160	-10	1100	10' rc	Dark green foliated to massive plagioclase-amphibolite ± quartz, sulfides.
2320	43	29	109	-0.1	0.3	2	-1	-5	15	25	-10	1600	10' rc	Dark green massive fine-grained biotite-amphibolite.
2321	85	8	80	-0.1	0.1	2	-1	-5	4	40	-10	1500	10' rc	Highly sheared amphibolite.
2322	57	7	57	-0.1	-0.1	2	-1	-5	3	200	-10	930	10' rc	Dark green massive amphibolite.
2323	58	9	64	-0.1	-0.1	2	-1	-5	3	30	-10	1100	10' rc	Dark green massive amphibolite.
2324	42	31	77	-0.1	0.2	3	-1	6	315	80	-10	690	1' cc	Granular weathered zone in marble.
2325	18	16	78	-0.1	-0.1	3	-1	8	115	40	-10	800	3' cc	Dark brown weathered marble and skarn.
2326	8	15	7	-0.1	-0.1	5	-1	-5	2	15	-10	280	1' cc	Light gray marble with green pyroxene.
2327	7	9	10	-0.1	-0.1	2	-1	-5	160	290	-10	85	1' cc	Quartz vein.
2328	6	7	9	-0.1	-0.1	4	-1	-5	22	30	-10	50	2' cc	Quartz vein.
2329	6	7	11	-0.1	-0.1	5	-1	-5	560	30	-10	140	rc	Quartz vein in layered calc-silicate quartzite.
2330	5	13	8	-0.1	-0.1	5	-1	-5	6	25	-10	260	3' rc	Green pyroxene-bearing marble.
2331	64	6	54	0.1	0.1	2	-1	-5	3	45	-10	1300	4' rc	Dark green foliated amphibolite.
2332	57	9	57	-0.1	0.1	2	-1	-5	5	30	-10	1500	4' rc	Gray green fine-grained massive amphibolite.
2333	8	6	8	-0.1	-0.1	4	-1	-5	40	15	-10	65	2' cc	Quartz vein.
2334	14	13	26	-0.1	0.1	4	-1	-5	32	40	-10	120	2' cc	Finely laminated quartzite.
2335	23	8	11	-0.1	0.1	5	-1	-5	12	90	-10	45	4" cc	Quartz vein.
2336	6	5	3	0.2	0.1	2	-1	-5	12	200	-10	95	20' rc	Quartz vein crosscutting foliation.
2337	6	7	5	5.2	0.3	4	-1	-5	20	65	-10	85	30' rc	Quartz vein running down center of trench.
2338	55	4	8	-0.1	-0.1	4	-1	-5	14	45	-10	170	4' rc	Quartz vein crosscutting foliation.
2341	24	9	33	-0.1	-0.1	4	-1	-5	50	30	-10	190	rc	Quartz vein parallel to foliation.

rc = composite chip sample
cc = chip channel sample
+ = greater than
- = less than
ND = Not determined
Hg in ppb, all others in ppm unless noted

Field no.	Cu	Pb	Zn	Au	Ag	Mo	Sb	Sn	W	Mg	As	F	Sample type	Description
2342	6	14	4	-0.1	-0.1	5	-1	-5	20	70	-10	45	12' rc	Milky white quartz vein with minor iron staining.
2343	8	8	102	-0.1	0.1	5	-1	-5	68	65	-10	640	rc	White micaceous quartzite.
2344	41	11	46	-0.1	-0.1	4	-1	5	18	170	-10	510	3' cc	Highly stained and fractured laminated quartzite.
2345	13	4	21	-0.1	-0.1	4	-1	-5	30	30	-10	55	3' rc	Highly stained and fractured quartz vein.
2346	65	22	85	-0.1	-0.1	4	-1	-5	215	70	-10	880	rc	Weathered granular layered marble zone above pegmatite.
2347	8	12	11	-0.1	-0.1	4	-1	-5	16	30	-10	340	rc	Quartz-feldspar pegmatite.
2348	10	9	63	-0.1	-0.1	21	-1	-5	3	25	-10	760	rc	Garnet-plagioclase-amphibole rock with minor sulfides.
2349	46	17	65	-0.1	0.2	5	-1	-5	520	70	-10	590	rc	Dark orange granular zone above marble.
2350	10	7	35	-0.1	-0.1	6	-1	-5	4	40	-10	190	rc	Iron stained gray marble.
2351	56	22	76	-0.1	0.3	6	-1	-5	85	90	-10	1300	3' rc	Dark brown granular marble zone.
2352	11	2	79	0.1	-0.1	46	-1	-5	2,438	185	-10	260	4' rc	Dark brown weathered pyroxene skarn with quartz vein.
2353	7	1	5	-0.1	-0.1	4	-1	-5	14	20	-10	40	rc	Quartz vein.
2354	74	8	171	-0.1	0.2	10	-1	5	790	40	-10	1000	rc	Strongly iron-stained schist.
2355	8	7	2	-0.1	-0.1	4	-1	-5	13	20	-10	50	rc	Quartz vein in biotite-muscovite-quartz schist.
2356	13	1	4	-0.1	-0.1	5	-1	-5	160	25	-10	35	1' rc	Iron-stained quartz vein.
2359	62	2	37	-0.1	-0.1	1	-1	1	1	350	-10	430	rc	Dark green fine-grained massive amphibolite.
2360	4	1	114	-0.1	-0.1	3	-1	1	1	60	-10	980	rc	Dark green fine-grained massive amphibolite.
2361	4	6	23	-0.1	-0.1	3	-1	-5	15	30	-10	340	7' rc	Blue-gray fine-grained quartzite.
2362	10	4	21	-0.1	-0.1	3	-1	-5	9	30	-10	370	8' rc	Blue gray fine-grained micaceous quartzite.
2363	52	6	55	-0.1	-0.1	1	-1	1	7	60	-10	740	rc	Green medium grained amphibole altered quartz-feldspar pegmatite.
2364	53	6	60	-0.1	-0.1	3	-1	-5	340	40	-10	1100	rc	Gray calc-silicate bearing micaceous quartzite.
2365	4	8	32	-0.1	-0.1	3	-1	-5	58	160	-10	780	rc	Retrograded calc-silicate marble.
2366	5	7	18	-0.1	-0.1	5	-1	-5	695	50	-10	550	3' rc	Green calc-silicate quartzite.
2367	4	2	2	3.6	0.3	4	-1	-5	16	30	-10	75	rc	Iron- and manganese-stained quartz vein parallel to foliation.
2368	44	33	38	-0.1	-0.1	3	-1	-5	8	115	-10	260	1' cc	Thinly interlayered marble, quartzite, and calcareous quartzite.
2369	18	6	34	-0.1	-0.1	2	-1	-5	3	255	-10	160	2' rc	Iron-stained layers in micaceous quartzite.
2370	15	4	24	-0.1	-0.1	4	-1	-5	8	110	-10	330	rc	Quartz vein with feldspar selvage.
2371	19	7	10	-0.1	-0.1	1	-1	1	3	30	-10	130	rc	Iron-stained white micaceous quartz schist.
2372	22	25	65	-0.1	-0.1	5	-1	-5	16	35	-10	290	2' rc	Altered, highly fractured iron- and manganese-stained micaceous quartz schist.
2373	33	3	48	-0.1	-0.1	2	-1	-5	4	140	-10	450	rc	Strongly iron-stained laminated quartzite.
2374	13	6	65	-0.1	-0.1	4	-1	-5	4	40	-10	580	1' rc	Iron-stained feldspathic micaceous quartzite.
2375	5	3	75	-0.1	-0.1	29	-1	-5	0.98%	125	-10	320	rc	Dark green medium-grained pyroxene skarn next to quartz vein.
2376	46	12	76	-0.1	-0.1	3	-1	35	17	ND	-10	500	10' rc	Granular orange altered zone in quartzite, schist, and marble.
2377	27	10	51	-0.1	-0.1	5	-1	-5	135	ND	-10	740	8' rc	Altered zone in thinly interlayered quartzite, schist, and marble
2378	42	22	106	-0.1	-0.1	3	-1	30	23	ND	-10	1100	5' rc	Granular, dark brown weathered marble zone.
2379	13	14	38	-0.1	-0.1	4	-1	8	13	ND	-10	430	rc	Quartz-feldspar vein or pegmatite.
2380	26	16	70	-0.1	-0.1	3	-1	38	63	ND	-10	580	2' rc	Alteration halo around quartz-feldspar vein.
2381	8	11	10	-0.1	-0.1	4	-1	-5	25	ND	-10	130	rc	Quartz-feldspar vein parallel to foliation.
2382	7	3	1	-0.1	-0.1	4	-1	-5	6	ND	-10	95	rc	Quartz vein with iron staining.
2383	4	10	18	-0.1	-0.1	5	-1	-5	6	ND	-10	100	rc	Blue-gray quartzite.
2384	138	2	45	-0.1	-0.1	1	-1	1	1	70	18	820	rc	Fine-grained massive amphibolite.
2385	2	2	1	-0.1	-0.1	5	-1	-5	3	ND	-10	30	rc	Quartz vein.
2386	9	13	12	-0.1	-0.1	4	-1	-5	3	ND	-10	60	rc	Quartz-feldspar vein with light green chlorite.
2387	6	7	6	-0.1	-0.1	2	2	-5	16	ND	-10	70	2' rc	Iron- and manganese-stained micaceous quartzite.
2388	4	3	4	-0.1	-0.1	3	2	-5	9	ND	-10	50	rc	Quartz vein with feldspar.
2389	4	5	41	-0.1	0.4	71	1	1	600	40	-10	220	rc	Dark green medium-grained pyroxene skarn.
2390	5	4	33	-0.1	-0.1	3	1	-5	6	ND	-10	65	19' rc	Quartz vein.
2391	3	3	1	-0.1	-0.1	4	3	-5	6	ND	-10	40	8' rc	Quartz vein.
2392	5	2	4	-0.1	-0.1	3	3	-5	6	20	-10	25	rc	Quartz vein.
2393	9	5	11	-0.1	-0.1	80	1	-5	9	30	-10	110	rc	1,304 ft, highly fractured, iron-stained quartz vein.

Table 4. Major oxide analysis for Gilmore Dome rocks.

sample	2288	2289	2291	2292	2293	2294
MAJOR OXIDES						
SiO2	54.66	71.54	58.89	59.70	58.52	75.56
Al2O3	22.15	14.37	21.30	17.93	18.31	13.20
Fe2O3	3.88	1.68	2.06	1.65	0.02	0.07
FeO	4.33	1.71	3.38	4.80	6.40	0.14
MgO	2.19	1.35	2.09	2.98	3.39	0.07
CaO	0.59	0.16	0.16	2.04	2.70	0.61
Na2O	0.82	0.65	0.74	1.77	1.53	3.81
K2O	6.21	4.27	5.12	5.22	5.04	4.46
TiO2	0.87	0.68	0.83	0.72	0.72	0.03
P2O5	0.12	0.04	0.05	0.10	0.09	0.07
MnO	0.08	0.09	0.04	0.16	0.18	0.02
LOI	2.55	2.24	3.48	1.14	1.34	0.27
H2O-	0.70	0.71	0.67	0.46	0.66	0.28
Fe2O3t	8.69	3.58	5.82	6.98	7.13	0.23
total	99.15	99.49	98.81	98.67	98.90	98.59
TRACE ELEMENTS						
Cu	48	37	32	43	18	9
Pb	10	8	11	8	8	31
Zn	109	62	94	90	92	3
Au	<10	<10	<10	<10	<10	<10
Ag	<0.1	<0.1	<0.1	<0.1	<0.1	<0.1
Mo	<1	1	1	<1	2	10
Sb	<1	<1	<1	<1	0	<1
Sn	1	1	2	1	1	1
W	1	1	1	1	3	5
Hg	80	50	40	40	60	40
As	20	<10	<10	<10	<10	<10
Co	18	5	11	17	17	<1
Ni	48	9	35	52	49	5
Fe	72500	30200	53900	65300	68100	2400
Mn	200	400	400	1200	1400	100
F	810	520	440	650	1400	210
Cr	92	99	77	102	103	42
Cd	<1	<1	<1	<1	<1	<1

Rock descriptions located in trace element tables 1,2,and 3.
All values in ppm except Au and Hg in ppb.

Table 4 continued.

sample	2357	2371	2389	2394	2395	2396
MAJOR OXIDES						
SiO2	94.59	90.39	66.22	61.08	71.52	89.26
Al2O3	2.76	4.47	5.48	18.93	13.98	4.81
Fe2O3	0.23	0.92	2.20	5.89	4.38	0.66
FeO	0.24	0.44	9.13	1.07	0.42	0.63
MgO	0.02	0.12	1.47	2.01	0.70	0.19
CaO	0.07	0.22	10.56	0.29	0.15	0.17
Na2O	0.10	0.90	1.32	1.41	0.49	0.77
K2O	0.30	0.90	0.12	4.56	3.17	1.03
TiO2	0.19	0.20	0.32	1.00	0.63	0.19
P2O5	0.01	0.03	0.21	0.12	0.11	0.05
MnO	0.00	0.04	0.67	0.11	0.01	0.07
LOI	0.91	0.72	0.42	2.79	2.99	0.53
H2O-	0.28	0.13	0.24	0.13	0.32	0.20
Fe2O3t	0.50	1.41	12.35	7.08	4.43	0.36
total	99.70	99.48	98.36	99.39	98.87	98.56
TRACE ELEMENTS						
Cu	7	19	4	2	8	27
Pb	5	7	5	4	5	10
Zn	6	10	41	91	24	16
Au	<10	<10	<10	<10	<10	<10
Ag	<0.1	<0.1	0.4	0.1	0.1	0.1
Mo	<1	<1	71	<1	<1	2
Sb	<1	<1	<1	<1	<1	<1
Sn	1	1	1	2	1	1
W	13	3	600	8	17	1
Hg	40	30	40	20	30	30
As	82	<10	<10	<10	<10	<10
Co	<1	2	6	21	5	3
Ni	8	8	20	56	13	6
Fe	4800	10200	51700	34300	32000	6000
Mn	<1	100	2300	800	100	100
F	170	130	220	420	290	90
Cr	43	64	65	44	55	86
Cd	<1	<1	<1	<1	<1	<1

Table 4 continued.

sample	2397	2398	2399	2400	2401	2404
MAJOR OXIDES						
SiO2	66.18	58.59	66.89	72.57	72.58	83.20
Al2O3	16.22	19.02	14.65	13.76	13.65	8.09
Fe2O3	2.15	1.47	3.99	2.43	2.15	1.65
FeO	3.96	5.56	2.79	0.35	0.60	1.23
MgO	1.59	1.64	1.64	0.83	1.13	0.59
CaO	1.05	0.46	0.67	0.32	0.44	0.20
Na2O	1.85	6.47	2.06	1.70	1.50	1.60
K2O	3.24	3.44	3.30	2.87	2.72	1.77
TiO2	0.88	1.02	1.07	0.68	0.66	0.45
P2O5	0.30	0.20	0.46	0.12	0.09	0.10
MnO	0.14	0.08	0.03	0.01	0.02	0.02
LOI	1.81	0.75	1.75	2.62	2.67	1.18
H2O-	0.24	0.06	0.15	0.16	0.14	0.03
Fe2O3t	6.55	7.65	7.09	2.82	2.82	3.02
total	99.61	98.76	99.45	98.42	98.35	100.11
TRACE ELEMENTS						
Cu	38	28	29	29	35	14
Pb	4	1	1	12	6	3
Zn	58	24	80	26	39	40
Au	<10	<10	<10	<10	<10	<10
Ag	<0.1	<0.1	<0.1	0.2	0.1	0.1
Mo	3	<1	1	3	2	2
Sb	<1	<1	<1	<1	1	1
Sn	1	1	1	1	1	1
W	1	1	1	4	5	2
Hg	30	40	30	30	110	30
As	<10	<10	<10	<10	<10	<10
Co	15	<1	16	5	3	6
Ni	37	51	47	8	7	17
Fe	46500	67200	55700	75800	23600	25700
Mn	400	500	100	<1	100	200
F	400	340	530	440	440	130
Cr	92	115	49	82	100	79
Cd	<1	<1	<1	<1	<1	<1

Table 4 continued.

sample	2405	2406	2408	2409	2410	2411
MAJOR OXIDES						
SiO2	90.63	63.47	69.76	59.04	89.85	68.44
Al2O3	4.36	16.78	13.98	19.71	4.07	15.74
Fe2O3	0.71	1.87	5.36	3.44	0.76	2.22
FeO	0.40	4.15	1.05	4.65	0.75	3.01
MgO	0.20	2.18	1.66	2.06	0.33	1.50
CaO	0.25	1.55	0.80	0.50	0.77	0.42
Na2O	1.29	1.34	1.71	1.30	0.79	1.10
K2O	0.72	4.47	2.97	5.10	1.22	3.30
TiO2	0.15	0.91	0.63	1.08	0.19	0.63
P2O5	0.21	0.14	0.14	0.21	0.07	0.11
MnO	0.05	0.07	0.17	0.09	0.06	0.06
LOI	0.46	1.67	1.72	2.34	0.51	2.47
H2O-	0.26	0.06	0.16	0.07	0.06	0.36
Fe2O3t	1.16	6.48	6.53	8.61	1.59	5.57
total	99.69	98.66	100.11	99.59	99.43	99.36
TRACE ELEMENTS						
Cu	27	49	9	88	11	51
Pb	7	5	1	4	6	5
Zn	36	86	74	100	15	60
Au	<10	<10	<10	<10	<10	<10
Ag	<0.1	<0.1	<0.1	<0.1	0.1	0.1
Mo	3	3	1	2	<1	<1
Sb	<1	<1	<1	<1	<1	<1
Sn	1	1	3	2	2	1
W	5	4	1	1	3	3
Hg	30	30	20	70	40	40
As	<10	<10	<10	<10	<10	<10
Co	4	20	19	26	4	12
Ni	5	45	39	43	12	32
Fe	7000	52500	32000	67300	11900	42300
Mn	300	300	700	400	400	200
F	120	500	470	490	90	270
Cr	73	99	120	94	94	129
Cd	<1	<1	<1	<1	<1	<1

Table 4 continued.

sample	2412	2413	2414	2415	2417	2418
MAJOR OXIDES						
SiO2	86.99	94.42	89.67	52.55	58.50	84.95
Al2O3	6.45	1.99	4.69	25.93	21.60	6.92
Fe2O3	0.92	0.39	0.39	1.97	4.52	0.73
FeO	1.11	0.66	0.81	2.77	3.13	1.37
MgO	0.46	0.19	0.40	1.96	1.66	0.50
CaO	0.39	0.18	0.39	0.31	0.20	0.59
Na2O	1.63	0.52	1.36	0.85	0.73	1.00
K2O	1.19	0.42	0.88	7.29	4.11	1.19
TiO2	0.31	0.10	0.23	0.93	0.90	0.34
P2O5	0.04	0.01	0.08	0.20	0.13	0.06
MnO	0.03	0.04	0.03	0.04	0.06	0.24
LOI	0.49	0.28	0.44	4.28	2.98	1.00
H2O-	0.16	0.14	0.26	0.29	0.24	0.10
Fe2O3t	2.15	1.12	1.75	5.05	8.00	2.25
total	100.17	99.34	99.63	99.37	98.76	98.99
TRACE ELEMENTS						
Cu	7	6	9	22	64	12
Pb	4	3	4	6	4	8
Zn	25	11	53	53	13	25
Au	<10	<10	<10	<10	<10	<10
Ag	<0.1	0.1	0.1	0.1	<0.1	0.3
Mo	<1	<1	<1	<1	<1	1
Sb	<1	<1	<1	<1	<1	3
Sn	2	2	2	2	1	2
W	1	6	11	1	1	2
Hg	20	40	50	60	50	40
As	<10	<10	<10	<10	<10	<10
Co	5	3	3	3	13	6
Ni	14	10	11	9	36	18
Fe	18200	7400	13100	42700	52100	14700
Mn	200	300	100	200	200	1000
F	90	100	100	560	480	170
Cr	109	165	94	52	119	120
Cd	<1	<1	<1	<1	<1	<1

Table 4 continued.

sample	2359	2360	2363	2384	2407	2430
MAJOR OXIDES						
SiO2	42.61	45.39	41.88	42.21	43.35	44.41
Al2O3	8.72	18.40	13.03	14.83	14.09	11.00
Fe2O3	4.94	1.67	3.69	1.83	2.21	2.07
FeO	7.26	10.44	9.28	11.46	10.08	8.68
MgO	17.53	6.08	7.89	8.01	7.56	9.81
CaO	10.42	10.24	15.27	12.36	13.59	15.65
Na2O	0.96	2.25	0.87	1.07	0.91	0.68
K2O	1.04	0.68	0.29	0.90	1.08	1.15
TiO2	1.93	0.69	2.49	2.52	2.56	2.19
P2O5	0.30	0.02	0.39	0.33	0.77	0.87
MnO	0.19	0.22	0.87	0.56	0.36	0.20
LOI	2.38	1.47	1.31	1.47	2.23	1.61
H2O-	0.21	0.29	0.23	0.22	0.07	0.14
Fe2O3t	13.01	13.27	14.00	14.56	13.41	11.72
total	98.49	97.84	97.49	97.77	98.86	98.46
TRACE ELEMENTS						
Cu	62	4	52	138	20	57
Pb	2	3	6	2	2	3
Zn	32	114	55	45	70	62
Au	<10	<10	<10	<10	<10	<10
Ag	<0.1	<0.1	<0.1	<0.1	0.1	0.1
Mo	2	<1	<1	<1	2	<1
Sb	<1	<1	<1	<1	<1	<1
Sn	1	1	1	1	2	1
W	1	1	7	1	4	5
Hg	350	60	60	70	40	280
As	<10	<10	<10	18	<10	<10
Co	30	21	31	58	26	24
Ni	189	45	109	284	121	129
Fe	56000	65800	55200	63300	75300	62100
Mn	400	1000	3000	1900	1700	900
F	430	980	740	820	1600	3800
Cr	660	78	370	290	280	300
Cd	<1	<1	<1	<1	<1	<1

Table 4 continued.

sample	2441	4630
MAJOR OXIDES		
SiO2	45.39	43.75
Al2O3	13.47	13.18
Fe2O3	2.35	1.76
FeO	8.35	9.73
MgO	7.37	8.66
CaO	13.92	12.83
Na2O	1.96	1.59
K2O	0.86	1.17
TiO2	2.98	2.98
P2O5	1.07	0.84
MnO	0.17	0.19
LOI	1.39	1.52
H2O-	0.31	0.03
Fe2O3	10.70	12.57
total	99.59	98.23
TRACE ELEMENTS		
Cu	22	139
Pb	4	3
Zn	43	38
Au	<10	<10
Ag	<0.1	0.1
Mo	<1	<1
Sb	<1	<1
Sn	1	1
W	1	1
Hg	90	150
As	<10	<10
Co	13	19
Ni	27	46
Fe	45900	58100
Mn	700	900
F	1400	660
Cr	69	32
Cd	<1	<1

Table 5. Major oxide data for amphibolites from Gilmore Dome.

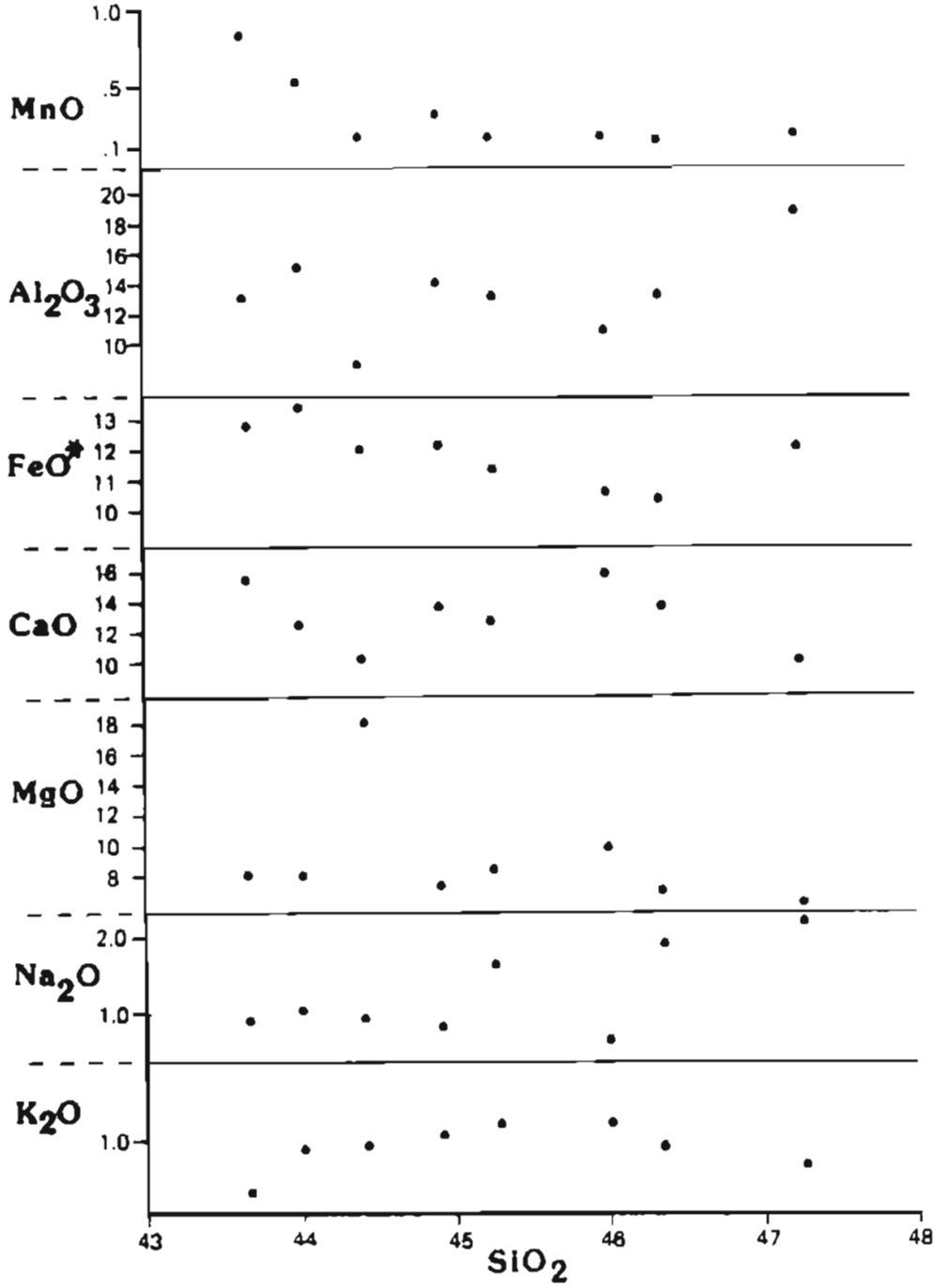

Table 6. Correlation coefficients for altered Gilmore Dome rocks.

	CU	PB	ZN	MO	SB	SN	W	HG	AS	F
CU										
PB										
ZN				0.45081 68		0.72219 68				0.82219 68
MO			0.45081 68			0.62200 82	0.59304 82			0.47957 82
SB										
SN			0.72219 68	0.62200 82						0.75534 82
W				0.59304 82						
HG										
AS										
F			0.82219 68	0.47957 82		0.75534 82				

only values greater than 0.45000 are shown
number of samples listed below each coefficient

Table 7. Correlation coefficients for unaltered Gilmore Dome rocks.

	CU	PB	ZN	MO	SB	SN	W	HG	AS	F
CU										
PB										
ZN										0.47892 61
MO										
SB									0.73005 63	
SN										
W										
HG										
AS					0.73005 63					
F			0.47892 61							

only values greater than 0.45000 are shown
number of samples listed below each coefficient

Table 8. Average crustal abundance of trace elements.

Element	Basalt	Granite	Shale	Limestone
Ag	0.1	.04	.05	1
As	0.1	.04	.05	2.5
Au	0.004	0.004	0.004	0.005
Cu	100	10	50	15
F	400	735	740	330
Hg	0.08	0.08	0.5	0.05
Mo	1	2	3	1
Pb	5	20	20	--
Sb	0.2	0.2	1	--
Sn	1	3	4	4
W	1	2	2	0.5
Zn	150	180	160	25

all values in ppm, -- indicates no data available.
Data from Levinson, 1974.